The Heat Pipe Injection Lance

by

Peter A. Botos

Department of Mining and Metallurgical Engineering
McGill University
Montreal, Canada

May, 1992

A thesis submitted to the Faculty of Graduate Studies
and Research in partial fulfillment of the requirements
for the degree of Master of Engineering

Imagination is more important than knowledge.

Albert Einstein

ABSTRACT

The heat pipe is a device which is capable of moving large quantities of heat over very small temperature gradients. Its ability to transport heat far surpasses the foremost solid conductor, silver, and its use in engineering applications is constantly increasing as innovators begin to realize its potential. To date, heat pipe technology has found little use in the metallurgical industry. This work focuses on the potential use of heat pipes in injection lancing; specifically, the need to preserve lances from consumption in the Mitsubishi continuous copper making process of the Kidd Creek smelter located in Timmins, Ontario, Canada.

The problems with the Mitsubishi lances presently used are two-fold:

i) the direct costs associated with continually feeding stainless steel lances into the molten copper bath.

ii) the indirect costs associated with improper control over the process since lance height relative to the bath is unknown.

A heat pipe injection lance is self-cooling, enabling it to maintain a surface temperature well below the Mitsubishi furnace temperatures. A cooled lance has an increased tolerance to furnace conditions, thereby decreasing its consumption rate. The furnace residence time of a heat pipe injection lance is orders of magnitude larger than a standard stainless steel lance, resulting in materials cost savings. During its operation, the exact location of a heat pipe injection lance is known, solving the second and perhaps more important problem with the Mitsubishi process; control of the lancing operation.

The work performed can be divided into three stages. The first stage involved the development and study of a transparent heat pipe which served to illustrate the principles of heat pipes, specifically, thermosyphons or wickless heat pipes. The second stage dealt with the conception, construction and study of a laboratory scale heat pipe injection lance. The knowledge gained in the laboratory was used to build two pilot scale heat pipe injection lances, Mark I and Mark II, in the third stage of this work. These lances were tested in the copper converting furnace at the Kidd Creek smelter. Through the development of pilot scale heat pipe

injection lances, it is shown that a self-cooled heat pipe lance has a furnace life orders of magnitude greater than a conventional stainless steel lance, with its exact location relative to the molten copper bath surface known.

Résumé

Le caloduc est un dispositif capable de transporter de grandes quantités de chaleur avec un faible gradient thermique. Sa capacité à transporter la chaleur est bien supérieure à celle du meilleur conducteur solide, l'argent, et son utilisation dans l'industrie augmente continuellement à mesure que les innovateurs réalisent son potentiel. Jusqu'à aujourd'hui, la technique du caloduc n'a trouvé que peu d'application dans l'industrie metallurgique. Ce travail a pour but d'étudier la possibilité d'utilisation de caloduc comme lance à injection, et en particulier, le besoin de préserver toute consommation des lances dans la procédé Mitsubishi de fabrication continue du cuivre de l'usine sidérurgique Kidd Creek localisée à Timmins en Ontario, Canada.

Les problemès rencontrés avec les lances Mitsubishi sont actuellement de deux ordres:

i) les coûts directs, engendrés par la consommation continue des lances en acier inoxydable dans la bain de cuivre.

ii) les coûts indirects, associés à un contrôle impropre du procédé, du à la mauvaix connaissance de la hauteur de la lance par rapport au bain.

Une lance à injection de type caloduc s'auto-refroidit, ce qui lui permet de maintenir une température en surface bien en dessous des température des fours Mitsubishi. Une lance refroidie résiste mieux aux conditions du four, et ainsi, son taux de consommation est diminué. Le temps de maintien dans le four d'une lance à injection de type caloduc est plusiers fois supérieur à celui des lances conventionelles en acier inoxydable, ce qui permet une économie dans le coût du matériau. Pendant son utilisation, la localisation de la lance à injection de type caloduc est exactement connue, ce qui résout le second problème posé et peut-être même d'autres problémes plus importants rencontrés dans le procédé Mitsubishi comme par exemple, le contrôle de l'opération d'injection par lance.

Le présent travail peut être divisé en trois parties. En premiière partie, le développement et l'étude d'un caloduc transparent permettent d'illustrer des thermosyphons ou des caloducs sans mèche. La seconde partie est consacrée à la conception, la fabrication et l'étude d'une lance à injection de type caloduc à l'échelle du laboratoire. Enfin, les connaissances acquises en laboratoire ont ensuite permis de fabriquer deux lances à injection expérimentales de type

caloduc, Mark I et Mark II. Ces lances ont été testées dans le four de cémentation du cuivre à l'usine Kidd Creek. Le développement des lances à injection expérimentales de type caloduc a permis de montrer que ces lances auto-refroidissantes ont une durée de vie dans le four plusieurs fois supérieure à celles des lances conventionnelles en acier inoxydable; de plus, leur localisation par rapport à la surface du bain de cuivre fondu est maintenant connue précisemment.

Acknowledgements

The author wishes to express his appreciation to his supervisor, Professor Frank Mucciardi, for his unending patience, support and enthusiasm. The many discussions held on a wide variety of topics were both engaging and illuminating.

The author is indebted to Ernest Mast and Dr. Mike Kozlowski; without their interest and backing this work would never have gone as far and as smoothly as it did.

Thanks go out to the members of the Metallurgical machine shop, particularly M. Knoepfel, as well as Walter Greenland of the Chemical machine shop for performing the difficult welding of the first two heat pipe injection lances.

To the staff and graduate students of the Department of Mining and Metallurgical Engineering, who were countlessly relied upon as a resource, the author would like to express his gratitude.

Finally, but most importantly, I would like to thank my parents, Eva and Alex Botos, and my family. Anyu and Apu, without your tireless love and support, I would never have been capable of such a work.

Contents

List of Figures

List of Tables

List of Micrographs

Nomenclature

A	area,
A_c	external surface area of condenser,
A_e	external surface area of evaporator,
A_l	cross-sectional area for liquid flow,
A_s	area of individual surface pores of the wick,
A_v	vapour core cross-sectional area,
C_l	wetted perimeter for liquid flow,
C_s	wetted perimeter of the individual surface pores of the wick,
d	screen wire diameter,
d_i	pipe inside diameter,
d_o	pipe outside diameter,
d_v	vapour core diameter,
D	diffusion coefficient,
d_v	dynamic pressure coefficient,
f_l	drag coefficient for liquid flow,
f_v	drag coefficient for vapour flow,
F_l	frictional coefficient for liquid flow,
F_v	frictional coefficient for vapour flow,
g	gravitational acceleration,
h_c	overall heat transfer coefficient at condenser,
h_e	overall heat transfer coefficient at evaporator,
k	thermal conductivity,
k_e	effective thermal conductivity of liquid saturated wick,
K	wick permeability,
L	effective heat pipe length,
L_a	length of heat pipe adiabatic section,
L_c	length of heat pipe condenser,

L_e	length of heat pipe evaporator,
L_t	total length of heat pipe,
M	molecular weight,
N	screen mesh number,
P	pressure,
P_c	capillary pressure,
P_{cm}	maximum capillary pressure,
$P_{cm,e}$	effective capillary pressure available for fluid circulation,
P_l	liquid pressure,
P_o	stagnation pressure,
P_{pm}	maximum effective pumping pressure,
P_{pw}	saturation vapour pressure at the pipe wick interface,
P_t	total pressure,
P_v	vapour pressure,
ΔP_l	liquid pressure drop,
ΔP_v	vapour pressure drop,
$\Delta P_\perp$	hydrostatic pressure in direction perpendicular to pipe axis,
Q	heat flow rate,
$Q_{b,max}$	boiling limit in heat transfer rate,
$Q_{c,max}$	capillary limit on heat transfer rate,
$Q_{e,max}$	entrainment or flooding limit on heat transfer rate,
$Q_{s,max}$	sonic limit on heat transfer rate,
$(QL)_{c,max}$	heat transport factor,
r	radius of cylinder,
r_b	bubble radius,
r_c	effective capillary radius,
$r_{h,l}$	hydraulic radius for liquid flow,
$r_{h,v}$	hydraulic radius for vapour flow,
r_i	inside radius of pipe,
r_n	boiling nucleation radius,

r_o	outside radius of pipe,
r_v	vapour core radius,
R	universal gas constant,
Re_l	liquid flow Reynolds number,
Re_v	vapour flow Reynolds number,
t	thickness,
t_p	pipe wall thickness,
t_w	wick thickness,
T	temperature,
T_g	gas temperature,
T_o	stagnation temperature,
T_{pw}	temperature at the pipe-wick interface,
T_v	vapour temperature,
T_{wv}	temperature at the wick-vapour interface,
V_l	liquid velocity,
V_v	vapour velocity,
w	groove width,
x	axial position,
x_{ref}	reference axial position from where x is measured,
x_{min}	axial position where capillary pressure is minimum,
x_{max}	axial position where capillary pressure is maximum,
β	profile coefficient for momentum flux,
γ_v	vapour specific heat ratio,
ϵ	wick porosity,
λ	latent heat of vaporization,
μ_l	liquid dynamic viscosity,
μ_v	vapour dynamic viscosity,
ρ	density,
ρ_l	liquid density,
ρ_o	vapour density at stagnation condition,

ρ_v	vapour density,
σ	surface tension coefficient,
σ	Stefan-Boltzmann constant,
τ_l	liquid frictional stress,
τ_v	vapour frictional stress,
ψ	heat pipe inclination measured from horizontal position,

Chapter 1

The Heat Pipe

1.1 Introduction

In 1942, R. Gaugler of the GM corporation, USA, filed a patent application[1] for a heat transfer device to be used in refrigeration systems. It was not until 1964 that the name heat pipe was given to the device by M. Grover, who independently reinvented the concept[2]. Grover added a brief theoretical analysis to describe his work with a stainless steel heat pipe. It soon followed that several articles were published on the application of heat pipes for cooling electronics, air conditioning, engine cooling and others[3,4,5]. Since Grover's invention, thousands of papers have been written on the subject of heat pipes, advancing the understanding of this important device to our present state. That state is only in its infancy as there is far more to be learned about this remarkable invention.

The heat pipe is essentially a heat transmission device which is capable of moving very large quantities of heat over minimal temperature gradients. The amount of heat that it can transport is orders of magnitude greater than any equivalently sized solid conductor. A suitable way to describe its heat transfer capabilities is to call it a super-conductor of heat, much like we refer to super-conductors in electrical applications. Among the many striking advantages of the heat pipe are: constructional simplicity, operational flexibility, accessibility to control and ability to transfer heat at a high rate over very small temperature gradients[6].

Typically, the heat pipe is a closed tube or chamber, varying in shape and size. Inside the heat pipe is a working substance and a capillary wick. The wick is not always necessary and when gravity can be exploited, no wick is required, in which case the pipe is termed a thermosyphon. Thermosyphon heat pipes are essentially the focus of this study and will be dealt with in detail later in this work.

A heat pipe can be divided into 3 regions: the evaporator section, the adiabatic section

and the condenser section. Figure 1.0 shows an illustration of a typical heat pipe. Initially, the heat pipe is evacuated so that the pressure in the container is at a minimum; ideally, zero atmospheres. Heat is absorbed in the evaporator section, conducted through the walls of the container and then transmitted to the working substance. The working substance is chosen

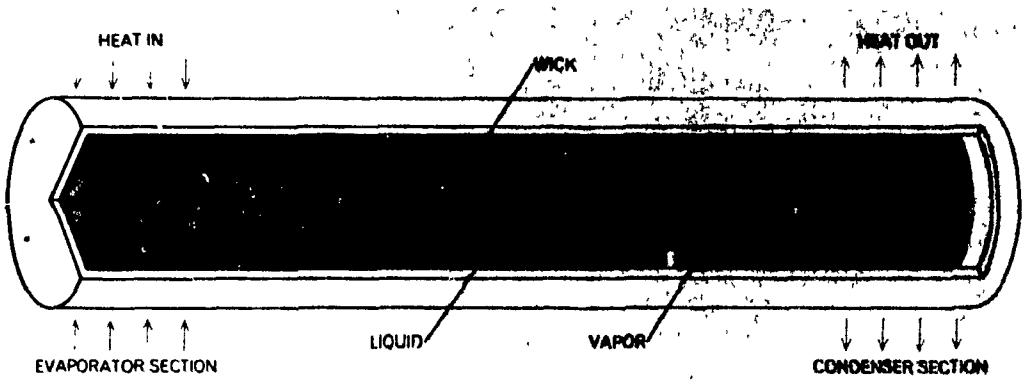

Figure 1.0 : Schematic of a Typical Heat Pipe

primarily because of its properties at the operating temperatures of the evaporator and the condenser. The substance chosen must have a normal boiling point at or near the evaporator temperature. The heat conducted through the walls of the evaporator section is absorbed through the vaporization of the working substance. As evaporation takes place a pressure gradient is established and the vapours generated travel to the other end of the pipe, the condenser.

In the condenser section, the environment is at a temperature well below the normal boiling point of the working substance so that the vapour is forced to condense on the walls of

the container. The latent heat of condensation is then released and conducted through the walls of the container and out into the environment. The condensate returns back to the evaporator by a capillary wick or by gravity when no wick is required (thermosyphon). In the case of a wicked heat pipe, depletion of liquid by evaporation causes the liquid vapour interface in the evaporator to enter into the wick surface and a capillary pressure is developed there. The resulting capillary pressure pumps the condensed liquid back to the evaporator for re-evaporation. In the case of a thermosyphon, the condensate flows down the walls as the force of gravity returns the liquid back to the evaporator either as a film or as droplets. In the adiabatic section no heat is transferred. The following figure is a schematic representation of a thermosyphon, heat pipe.

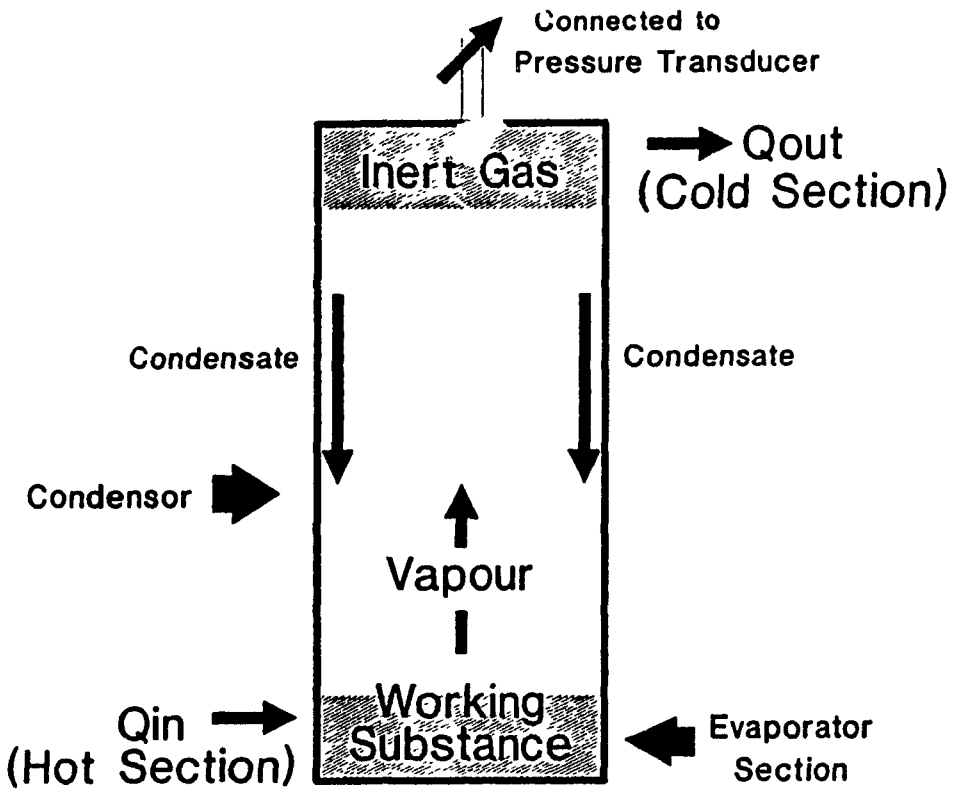

Figure 1.1 : Schematic of a Thermosyphon Heat Pipe

The evaporation and condensation processes will continue if no blockage of flow is incurred and the heat pipe is in a feasible operating temperature range. Thus, an equilibrium condition is set up where continuous vapour and liquid flow take place.

The key to the heat pipe's tremendous ability to move heat is in the energy absorbed and released by phase changes. This energy can be absorbed at one location, transported to another and released without any significant losses. Thus, the heat pipe essentially re-distributes heat energy very effectively. This is a valuable property that can be incorporated into many engineering applications. It is also this property that has enabled the Heat Pipe Injection Lance to perform successfully.

1.2 Applications

Heat pipes are used in a wide variety of applications most of which involve a heat exchange device. The following are descriptions of patents for a variety of heat pipe applications.

Heat Recuperator[7]:

A large portion of the heat which is entrained and lost in the exhaust gas of a fireplace can be recovered by a heat recuperator. It is essentially comprised of heat absorbing elements (evaporators) and heat distributing elements (condensers), with a heat carrier medium in circulation (the working fluid). This patent claims that 20-35% of the heat released by burning wood can be recovered by this system. Referring to Figure 1.2, water, the working substance, evaporates in duct 2 and condenses in duct 5 using the burning wood, 3, as the heat source. The condensate is returned through tube 11 to the evaporator and a fan, 15, convects the heat given off at the condenser into the room.

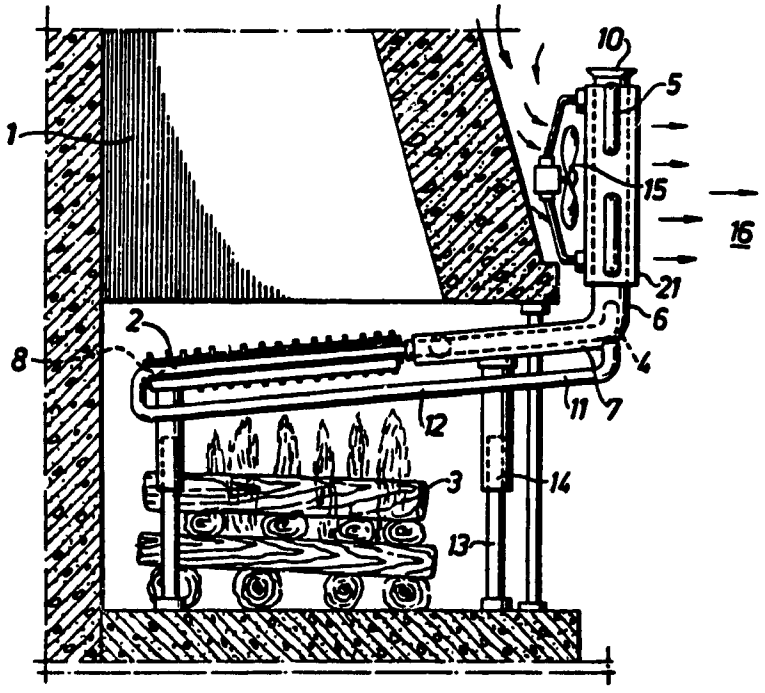

Figure 1.2 : Heat Pipe Fireplace Application

Solar Collector[1]:

Figure 1.3 shows a device which harnesses the energy of the sun to heat household water. A solar collector, 10, has an inlet, duct 11, for a first fluid to be heated and an outlet, duct 12, for the spent solar heated fluid. A solar collector is mounted in a rectangular frame, 13. Onto a second, smaller rectangular frame, 14, is mounted a tank, 15, used for containing a heat transfer fluid, 16. This tank is metallically lined and insulated.

The first ducting in the tank interior, 17, takes the heat collected by the first fluid and transfers it to the second fluid body, 16, in the tank interior. That same ducting shown at 18, is in series with inlet 11 and outlet 12 to heat the second fluid 16. The first fluid contained in ducting 18, may be freon. It is vaporized in the collector and condensed in duct 18, releasing its energy to the second fluid, 16, in the tank. A third fluid, water, is passed through ports 21a and 21b to pick up energy from the second fluid. This heated water can then be used in the house.

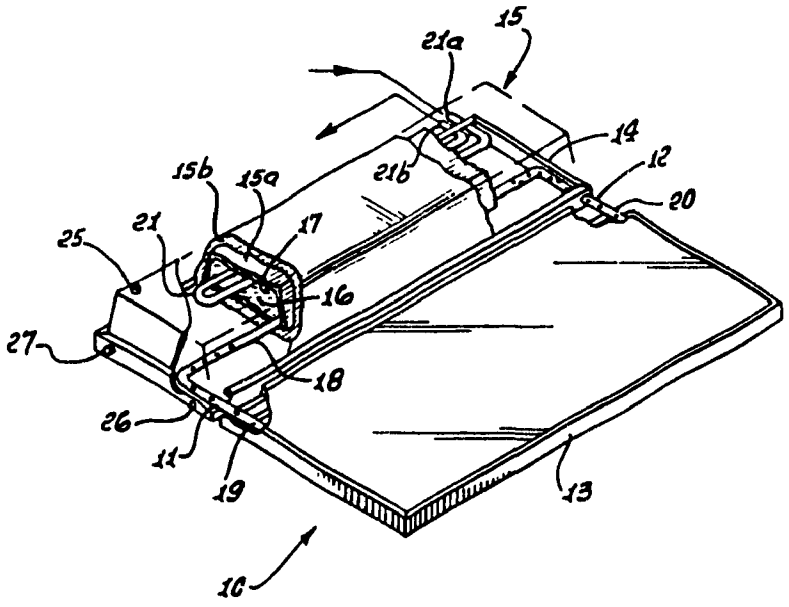

Figure 1.3 : Solar Collector

Industrial Solids Heat Exchanger[9]

A patent describing apparatuses and methods for transferring heat from a relatively hot stream of solid materials exists. Referring to Figure 1.4 which follows, two streams of solids cascade downward by the force of gravity over a series of heat pipes. The heat pipes are arranged so that they exchange heat from the hot stream to the cold stream, allowing counter-current heat transfer to take place. This invention is applied to a process which recovers hydrocarbons from shale rock.

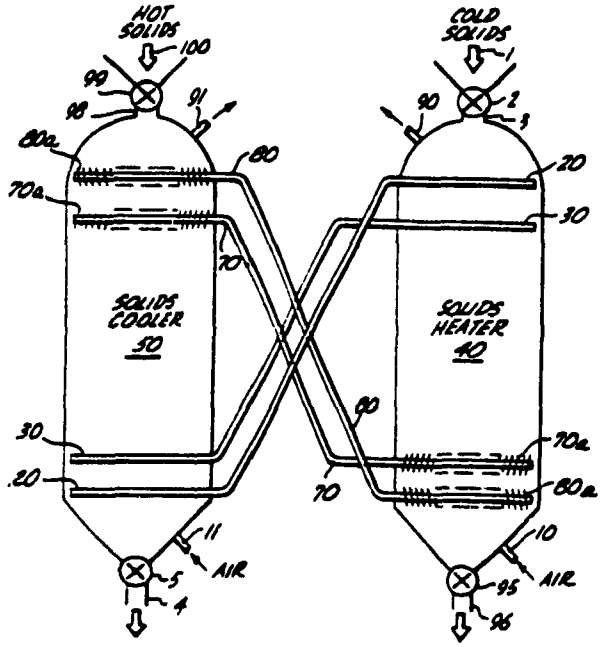

Figure 1.4 : Industrial Solids Heat Exchanger

Cooling System for Internal Combustion Engine[10]

According to a patent by Daimler-Benz, heat pipes can be used to cool an internal combustion engine of an automobile. Such a system has the advantage of dispensing with pumps to provide the necessary air cooling of the engine. Instead, the evaporation and condensation of a working fluid can be used to cool the engine, at exact critical locations as Figure 1.5 illustrates. Locations 2, 3, 6a, 6b, and 7 indicate the engine space, a conventional combustion engine, 4 cylinder head, the evaporator and a common condenser, respectively.

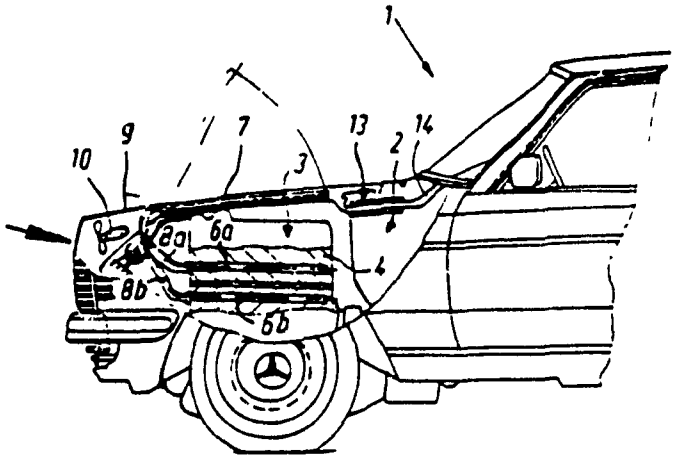

Figure 1.5 : Cooling System for Internal Combustion Engine

Heat pipe applications are far less common in the metallurgical industry than they are in other engineering fields, but they do exist. According to the patent of the Institut de Recherches de la Siderurgie Francaise (IRSID), heat pipe technology can be used to eliminate complications caused by aggressive hot slags in the refractory lining of metal smelting equipment.[11] This can be done by arranging heat pipes of high thermal conductivity in the upper annular zone of the refractory lined smelter, or in the zone where slag is forming. The heat pipes remove heat between the upper and lower levels of slag, thereby cooling the region and reducing the damaging effects of the slag.

A patent was found that describes a heat pipe application for cooling blast furnace tuyeres[12]. Essentially, a blast furnace tuyere is a large copper block with a hole through which air is blown. Typically, water cooling is used to cool the copper blocks. This is not the safest way. If the blocks fail, which they eventually will, water may leak into the blast furnace and cause an explosion. A heat pipe cooled tuyere would draw the heat back to a more manageable location where it could be cooled safely, with water.

From the extensive literature survey carried out on the subject, it is clear that the metallurgical industry is not benefitting from heat pipe technology. It was felt that with the right application and the proper exposure, this could change. With a view towards increasing the metallurgical industry's awareness of heat pipe technology, investigations into a heat pipe injection lance began.

Chapter 2

The Heat Pipe Injection Lance

2.1 Introduction

Realizing the potential of this unique device, and the importance of heat energy in the metallurgical industry, part of the motivation of this work was to elevate the industry's awareness of heat pipes by finding a suitable application that could demonstrate its abilities. Ideally, the application would illustrate the properties of a heat pipe and how these properties can be exploited to improve a metallurgical process, thereby generating more interest in the use of heat pipes as a metallurgical tool. At the same time, the development of such an application would further our understanding and expertise of heat pipes so that any outside interest generated from our work could be properly dealt with.

A number of possibilities were considered as applications by Professor F. Mucciardi and the author, at the outset of this work. We were joined by E. Mast of the Noranda Technology Center, Pointe Claire, Quebec, Canada, in our search for an appropriate application. E. Mast also believed that the heat pipe was a device with a tremendous potential in the metallurgical industry. Through E. Mast's contact with Dr. M. Kozlowski of Kidd Creek Mines, Timmins, Ontario, Canada, and discussions with Dr. F. Mucciardi and the author, the idea of using a heat pipe in injection lancing was put forth.

The objective of this work was to develop a lance, whereby heat pipe technology would be used to engineer a self cooling injection lance that could replace the present injection lancing system used in the Kidd Creek smelter. The potential benefits of using a heat pipe injection lance are:

i) Savings in lance material costs and,

ii) Control over the lancing operation

This novel lance would essentially be an annular, wickless heat pipe (thermosyphon) with the

injection chamber being the center of the annulus. The heat pipe injection lance would be implemented into the Mitsubishi process used at the Kidd Creek smelter.

2.2 The Mitsubishi Process

2.2.1 Introduction

Since the early sixties, copper producers have focused on a process that could continuously produce molten copper from its concentrates. Although the goal was the same, a variety of very different processes have emerged. The dominant copper converting processes existing today are the Outokumpu and Inco flash furnaces processes, the Noranda process and the Mitsubishi process. Perhaps none but the Mitsubishi process is truly continuous as the other processes still use conventional Pierce-Smith converters performing batch operations as opposed to the continuous matte conversion of the Mitsubishi process[13]. Although these new processes have in common an intent to reduce fuel consumption by utilizing the heat of oxidation of iron and sulphur contained in the copper concentrates, the technical procedures followed by each differ significantly[14]. In the flash furnace processes, the main reaction proceeds within a solid-gas dispersion system causing the dust loading of the off-gas to be rather high. Also, a need exists for a separate vessel to treat high magnetite slag due to excess magnetite generated at the reaction shaft. In the Noranda process, the raw materials are spread over the bath and oxidation air is blown through tuyeres at the bottom of the reaction vessel. In the Mitsubishi process raw materials and oxidizing air are blown into the molten bath through lances situated just above the bath.

It was in 1968 that the Mitsubishi Metal Corporation started a test pilot plant of a continuous copper smelting and converting process at the Onahama smelter. The basic notions behind the design of the new process were:

a) Smelting and converting reactions take place in separate furnaces.
b) Transportation of melt to be carried out through launders connecting the furnaces.
c) Top blow lances to be used for air blowing and solid materials feeding.

In 1971, a semi-commercial plant was started at the Onahama smelter. After a number of years a full scale plant began in March 1974, at the Naoshima smelter. In June 1981, the second Mitsubishi process was commissioned at the Kidd Creek smelter in Timmins, Ontario, Canada.

2.2.2 The Kidd Creek Smelter

Figure 2.0 shows a schematic flowchart of the Mitsubishi process at Kidd Creek. The process comprises three steps: smelting of raw materials at the S-furnace, separation of the resulting slag and matte at the SH-furnace and converting of high grade matte at the C-furnace[14]. Slag losses can be controlled to achieve acceptable economic levels and converter slag can be recycled to the smelting stage.

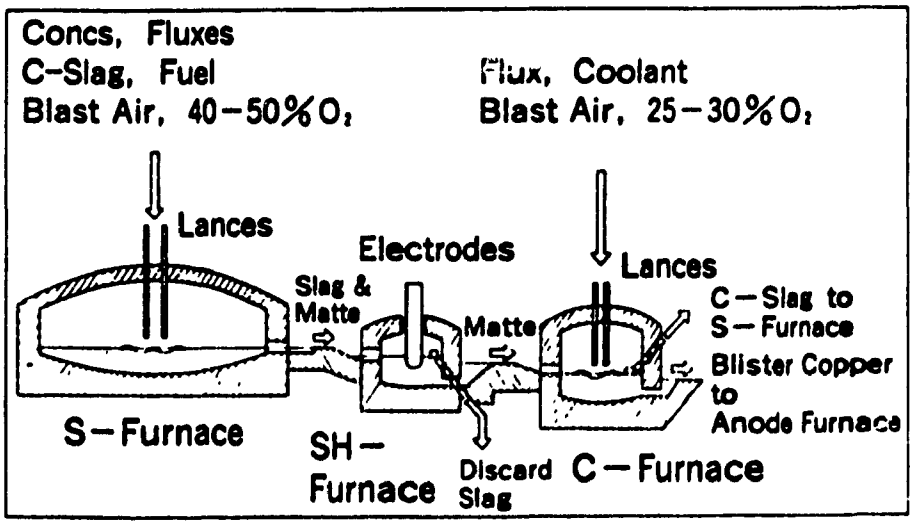

Fig ıre 2.0 : Schematic of Mitsubishi Process

The Smelting Stage

A mixture of copper concentrates, fluxes, reverts and pulverized coal combined with oxygen enriched air (40-50%) is injected through vertical lances into the molten bath of the S-furnace at speeds of up to 150-300 m/s. In all there are ten process lances, five of which shroud the feed pipes[15]. The height of the lances above the bath is approximately 50 cm. Lances are rotated continuously with periodic adjustments to maintain proper height. The lances are consumed and replaced periodically.

The consumable lance is made of a stainless steel pipe with no external cooling. Contained in the S-furnace is a molten bath comprised mostly of matte and a thin layer of slag. This can allow for deep penetration of the jet even without submersion of the lances. Penetration depths have been calculated in a model developed by Kimura[16] to be in the order of 1.4 m. Hearth erosion just below the lances support this model.

The Converting Stage

Molten copper matte is converted to blister copper by gas injection through stainless steel lances. The injection lances, like the S-furnace, are above the bath. The injection is a mixture of pulverized flux and oxygen enriched air. The structure and the operating principles of the C-furnace are essentially the same as the S-furnace.

The predominant reactions in the C-furnace are as follows:

$$FeS_{(matte)} + Cu_2O_{(slag)} = Fe_{(slag)}O + Cu_2S_{(matte)}$$

$$3FeO_{(slag)} + Cu_2O_{(slag)} = Fe_3O_{4(slag)} + 2Cu$$

$$Cu_2S_{(matte)} + 2Cu_2O_{(slag)} = 6Cu + SO_2$$

Oxygen blown through the lances can oxidize dissolved sulphur in the matte as well as copper to regenerate cuprous oxide. The reactions are as follows:

$$S_{(in\ copper)} + O_2 = SO_2$$

$$2Cu + 0.5O_2 = Cu_2O_{(slag)}$$

Plant data relating copper loss to the C-Slag and %S in the blister copper is shown in the following figure:

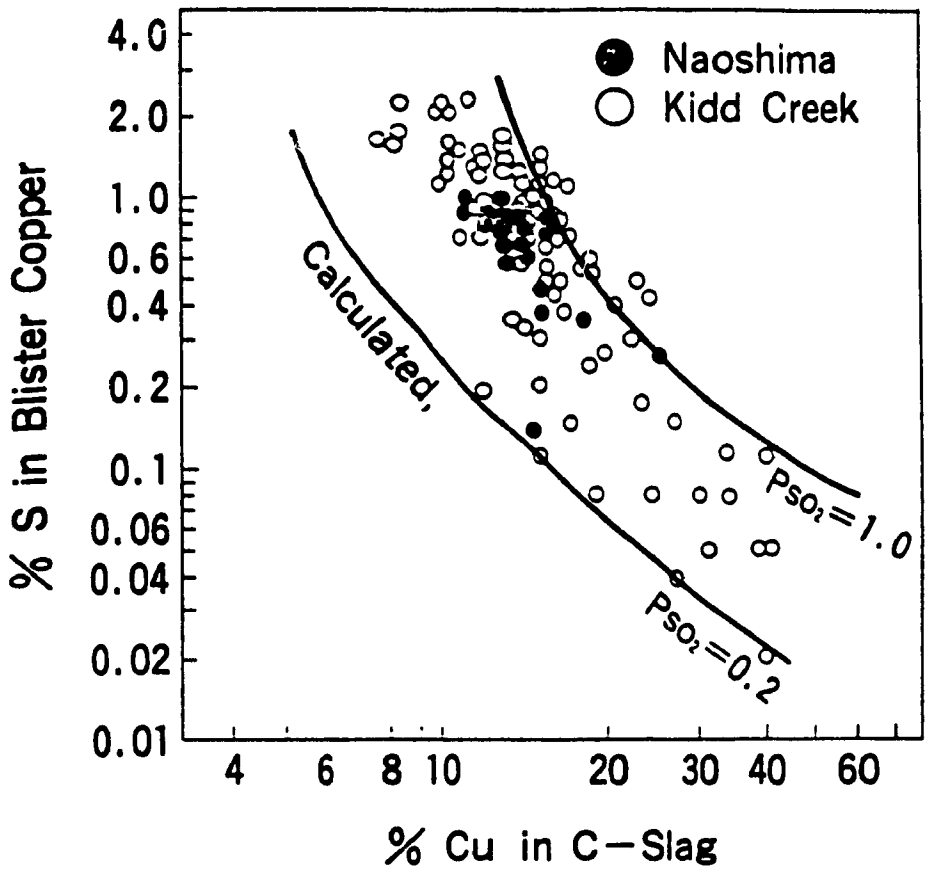

Figure 2.1 : %S in Blister Copper versus Copper Losses to C-Slag

From the plant data we can see that both plants operate close to P_{SO2} = 1 atm. This suggests that SO_2 attack is one mechanism for the chemical deterioration of the consumable lances since the atmosphere in which the lances operate is predominantly sulphur dioxide. This attack is much more severe in the C-furnace than in the S-furnace. The result is greater consumption of the lances in the C-furnace.

2.2.3 Mitsubishi Lances

One of the fundamental differences of the Mitsubishi process versus the Noranda process or the Flash Furnace processes is the top blowing of oxygen enriched air and fluxes into a molten bath. Top blowing is vital in allowing the continuity of the process since no complete shutdown of production is required to replace the lances, unlike the tuyeres in the Noranda process. Lances can be replaced one by one allowing continuous blowing from the other lances. The tuyeres must be constantly replaced in the Noranda process requiring periodic shut down of the reactor.

Top blowing also allows the system to be closed, favouring better control of the off-gas. Rather than large fluctuations from no off-gas to peak off-gas as in the Noranda process, where the handling system must be designed for peak operation, the Mitsubishi process needs only to deal with a much smaller steady stream of gas. Environmentally it is much more sound.

Top blowing allows for the three furnace design by not interrupting the cascading flow of the matte and slag from one furnace to the other. This design was fundamental to the Mitsubishi process since the very beginning of the developmental work[17].

Figure 2.2 shows the Mitsubishi process furnace arrangement at Kidd Creek, illustrating the placement of the lances and the cascading liquid delivery system. The off-gases from the S-furnace and C-furnace are removed by a fume-hood venting system which in turn delivers the off gases (predominantly SO_2) to an acid plant.

It is clear that the injection lances of the Mitsubishi process play a key role in the system. Ideal operation of the Mitsubishi process requires that the process lance tips in both the smelting and converting furnaces are maintained close to 0.5 m above the bath surface. Due to the harsh conditions in the furnaces, stainless steel lances are consumed and periodically replaced by threading on a new section. Unfortunately, it is not quite as simple as just replacing the lance. A major problem with consumable lances is the fact that their exact whereabouts within the furnaces are unknown. If the rate of consumption was uniform and predetermined, the location of the lances could be easily calculated. However, this is not the case and the result is a process which lacks good control. Presently, the only method of determining lance location is by visual inspection which can only occur when the furnaces are shut down. Proper adjustments are then made. This is not an ideal means of control. Certainty of penetration depths cannot be had so

that optimization of the process is not achieved.

(Kidd Creek)

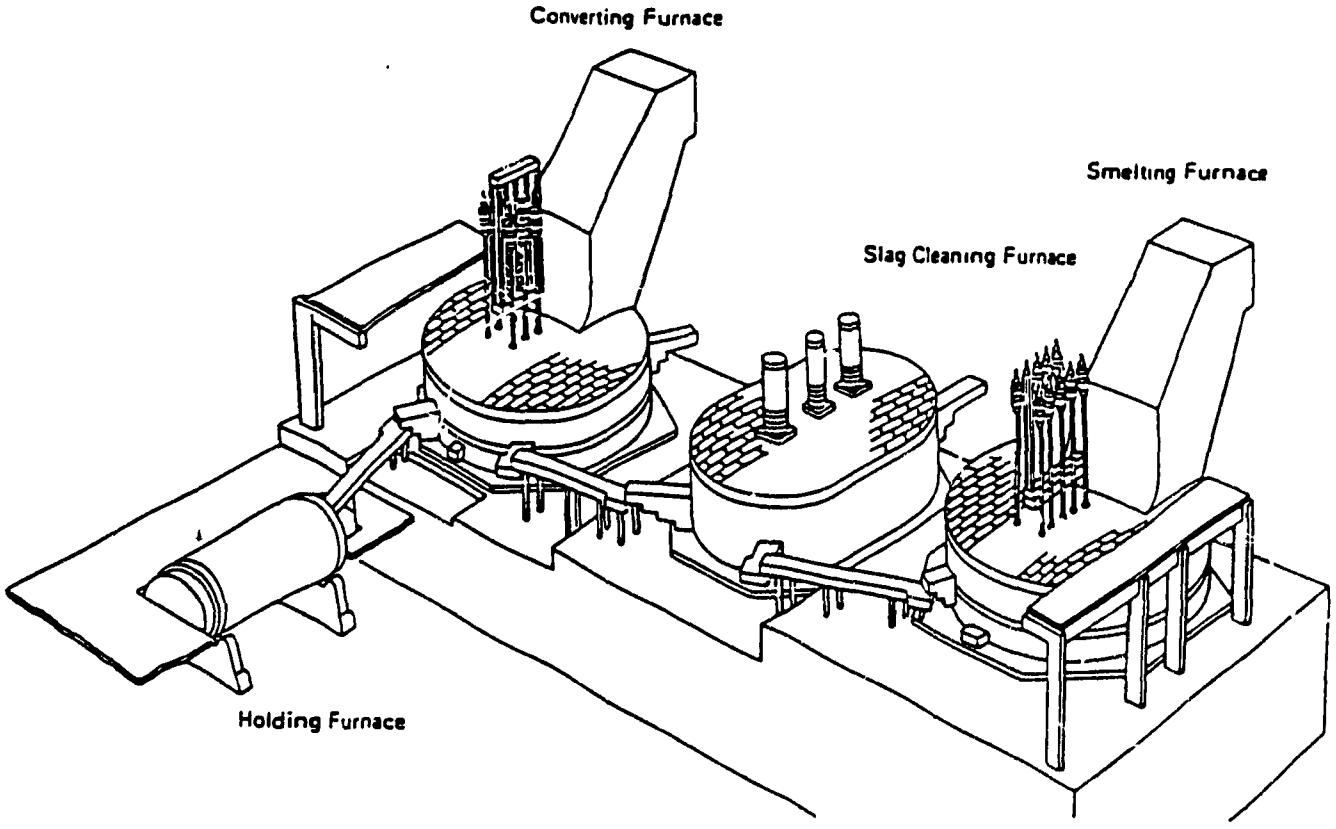

Figure 2.2 : Mitsubishi Process Furnace Arrangement at Kidd Creek

2.2.4 Lance Consumption

The freeboard environment in the smelting and converting furnaces is both sulfidizing and oxidizing with temperatures well above the maximum working limit for any steel. Stainless steel is also dissolved by both matte and blister copper. The conditions that the process lances have to endure are not steady. Due to the cyclic nature of the solids delivery system, variations in furnace freeboard temperature and SO_2 levels and changes in lance cooling offered by the injection are encountered. Splashing from the injection causes accretions of matte and slag to form on the lances which can be seen during visual inspection. Accretions can become very large during standard operation of the furnaces. The following problems have been encountered during lance operation:

a) Dissolution of the lance tip if lowered into the melt.

b) Melting of the lance tip in proximity of the reaction zone.

c) Enhancement of mechanism b) by sudden loss of protective accretion.

d) Mechanical failure of the lance body under a large asymmetric rotating load (accretion) at high temperature in a corrosive environment.

e) Lances which have burned back to the roof may cause localised heating and shorten the lives of other lances.

f) Thermal cycling.

Investigations into improving lance reliability have been ongoing since the plant was commissioned. The reasons for these investigations are two-fold; firstly, the direct cost of lance material and secondly, and perhaps of greater importance is the indirect costs of process efficiency related to poor control of the lance height.

Tests have been conducted by Kidd Creek both in the plant and in a laboratory. The tests focused on evaluating the performance of different lance materials taking costs into account. A number of different candidate lances were tested. The results are presented in the following table.

Table 2.0 : Results of Field Trial Tests for Different Lance Materials

Mild Steel On S-Furnace	Inexpensive But Poor Performance
Assorted Refractory Clad Lances	Uncertain Fates-Poor Choice
Diffusion Coated Lances	No Improvement
Type 304L	No Improvement
Type 316	Poor Performance
High Chromium Stainless Steel	Large Improvement
Corguard Lance	Poor Performance

The investigations found that High Chromium stainless steel (HC) lances could last an order of magnitude longer than the lances being used. Even with the much higher material costs, large costs savings in lance consumption were realized when the HC lances were implemented .

Although the HC lances have improved the situation in the S-Furnace and the C-furnace, lances are still consumed and lance location is still unknown.

2.2.5 The Heat Pipe Lance Concept

The bulk of the experimentation carried out for this work took place at the Kidd Creek Smelter. The work that preceded it was preparatory lab scale work. The goal of this work was to investigate the potential of using heat pipe technology to build a self-cooling lance which could be incorporated into the Mitsubishi Process in the Kidd Creek furnaces. The reasoning behind a self-cooling lance is: if a quantity of accretion can be frozen onto the lance and maintained due to the lower temperature of the lance, the lance can be protected from the atmosphere. Maintaining the lance at a much lower temperature will also slow down the kinetics of the reactions at the interface, exponentially. If the life of a lance can be improved so that it is several orders of magnitude larger than the present situation and the exact location of the lance

relative to the bath known, materials costs can be reduced and process optimization can be had. The full potential of top blowing could be realized as direct control over the process would be achieved.

Chapter 3

Heat Pipe Theory

3.1 Introduction

With the objectives of this work stated, details of the heat pipe's operating principles now follow. During the operation of a heat pipe it is often desirable to maximize the circulation of working fluid thereby maximizing heat transport. Four limitations affecting the circulation of working fluid may be encountered during heat pipe operation. These limitations are the capillary limit, the sonic limit, the entrainment limit and the boiling limit. Besides the design criteria and material constraints, it is these limitations that determine the heat removal ability of the heat pipe. More specifically, depending on the particular heat pipe system and operating criteria, it will be one of the aforementioned limits which will determine the maximum possible heat removal rate of the heat pipe system.

Based on previous work and his own work, Chi includes in his book entitled " Heat Pipe Theory and Practice: A Sourcebook"[6] some practical equations and examples to determine the aforementioned limitations. These equations will be briefly described and then applied to a conventional heat pipe example. All the symbols used in the equations are defined in the nomenclature section. The solutions to the example are worked out in Appendix A.

The equations which follow incorporate the laws of fluid mechanics and heat transfer to establish the theory for predicting heat transport limitations.

3.2 Capillary Limit

In wicked heat pipes, the amount of heat that can be transported is restricted by the amount of liquid which can be returned by the wick, which in turn is a function of the capillary pressure in the wick. The capillary pressure is a result of pressure differences between the vapour and the liquid. As vapour flows from the evaporator to the condenser, there exists a

vapour pressure gradient along the length of the pipe. The pressure is higher on the evaporator side than on the condenser side. Similarly, a liquid pressure gradient exists along the length of the pipe as the condensate flows from condenser to evaporator. For a capillary pressure to exist these two pressures must be different.

This pressure difference between the two sides of the liquid-vapour interface, the capillary pressure, is established by the menisci that form at the interface, i.e. by forcing the interface back into the wick structure. The pressure balance can be described mathematically as follows:

$$[P_v(x_{ref})-P_v(x)]+[P_v(x)-P_l(x)]+[P_l(x)-P_l(x_{ref})]+[P_l(x_{ref})-P_v(x_{ref})]=0 \quad (1)$$

If we introduce into this equation the capillary pressure, P_c, defined as the difference between the vapour pressure and liquid pressure at the vapour-liquid interface, we have:

$$P_c(x)=P_c(x_{ref})+\Delta P_v(x-x_{ref})+\Delta P_l(x_{ref}-x) \quad (2)$$

There exists a maximum capillary pressure that can develop for a given liquid-wick system. As the heat rate into the pipe increases, the evaporation rate of fluid in the evaporator increases, placing a greater demand on the wick to pump the condensed liquid back to the evaporator. When the wick can no longer return liquid to the evaporator at a rate equal to the rate of evaporation, the capillary limit is reached. The evaporator dries out and the temperature rises drastically. Unless the heat source is reduced, the pipe will cease to operate properly and may eventually fail.

The general equation for the capillary limitation on heat load according to Chi is:

$$P_{cm,e}=2\frac{\sigma}{r_c}-\Delta P_\perp=\int_{x_{min}}^{x_{max}}\left(\frac{dP_v}{dx}-\frac{dP_l}{dx}\right)dx \quad (3)$$

The liquid pressure gradient can be found from:

$$\frac{dP_l}{dx}=-F_lQ\pm\rho_l g\sin\psi \quad (4)$$

In this equation the frictional coefficient for liquid flow is:

$$F_l = \frac{\mu_l}{KA_w \lambda \rho_l} \tag{5}$$

and the wick permeability is:

$$K = 2\epsilon \frac{r_{h,l}^2}{(f_l Re_l)} \tag{6}$$

Similarly for the vapour pressure gradient we have:

$$\frac{dP_v}{dx} = -F_v Q - D_v \frac{dQ^2}{dx} \tag{7}$$

where the frictional pressure coefficient for vapour flow is:

$$F_v = (f_v Re_v) \frac{\mu_v}{2r_{h,v}^2 A_v \rho_v \lambda} \tag{8}$$

and the dynamic pressure coefficient for vapour flow is :

$$D_v = \frac{\beta}{A_v^2} \rho_v \lambda^2 \tag{9}$$

These equations can be combined to yield a simplified form:

$$2\frac{\sigma}{r_c} - \Delta P_\perp - \rho_l g L_t \sin\psi = \int_0^{L_t} (F_l + F_v) Q dx \tag{10}$$

This equation, which is for a conventional heat pipe, assumes that at x = 0, the end of the condenser, the capillary pressure is a minimum and at x = L_t, the end of evaporator, the capillary pressure is a maximum.

From equation 10 an expression for capillary limitation can be found by first establishing an expression for the heat transport factor:

$$(QL)_{c,max} = \int_0^{L_t} Q dx \tag{11}$$

The capillary limit can be found from the heat transport factor $(QL)_{c,max}$ using the following relation:

$$Q_{c,max} = \frac{(QL)_{c,max}}{0.5L_c + L_a + 0.5L_e} \tag{12}$$

In order to demonstrate capillary limit calculations, the following example taken from Chi[6] will be considered. This same example, which may be regarded as a typical heat pipe situation, will also be considered for sonic limit, entrainment limit and boiling limit calculations. The latter operating limits will be described in the following sections. The calculations for this example are worked out in Appendix A.

Example 1. A 0.5m long water heat pipe, operating at 373.15 K with a wrapped-screen wick has the following characteristics:

Copper tube o.d., $d_o = 2.54 \times 10^{-2}$ m.
Wire screen mesh number, $N = 7.87 \times 10^{-5}$ m^{-1}.
Screen wire diameter, $d = 6.25 \times 10^{-5}$ m.
Screen wick thickness, $t_w = 1 \times 10^{-3}$ m (8 layers approx.).
Copper tube i.d., $d_i = 2.21 \times 10^{-2}$ m.
Vapour core diameter, $d_v = 2.01 \times 10^{-2}$ m.
heat pipe inclination, $\psi = 0$ rad.
Condenser length, $L_c = 0.1$ m.
Adiabatic Length, $L_a = 0.3$ m.
Evaporator Length, $L_e = 0.1$ m.

Using equation 10 and referring to Appendix A, we can see that the theoretical capillary limit for this pipe is 84.5 W.

3.3 Sonic Limit

The sonic limit is encountered when the vapour velocities in a heat pipe reach sonic speeds. In a heat pipe with constant vapour core diameter, the vapour stream velocity is controlled by evaporation and condensation of the working substance. As more vapour is generated, i.e. increased heat load, the velocity of the vapour will increase to accommodate the greater mass flow rate of vapour. In turn, more condensation will take place. We can compare this situation to a compressible fluid flowing through a converging-diverging nozzle. Velocity variations in such a situation result from a constant mass flow through a variable area. In the case of the heat pipe, the situation is reversed; the area is constant but the mass flowrate changes. In both cases, as the fluids are compressible, the velocities change with the changes in pressure that arise from either a decrease in area or an increase in the mass flowrate.
The sonic limit of a heat pipe can be expressed in the following equation:

$$Q_{s,max} = A_v \rho_o \lambda \left[\frac{\gamma_v R_v T_o}{2(\gamma_v + 1)} \right]^{1/2} \tag{13}$$

When the sonic limit is reached, a choked flow condition results wherein the flowrate will no longer increase. Increasing the heat rejection rate beyond the sonic limit serves only to decrease the condenser temperature, creating large axial temperature gradients without increasing the heat transfer rate.

In Appendix A, the sonic limit is calculated for the water heat pipe in example 1. The sonic limit is found to be, $Q_{s,max} = 9.19 \times 10^4$ W, which is orders of magnitude higher than the capillary limit.

3.4 Entrainment Limit

Inside the heat pipe a two phase (i.e. liquid and vapour) system exists, where one phase flows in the opposite direction of the other. As the heat input into the heat pipe increases, so do the velocities of both phases. Since the phases are travelling in opposite directions, any increase in heat flux amplifies the net change in velocity between the vapour and liquid. Shear forces exist at the vapour-liquid interface due to the relative vapour to liquid velocity. If the

relative vapour velocity is high enough, a critical limit is reached resulting in vapour tearing away liquid from the surface and entraining it in its flow. This entrainment limit is reached when the demand on the liquid return system exceeds its ability, resulting from the excess entrained liquid which it must accommodate but cannot. The evaporator becomes depleted and eventually dries out.

The equation to determine the entrainment heat transport limit in a conventional heat pipe is:

$$Q_{e,max}=A_v\lambda\left(\frac{\sigma\rho_v}{2r_{h,s}}\right)^{1/2} \tag{14}$$

The entrainment limit for the heat pipe in example 1 is calculated in appendix A to be 1.64 x 10^4 W. This value is smaller than the sonic limit but still orders of magnitude larger than the capillary limit.

3.5 Boiling Limit

The occurrence of evaporation at a solid-liquid interface is termed boiling. This process occurs when the temperature of the surface exceeds the liquid saturation temperature[18]. If it is exceeded by a large enough temperature, vapour bubbles form at the solid surface. In a heat pipe, when evaporation occurs within the liquid pool of the evaporator, bubbles can form and disturb the circulation of liquid. If the circulation of fluid to the walls of the pipe is interrupted, "hot spots" can form and damage the pipe wall. This is another limit which must be considered when calculating the maximum theoretical heat which can be transported. To determine the boiling limit, the theories of nucleate boiling must be considered. Two separate processes are involved, (i) nucleation or the formation of bubbles and (ii) growth and motion of these bubbles. At equilibrium, a spherical bubble near the pipe-wick interface will follow the relation:

$$\pi r_b^2(P_{pw}-P_l)=2\pi r_b\sigma \tag{15}$$

The liquid pressure is equal to the vapour pressure minus the capillary pressure at the liquid vapour interface. Using this and the Clausius-Clapeyron equation, T and P can be related along

the saturation line to yield:

$$T_{pw}-T_{wv}=\frac{T_v}{\lambda\rho_v}\left(\frac{2\sigma}{r_b}-P_c\right) \tag{16}$$

where $(T_{pw}-T_{wv})$ is the temperature drop across the wick structure at the evaporator section. Using conduction theory, the following relation can then be calculated:

$$(T_{pw}-T_{wv})=\frac{Q\ln(r_f/r_v)}{2\pi L_e k_e} \tag{17}$$

Equating these two equations and replacing r_b with r_n, the initial radius of the vapour bubbles at equilibrium, the vapour bubbles will form and grow if:

$$Q_{b,max}=\frac{2\pi L_e k_e T_v}{\lambda\rho_v \ln(r_f/r_v)}\left(\frac{2\sigma}{r_n}-P_c\right) \tag{18}$$

Values of r_n have been experimentally determined by Griffith and Wallis[19]. Their results indicate that r_n varies from 1×10^{-4} to 10^{-3} in. In the absence of non-condensible gases, these values are much lower. A good estimate for r_n in heat pipes is 10^{-3} to 10^{-5} in., depending on how good the vacuum is. The boiling limit is calculated for example 1 in Appendix A and is found to be 1394 W.

When considering the four limitations for the conventional heat pipe in example 1, it is clear that the sonic limit is the least worrisome, with a value of 9.19×10^4 W. The entrainment limit closely follows with a value of 1.64×10^4 W. The boiling limit is an order of magnitude smaller than these limits but still not the determining factor. As suspected the capillary limit is the limiting factor in heat transport, allowing the heat pipe to transport only 84.5 W.

Chapter 4

Previous Work

4.1 Introduction

Since the heat pipe's re-invention by M. Grover in 1963, the acceptance and use of heat pipes has grown. Besides the specific applications mentioned earlier in this work, vast amounts of scientific research have been carried out in an effort to better understand the fundamental principles of the heat pipe. Investigations into the performance characteristics of heat pipes such as heat transport capabilities[20,21], compatibility and reliability of heat pipe materials[22], and operating limits of heat pipes[23] have been undertaken.

Even though general heat pipe concepts are straightforward, one finds that the transport phenomena taking place within a heat pipe are rather complicated. Modelling heat pipe systems requires a solid understanding of the two-phase flows that occur during operation. The study of heat pipes incorporates the sciences of heat transfer, fluid dynamics, materials and thermodynamics[6]. All of these disciplines must be understood to develop accurate mathematical models of a heat pipe system.

Work has been done to mathematically model the operation of heat pipes through numerical analysis by Faghri and Parvani[24] and Faghri and Chen[25]. These works describe the operation of the heat pipe, predicting the pressure drop and velocity variations within the pipe. In other work by Faghri, concentric annular thermosyphons as well as heat pipes are considered wherein fundamental analysis of vapour flow, capillary limit and heat transfer characteristics is done[26,27,28]. Faghri's main concern is with the numerical analysis of the fundamental transport phenomena taking place during heat pipe operation. One of his most recent publications dealt with the mathematical modelling of heat pipes during start-up[29].

The operating limits of a heat pipe are a concern in any application. Factors such as capillary limit, sonic limit, entrainment limit and boiling limit must be considered in any heat

pipe design. Ivanovsky et al., investigated the capillary limit in sodium heat pipes wherein they discuss the optimization of geometric parameters for improving capillary limit[30]. Fukano et al.[31], determined the operating limits of a copper-methanol two phase thermosyphon by assessing the effects of tube diameter, system pressure and amount of working fluid on the periodic oscillations arising from the flooding limits. Dobran analytically investigated dry-out and flooding of a two-phase thermosyphon based on a lumped parameter description of the system[32]. Dobran also investigated the suppression of the sonic limit in high temperature heat pipes through optimization of heat pipe geometry and selection of working fluid[33]. He found that high rates of heat transfer can be achieved with large vapour flow cross-sectional areas, small lengths of the evaporator and adiabatic regions, and normal-to-the-main-flow liquid evaporation in the evaporator.

Studies on the effect of inclination angle of the heat pipe have also been done. Typical questions that need to be answered might be as follows. What are the influences of inclination angle on heat transfer performance? What is the relationship between inclination angle and the amount of working fluid required? A study by Negishi and Sawada[34] revealed that it is necessary to fill between 40 and 45% of the evaporator inner volume with ethanol as the working fluid in a thermosyphon with an inclination angle of no less than 5 degrees to obtain a steady high heat transfer rate.

4.2 Heat Pipes in the Metallurgical Industry

There has been work done regarding metallurgical investigations of heat pipe technology but only to a very limited extent. Most of the heat pipe work reported in the literature related to metals casting, with a view towards controlling solidification rates. This can be done by strategically locating heat pipes in a casting assembly and using pressure control and temperature control to regulate the amount of heat that is removed from the casting. Bahadori[35] published a paper on this subject in 1970. The latent heat of fusion of the liquid metals provides the heat required for evaporation in a gas-controlled heat pipe. The heat of fusion can be conducted away at different rates by the heat pipe depending on the rate of cooling desired. It is well understood that cooling rates have a profound effect on microstructure, thereby the final properties of the casting.

Work has also been conducted on heat pipe controlled solidification in Czechoslovakia. Zuzanak[36] uses a simple numerical model to examine the effect of heat pipes on casting solidification and defines fundamental conditions to control the entire process. In a more involved work Zuzak et al., investigate actively chilling steel in a sand mold casting system[37] using a sodium heat pipe. Three parts were cast, a plate, a cylinder and a gear wheel, and numerous experiments were conducted. The goal of the work was to attain practical applicability of the acquired knowledge to foundry technology.

Wells et al., have developed a computer program aimed at studying the effects of a heat pipe on the temperature distribution throughout a solidifying alloy[38]. A computer program was generated that could be used to predict the transient, two dimensional temperature distribution in a solidifying alloy of non-eutectic composition with temperature dependent thermal properties. When using a heat pipe in conjunction with a conventional chilling system, the model predicted that the rates of solidification for all locations across the casting could be increased.

Recently, at McGill University, work concerning metallurgical heat pipe applications was undertaken. H.C. Choi completed his Ph.D entitled "Techniques for the Continuous Measurement of Melt Temperature" wherein two approaches to the problem of continuous temperature measurement in steel were discussed[39]. The first involved a numerical technique using inverse heat conduction. The second investigated the use of a self cooling heat pipe sleeve to protect the thermocouple from the molten steel. Choi's heat pipe investigations comprised a variety of tests with different materials. In his most conclusive test a shell of copper matte was frozen onto a stainless steel heat pipe in conditions that had previously dissolved a plain stainless steel pipe. He thus proved the concept of continuous temperature measurement by demonstrating that the shell formed by the cooled heat pipe could protect the pipe from the otherwise damaging environment.

The author has also worked with fellow researchers on flow visualization in a transparent thermosyphon. Valuable insight was gained in understanding the flow phenomena in a thermosyphon heat pipe. Boiling and condensation phenomena were observed and parameters such as condensate flow velocities, condensate film thickness and vapour velocities were calculated and summarized in an internal report[40]. The transparent thermosyphon work laid the foundation for much of the work which follows in this thesis.

Chapter 5

The Transparent Heat Pipe

5.1 Introduction

This section describes work that was conducted with a Pyrex tube thermosyphon heat pipe, that contained Freon 11 as the working fluid. The heat pipe was of typical design, and was operated in the vertical position, making full use of gravity to return the working fluid back to the evaporator.

The previous work with heat pipes conducted at McGill had been successful, yet still the inner-workings of a heat pipe were somewhat of a mystery. It was felt that a transparent heat pipe could shed light on the fluid flow phenomena inside the pipe and be used as a working model to demonstrate the principles of a heat pipe to others. It was also felt that the transparent thermosyphon work conducted at low temperatures could be used to determine the most suitable heat transfer models to use, i.e. whether the condensation is film or dropwise or whether the regime is laminar or turbulent. Once calculations were made they could be verified visually. Although the verifications would not be rigorous, i.e. no physical measurements of film thickness or vapour velocities were taken, they would determine whether calculations were reasonable or not, i.e. a film thickness of 3 mm versus .1 mm could be discerned by the naked eye. The calculations and modelling would improve our understanding of the fluid flow and heat transfer phenomena within the pipe, so that high temperature heat pipes could be better engineered. It was felt to be a worthwhile endeavour, since with low temperature systems the operating conditions are very mild making experimental design and construction relatively quick and easy.

5.2 Design and Construction

Originally, the pipe was to be constructed from plexi-glass due to its transparency and relative toughness as compared to glass. A working fluid with a low operating temperature was

then required in order to be compatible with the low melting point of plexiglass. Several fluids were considered and are outlined in the following table:

Table 5.0 : Low Temperature Working Fluids and Their Physical Properties

Fluid	Chemical Formula	Boil. Temp. (°C)	Melt. Temp. (°C)	Latent Heat (kJ/kg)	Pressure Vapour (bar)	Useful Range (°C)
Refrig. 11	$CFCl_3$	23.9	-101	183.4	1.1341	-40-120
Refrig. 12	CF_2Cl_3	-29.6	-114	-	6.8491	-
Acetone	C_3H_6O	56.3	-94.5	552	0.0318	0-120
Methanol	CH_4O	64.7	-97.5	1165	0.1860	10-130
Pentane	C_5H_{12}		-159	367	-	-
Ethanol	C_2H_6O		-143	788	-	0-130

note: thermophysical properties taken at 27 °C and/or 1 bar

The factors which must be considered when choosing a working substance are as follows[41]:

- Compatibility with wick and wick material
- Good thermal stability
- Wettability of wick and wall materials
- Vapour pressures not too high or too low over the operating temperature range
- high latent heat of vaporization
- high thermal conductivity
- low liquid and vapour viscosities
- high surface tension

These are the scientific factors which must be considered and optimized, but in the real world we must always yield to cost and availability as they most often govern the materials we

use. Refrigerant 11 was a good candidate from a scientific perspective as it adhered rather well to the aforementioned criteria. It was readily available and it was non-flammable.

As was previously mentioned, the original heat pipe thermosyphon, or simply thermosyphon, was to be made of plexi-glass, but problems were encountered when the plexi-glass was heated in a hot water bath. The temperature gradients and the pressures developed in the pipe would cause stress fractures. A number of tubes were tested with the final plexi-glass tube having a wall thickness of 1/8 inch, which still was not adequate as it eventually cracked as well. It was decided to switch to pyrex glass, an extremely temperature resistant material that could withstand fairly large pressures. Although it was originally hoped that glass could be avoided due to the risk of shattering while in operation, in the end it was the only option that time permitted.

5.3 Experimental Procedure

The tube which was to be the thermosyphon container had the following specifications:

- Material: Standard Corning Pyrex Glass
- Outside Diameter: 29 mm
- Inside Diameter: 26 mm
- Total Length : 860 mm

Thermocouples were situated along the length of the thermosyphon, pressed to the outside of the pipe by a layer of styrofoam insulation held by a plastic ti-wrap. The thermocouples were attached to wires which led to the data acquisition system. A pressure transducer was also connected to a *Swagelok* t-connection consisting of two Nupro valves; one leading to the pressure transducer and the other leading to a vacuum pump. The pressure transducer was connected to a power supply and to the data acquisition system. The pressure transducer was an *Omega* type which employs a strain gauge situated in front of a pressure sensitive diaphragm. When the diaphragm is compressed it alters the resistance in the wheatstone bridge arrangement within the strain gauge correspondingly with the pressure causing the displacement of the diaphragm. This reading is calibrated according to a simple equation in the data acquisition system. The experimental set-up is shown in the following figure.

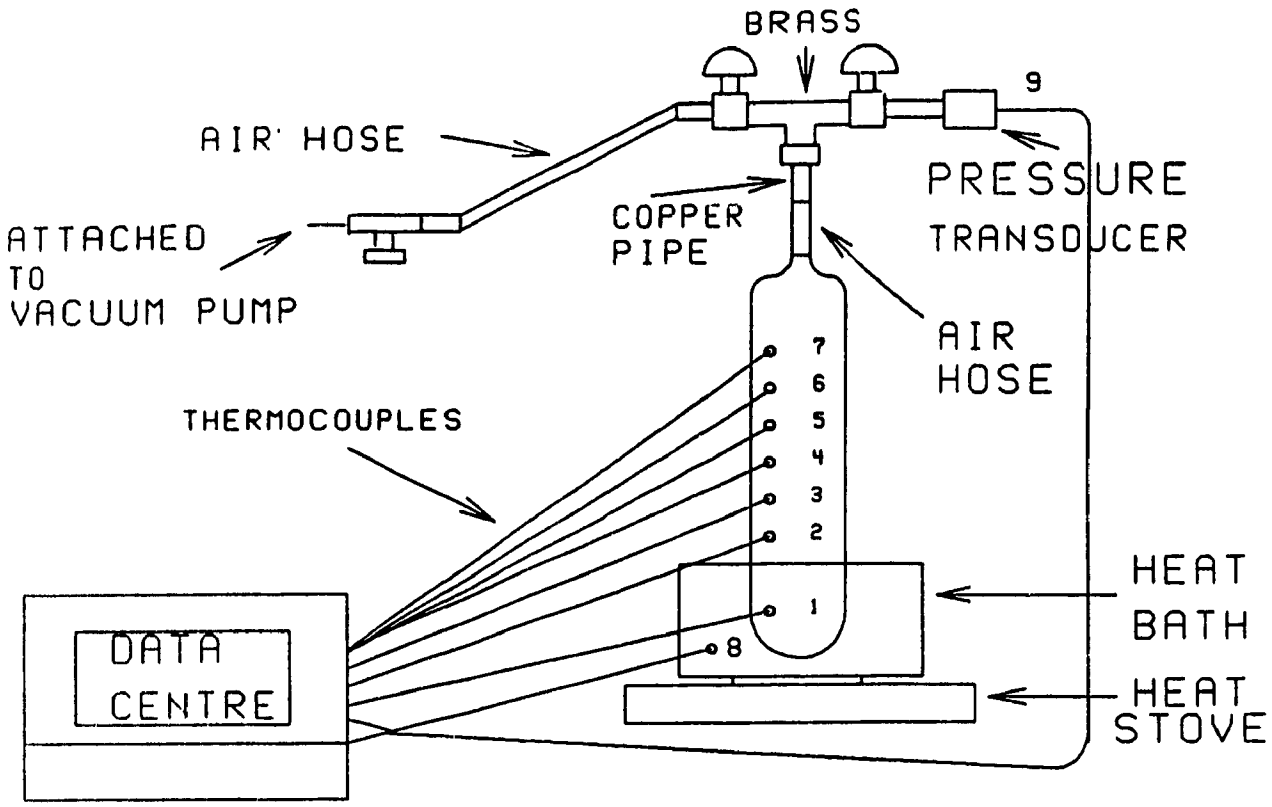

Figure 5.0 : Schematic of Experimental Set-up of Refrigerant 11 Thermosyphon

Glass blowing was used to seal the pipe on the evaporator side and to create a nipple on the condenser side. Plastic tubing was connected to the nipple at one end and to copper tubing, leading into the tee, at the other end.

The following lists the experimental apparatus that was required to perform the investigations:

- one heating stove
- one metallic heating bath
- one pyrex glass tube
- eight E-type thermocouples
- 70 ml Freon 11 (CCl_3F)
- one varying voltage transformer
- one vacuum pump
- one thermometer

- one omega pressure transducer
- two nupro pressure valves
- swagelok tee-assembly
- Data acquisition system consisting of a voltmeter and Hewlitt Packard computer

A typical experiment involved first charging the pipe with Freon so that it surpasses the evaporator level by about 10%. Since Freon is lost when the pipe is evacuated this was considered to be 100% of the evaporator volume, which is standard procedure when filling a heat pipe[41]. The data acquisition system was then turned on to begin recording results. The heat pipe was evacuated to removes excess air entrapped in the system to a pressure of approximately 0.1 atm with a vacuum pump. In actuality, the system was purged and the pressure reading indicated the pressure of freon in the pipe at room temperature. The heating stove and controller were then switched on and allowed to heat the water for a few hours until the desired amount of data was collected. Safety glasses were used at all times for precaution against shattering of the pyrex glass. The pressure that was maintained during experimentation was in the vicinity of one atmosphere so that no net forces were imposed on the pipe.

5.4 Results and Discussion

Video tape was made of the transparent thermosyphon during its operation which proved to be extremely useful in explaining the principles of a heat pipe to those unfamiliar with the topic. Showing the transparent thermosyphon during operation to those who would later fund the work in co-operation with McGill on the Kidd Creek Lance project, in the authors opinion, was a turning point in getting the project under way. It served to illuminate discussions on the topic of heat pipes so that a better understanding could be had by all. Besides its use in illustrating to others the principles of heat pipes, it shed light on the fluid flow phenomena in the pipe and dispelled any scepticism the author had regarding heat pipes. Thus, the first objective in building a transparent thermosyphon was met.

The second objective was to determine the most appropriate heat transfer model to use in calculating the operating parameters of the heat pipe, i.e. heat fluxes, vapour velocities, fluid velocities. It was evident that a laminar film of significant thickness was continually running

down the walls of the pipe, growing thicker as it reached the bottom. From our visual observations, it was decided that the most appropriate heat transfer analysis to use was that of laminar film condensation originated by Nusselt. Some of the details of the analysis are discussed in "Fundamentals of Heat and Mass Transfer" by Incropera and De Witt[19] in the section entitled "Boiling and Condensation". The heat transfer calculations describing the transparent thermosyphon which includes the laminar film condensation analysis are presented in Appendix B. The results of those calculations will be discussed.

5.5 Heat Transfer Model of Transparent Thermosyphon

The four phenomena of heat transfer considered in this analysis are straight forward and can be found in any text written on the subject of heat transfer. The books referred to in this work were "Fundamentals of Heat and Mass Transfer" by Incropera and De Witt, previously mentioned, and "Heat Transfer" by J.P. Holman[42]. The four mechanisms are Natural Convection and Radiation from the outer surface of the pipe to the atmosphere, Conduction through the walls of the pipe and laminar film condensation within the pipe.

The aim of the analysis was to determine the heat flux dissipated by the pipe, the vapour velocity and liquid film velocity of the working substance within the pipe and the film thickness. Knowing these parameter and how to calculate them would allow proper design of future high temperature thermosyphons.

Typical values obtained were:

Heat dissipated by pipe, $q = 100.7$ W

Vapour velocity, $v_{vapour} = 0.176$ m/s

Condensate velocity, $v_{cond} = 0.07$ m/s

Chapter 6

The Laboratory Scale Heat Pipe Injection Lance

6.1 Introduction

Upon completion of the transparent heat pipe experiments, a laboratory scale heat pipe injection lance was constructed. Essentially. the lance was an annular heat pipe or thermosyphon (no wick was employed). It consisted of a pipe within a pipe, with plates welded at the ends to seal it. The following figure is a schematic of the laboratory scale heat pipe injection lance (LSHPIL) showing dimensions and materials.

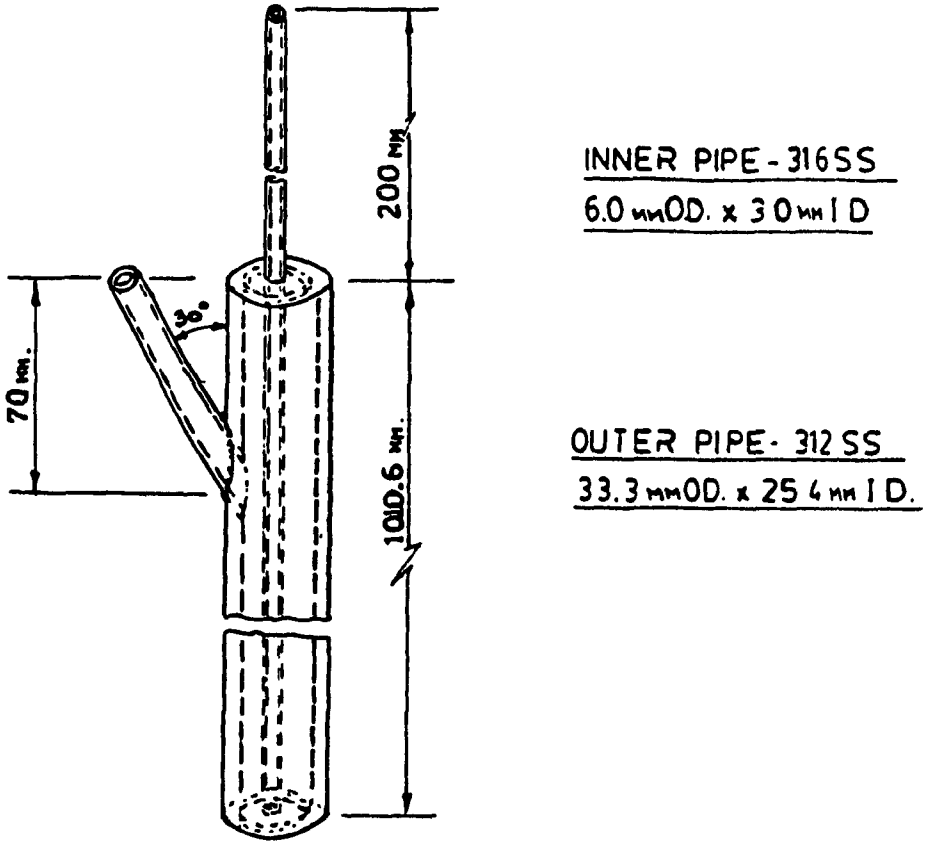

Figure 6.0 : Dimensions and Materials of Laboratory Scale Heat Pipe Injection Lance

The LSHPIL was tested at McGill University's Metallurgical Furnace Laboratory and at the Noranda Technology Center (NTC). The tests at McGill were run in a 30 kW, 10 000 Hz induction furnace. At Noranda, the experiments were conducted in an electric resistance furnace capable of reaching temperatures of 1300 °C.

A number of trial runs were first attempted at McGill to condition the LSHPIL. When charging the sodium, impurities may find their way into the pipe in addition to the impurities associated with commercial grade sodium. The conditioning process involved heating the LSHPIL to red hot temperatures for short periods of time so that the sodium in the annulus could vaporize. The lance was then allowed to cool until it was warm to the touch. The lance was then re-evacuated to remove any impurities which may have been ejected from the sodium and the container. The procedure was repeated several times until a vacuum below .01 atm could be maintained after the heating and cooling down procedures.

The experiments conducted at the NTC involved laboratory scale simulations of some of the expected conditions in the Kidd Creek C-furnace. Radiation atmospheres comparable to Kidd Creek's C-furnace were tested with air injection through the center of the lance and external cooling by a fan on the outside of the lance, simulating plant conditions. Unfortunately, a sulphidizing atmosphere like that of the C-furnace could not be arranged.

The section which follows is arranged into two parts. The making of the LSHPIL at McGill and the testing of it at Noranda. The results of the Noranda tests are then discussed.

6.2 The Making of the LSHPIL

The three basic components of a heat pipe are the working substance, the container and the wick. In our case, a thermosyphon heat pipe was decided upon as the lance would operate vertically so that gravity could be fully exploited. This being the case, no wick was required. The working substance was chosen based on the criteria listed in chapter 5. The following table lists some of the more common working substances.

Table 6.0 : Common Working Substances and Operating Ranges

Medium	Melting Point (°C)	Normal Boiling Point (°C)	Useful Range (°C)
Helium	-272	-269	-271 to -269
Nitrogen	-210	-196	-203 to -160
Ammonia	-78	-33	-60 to 100
Freon 11	-111	24	-40 to 120
Acetone	-95	57	0 to 120
Methanol	-98	64	10 to 130
Ethanol	-112	78	0 to 130
Water	0	100	30 to 200
Toluene	-95	110	50 to 200
Thermex	12	257	150 to 395
Mercury	-39	361	250 to 650
Cesium	29	670	450 to 900
Potassium	62	774	500 to 1000
Sodium	98	892	600 to 1200
Lithium	179	1340	1000 to 1800
Silver	960	2212	1800 to 2300

Possible candidates for the working substance required by the LSHPIL were potassium, sodium or lithium. It was felt that potassium would have too high of a vapour pressure at the operating temperatures of the C-furnace ($\sim$ 1200 °C) and that lithium's would be too low. Sodium, the least expensive of the three metals, was ideal since its operating range seems to coincide very well with that of the C-furnace. It has good thermal stability and a high latent heat of vaporization. The viscosities of the liquid and vapour are low and the surface tension is high. As well, the thermal conductivity of sodium is very good. It appeared that sodium was perfect for our application.

The next step was to choose the container material. Taking into account the elevated temperatures the lance would be operating at, metals such as aluminum and copper could not

be considered. Although nickel has a high melting point, its compatibility with a copper/sulphur environment is poor. Nickel is very soluble in copper. Nickel is also not available in a wide variety of shapes and sizes. More exotic metals such as titanium, tantalum and niobium could not be considered due to their very high costs. In industry, cost is the bottom line. The use of such metals could not be justified from an economic perspective since commercialization of a heat pipe lance is the end goal.

Stainless steel comes in a wide variety of forms and sizes. It is readily available and reasonably priced. It is the material used for the Mitsubishi lances and according to literature, it is compatible with sodium[42]. Its compatibility with sodium is addressed in the S.E.M. section of this work. Stainless steel is not completely compatible with the environment of the Kidd Creek furnaces, as is well known by the Mitsubishi process, but that is as a normal lance, not as a heat pipe lance. Stainless steel was the best choice for the pipe container once all the factors were considered.

The lance was machined and then welded. The welding of the lance was not a simple task. Great care must be taken in ensuring not only a strong weld but a leak proof weld; one that ensures the container can support a vacuum.

6.3 Cleaning and Filling of the pipe

Once all the machining had taken place, the heat pipe's components were thoroughly cleaned to minimize any impurities in the system. The cleaning procedure for stainless steel used was the one outlined in Chi[6] and is as follows:

1. Clean in 1,1,1-trichloroethane and periodically agitate and brush with bristle brush.
2. Rinse with cold trichloroethane and force dry with air.
3. Immerse in a passivating solution of sodium dichromate (7.5-30 kg/m^3) and nitric acid (15-30% by volume) at room temperature for 30 minutes to 2 hours followed by a tap water rinse.
4. Thoroughly dry with forced air.
5. Rinse with anhydrous isopropyl alcohol.
6. Insert wick, rinse with isopropyl alcohol, and dry as in step 4.

Once cleaning was finished, the pipe was welded. In some situations where it is feasible, welding should take place first. The pipe can then be cleaned as a sealed vessel, the only aperatures remaining open being the sodium feed holes. The pipe can then be temporarily sealed at the feeding locations and agitated with the cleaning fluids inside the pipe, instead of immersing the entire pipe in a bath. In this way, no fluxes or soot resulting from welding find their way into the pipe. It also makes the cleaning process easier and less wasteful since only the inside of the pipe truly needs to be cleaned.

The final stage before the pipe is sealed is the filling stage. Many difficulties were encountered when attempting to feed sodium into the annulus of the heat pipe. Sodium is a very reactive element which has a high affinity for oxygen. In liquid form, it will ignite when in contact with oxygen and will explode if contacted by water. Great care was taken in handling sodium. In solid form, it can be handled with gloves given one has an understanding of its hazards. A number of methods for charging sodium into the heat pipe were contemplated. Liquid filling was attempted in the past but met with problems. It was attempted again in this work and once again was not met with great success. When charging the sodium in liquid form great care must be taken in ensuring that an inert atmosphere prevails. This implies a fairly sophisticated charging is required since uniform heating and the absence of both oxygen and water is necessary. It was found that the simplest and safest way to charge sodium was in solid form. It is much safer since the activity of the species greatly decreases when in the solid form. The formation of an oxide layer protects the sodium from rapid oxidation and reduces its reactivity. The solid form of sodium can be easily cut into pieces with a knife, as sodium is soft, and then it can be handled with gloves.

The sodium used in the LSHPIL was commercial grade. It was cut into pieces in an inert atmosphere, i.e. under a positive pressure of nitrogen, in a closed environment where it could be manipulated. In the same closed environment it was charged into the feed tube of the heat pipe. Once the pipe was filled, it was closed using *Swagelok* fittings and valves. The heat pipe was then evacuated to remove any air present in the annulus to prevent further oxidation of sodium. It is very difficult to avoid oxidation of the sodium. The oxide is relatively inert and does not affect the operation of the heat pipe. However, it does react with water to form hydroxide so it should be kept at a minimum. The following picture shows knife-cut sodium

inside a sealed plastic *Ziploc* bag.

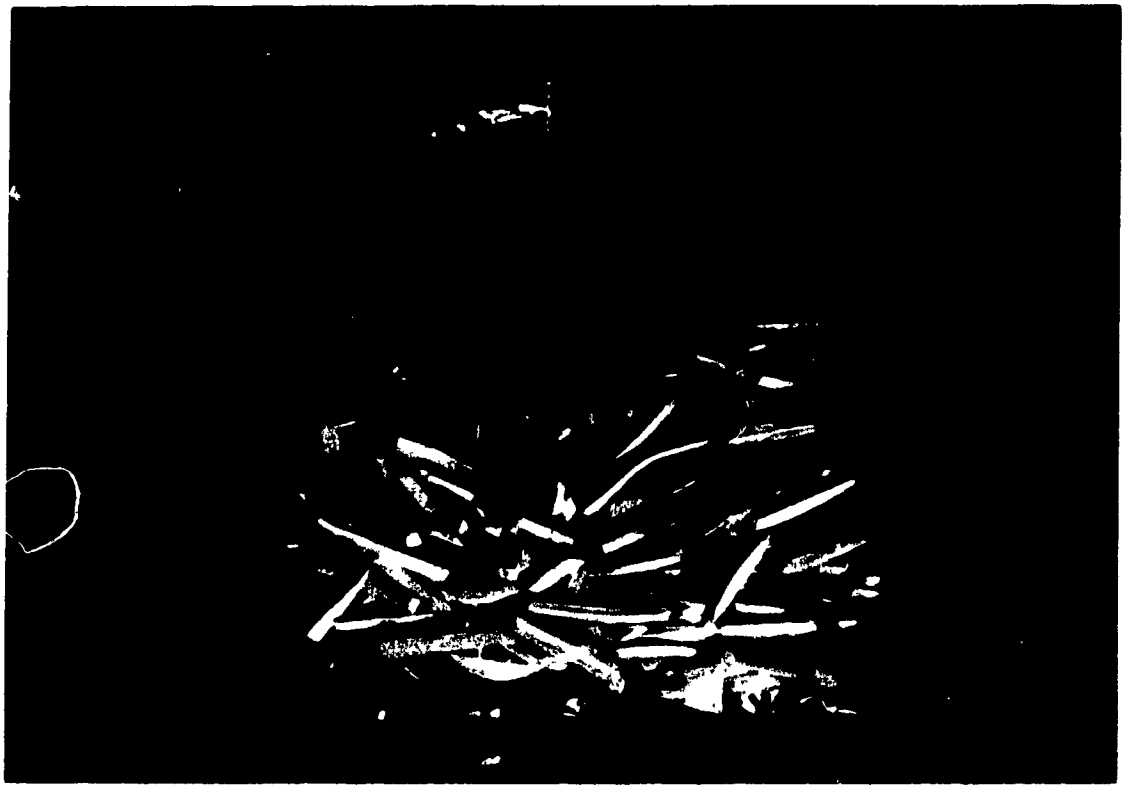

Figure 6.0 : Sodium Cut by a Knife

6.3 Experimental

Once the pipe had been closed and evacuated, it was ready to be heated. As was mentioned earlier, a number of conditioning tests were run in an induction furnace to remove impurities and prepare the LSHPIL for operation. The LSHPIL was then brought to the Noranda Technology Center for simulation experiments in an electrical resistance furnace. The following photograph shows the set up at the NTC:

Figure 6.1 : LSHPIL - Kidd Creek Simulation Experiments

The set-up consisted of:

- 1 resistance furnace capable of temperatures exceeding 1300 °C
- 1 Lab Scale Heat Pipe Injection Lance (LSHPIL)
- 3 thermocouples, T/C #1, T/C #2, and T/C #3 were situated 35, 50 and 76 cm from the bottom tip of the lance, respectively
- 1 pressure transducer
- 1 industrial size fan
- 1 air hose capable of a 90 Nl/min air injection
- assembly to hold LSHPIL in place
- 2 voltmeters

The independent parameters manipulated were the furnace temperature, the air flowrate through the lance and the speed of the fan blowing air on the outside of the pipe. The dependent parameters were the pressure, wall temperatures and condenser lengths. The evaporator section was that which was submerged into the furnace atmosphere. Heat supplied by the furnace served to vary the pressure inside the lance, the outer wall temperature of the lance and the condenser length. The condenser section was that section which was outside the furnace and was glowing "red hot". The inert gas section was near the top of the lance and had the same appearance as it did at room temperature.

6.5 Results and Discussion

The tables which follow summarize the tests that were run on July 3, 1991 at the NTC. In both tables, the LSHPIL was 30.5 cm inside the electric-resistance furnace. The conditions for both sets of experiments were the same with the exception of a cooling fan which was used for experiments 10 to 18.

Table 6.1 : LSHPIL - Kidd Creek Simulation Experiments, No External Cooling Fan

Furnace Set Point Temperature (°C)	1150			1200			1250		
Experiment Number	1	2	3	4	5	6	7	8	9
Gas Flowrate (Nl/min)	0	50	90	0	50	90	0	50	90
Pressure (atm)	0.97	--	0.54	1.30	0.97	0.74	1.56	1.30	1.03
Wall Temp.(°C)									
T/C #1	788	747	725	805	780	766	832	824	790
T/C #2	775	732	716	795	767	764	810	802	780
T/C #3	296	193	248	48	460	377	687	610	677
Approx. Condenser Length (cm)	34	33	34	36	36	30	43	38	40

Table 6.2 : LSHPIL - Kidd Creek Simulation Experiments, External Cooling Fan

Furnace Set Point Temperature (°C)	1150			1200			1250		
Experiment Number	10	11	12	13	14	15	16	17	18
Gas Flowrate (Nl/min)	0	50	90	0	50	90	0	50	90
Pressure (atm)	0.37	---	---	0.74	0.57	0.58	0.80	0.70	0.66
Wall Temp.(°C)									
T/C #1	660	659	635	718	708	703	752	736	737
T/C #2	580	587	536	617	596	534	640	616	618
T/C #3	57	41	31	214	265	279	495	450	404
Approx. Condenser Length (cm)	--	34	20	29	25	20	34	30	30

Several useful conclusions may be drawn from these results:

1. The condenser/evaporator length ratio varied between 0.6 and 1.4 with a value of 1 for experiment 1, the standard.
2. The outer condenser region could be reduced by as much as 41% when a cooling fan was introduced.
3. The pressure inside the LSHPIL dropped to 42% of its original value when air was both injected through the middle and blown on the outside of the lance.
4. The inert gas/vapour interface is not flat as originally suspected.
5. There exists a sharp decrease in temperature towards the end of the condenser region over a small distance.

The above conclusions are very important from a plant application point of view. The discovery of a one to one ratio of evaporator to condenser for the standard test (experiment 1) was essential in determining the pilot scale lance length requirements. By knowing the required depth of insertion into the C-furnace for the pilot scale heat pipe lance (the evaporator length), the total required length of the lance could be determined. It can be seen that the ratio of the condenser length to the evaporator length increases as the temperature of the furnace increases. This results from the increasing heat flux into the evaporator causing a need for an increased condenser area to dissipate the heat. This translates into an increase in length since the circumferences of the evaporator and condenser are the same.

The ability to drop the external condenser by as much as 41% with a cooling fan (experiment 12 vs 3), if required, is reassuring from an operations point of view. If during operation the condenser rises to an undesirable or unsafe height, it could be lowered with an external, air cooling device. Safety for the operators and the workers on the floor is always a concern.

It was interesting to learn that the pressure in the lance could drastically be reduced by the simultaneous external and internal cooling of air. It was originally believed that the pipe could be cooled down in this way, but not by such a significant amount. What led to this discovery was the abnormal behaviour of the condenser. The norm being in a way that a straight, flat interface would behave, i.e. moving up and down in accordance with the pressure

changes in the LSHPIL. The condenser that was perceived on the outside did not always fluctuate with the pressure changes. The injection air down the middle of the pipe would drop the pressure but not the visible external condenser (experiments 1 and 3, 4 and 5, 17 and 18). This implies that two condensers exist, one on the inside pipe and one on the outside pipe. When air is blown on the outside pipe the condenser visually drops as the condenser cools down, causing the red hot glow to disappear. When air is blown through the middle, the outer condenser does not necessarily change but the inner one does, indicated by the pressure drop, i.e. less vapour pressure implies less condensation, which must be taking place on the inner wall if no changes occur on the outside. Thus an annular thermosyphon (the LSHPIL) will not necessarily have a flat interface; it could be slanted under certain operating conditions.

The fact that the temperature rapidly decreases over a short distance above the visible condenser results from the (inert gas)/(vapour) interface that exists in heat pipes. Any non-condensible gases that have found their way into the LSHPIL (imperfect vacuum, impurities from sodium) are pushed to the top of the chamber by the rising vapour. A diffusion layer exists as the interface between the rising vapour and the inert gas is not completely discrete, i.e. mixed. The temperature drop which takes place over the short distance reflects this. In Figure 6.2, which follows, the schematic illustrates how the flow of the rising vapour causes the non-condensible gases to be suspended at the top of the container. Only a diffusive layer exists where the inert gas is driven downwards by diffusion and buoyancy forces. Eventually, they are forced back up by the rising vapour molecules. Note that the schematic does not show a perfectly even distribution of molecules, as it should be.

More tests were run at NTC two days later on July 5, and similar results were found. Photographs were taken to illustrate the change in condenser with changes in conditions. The five conclusions drawn previously are illustrated in Figures 6.3 through to 6.9, on the pages which follow.

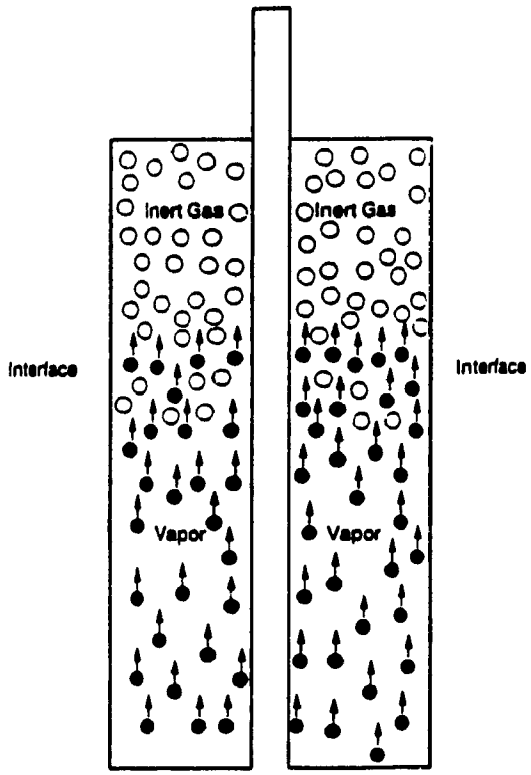

Figure 6.2 : Illustration of Diffusive Layer of the Inert Gas/ Vapour Interface and Inert Gas Hold-Up

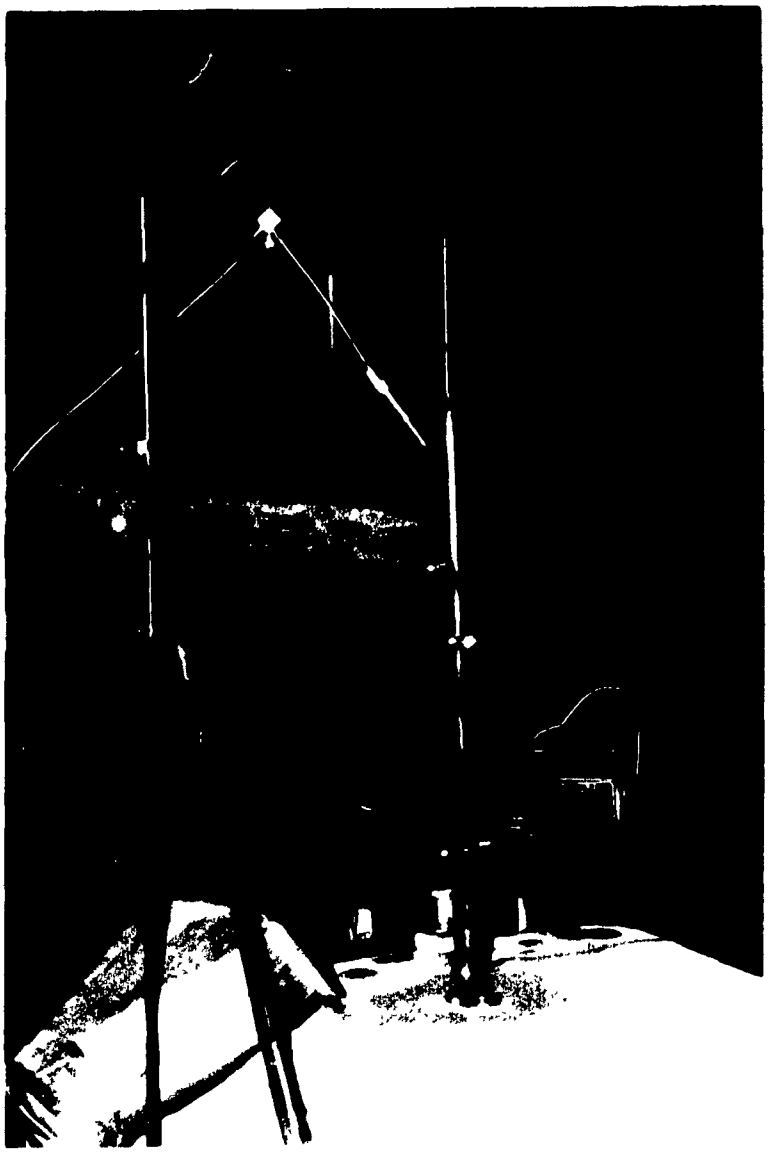

Figure 6.3 : LSHPIL Tests at NTC: Furnace Temperature = 1150 °C, Gas Flowrate = 0 l/min No Fan, Pressure = 0.8 atm, Condenser length = 40 cm

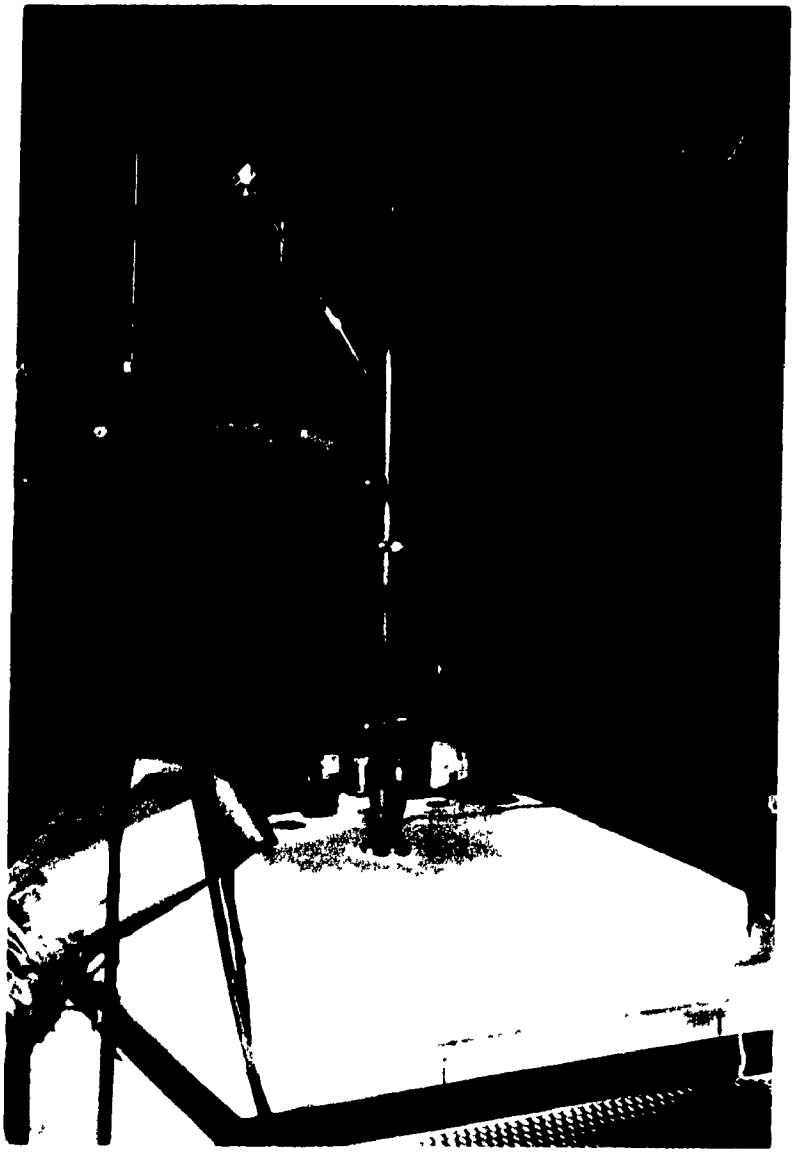

Figure 6.4 : LSHPIL Tests at NTC: Furnace Temperature = 1200 °C, Gas Flowrate = 0 l/min, No Fan, Pressure = 0.97 atm, Condenser length = 48 cm

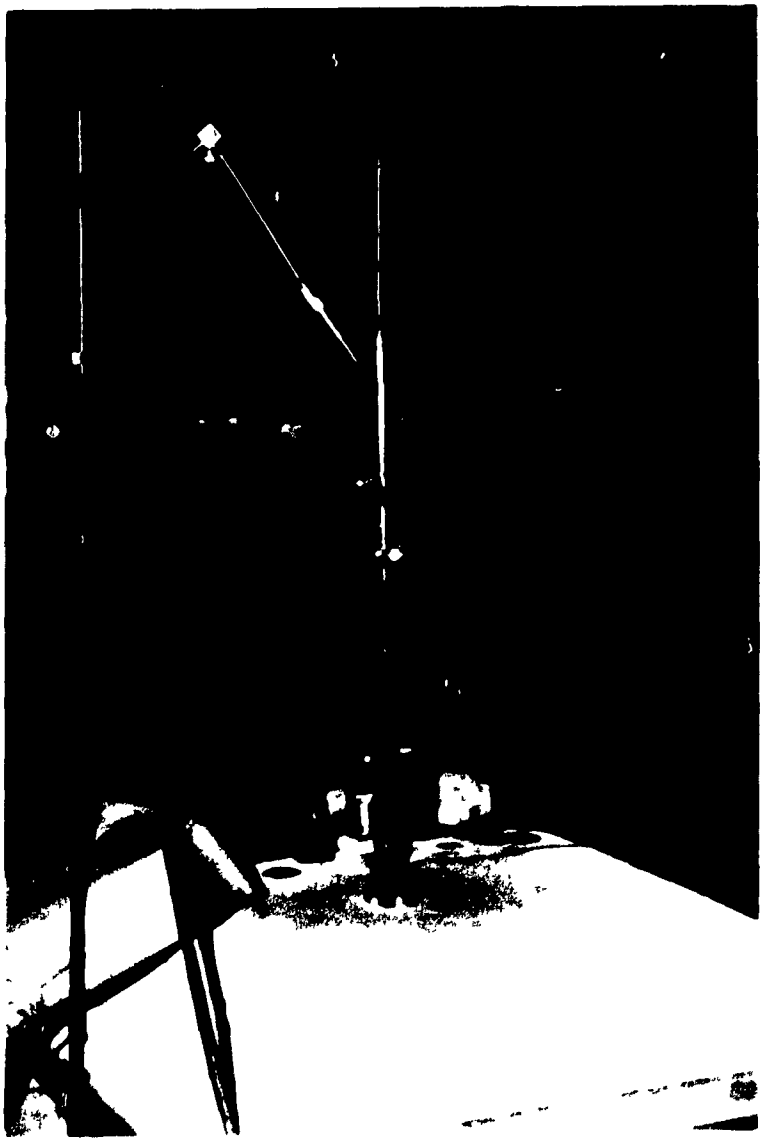

Figure 6.5 : LSHPIL Tests at NTC: Furnace Temperature = 1200 °C, Gas Flowrate = 50 l/min, No Fan, Pressure = 0.88 atm, Condenser length = 43 cm

Figure 6.6 : LSHPIL Tests at NTC: Furnace Temperature = 1200 °C, Gas Flowrate = 90 l/min, No Fan, Pressure = 0.73 atm, Condenser length = 41 cm

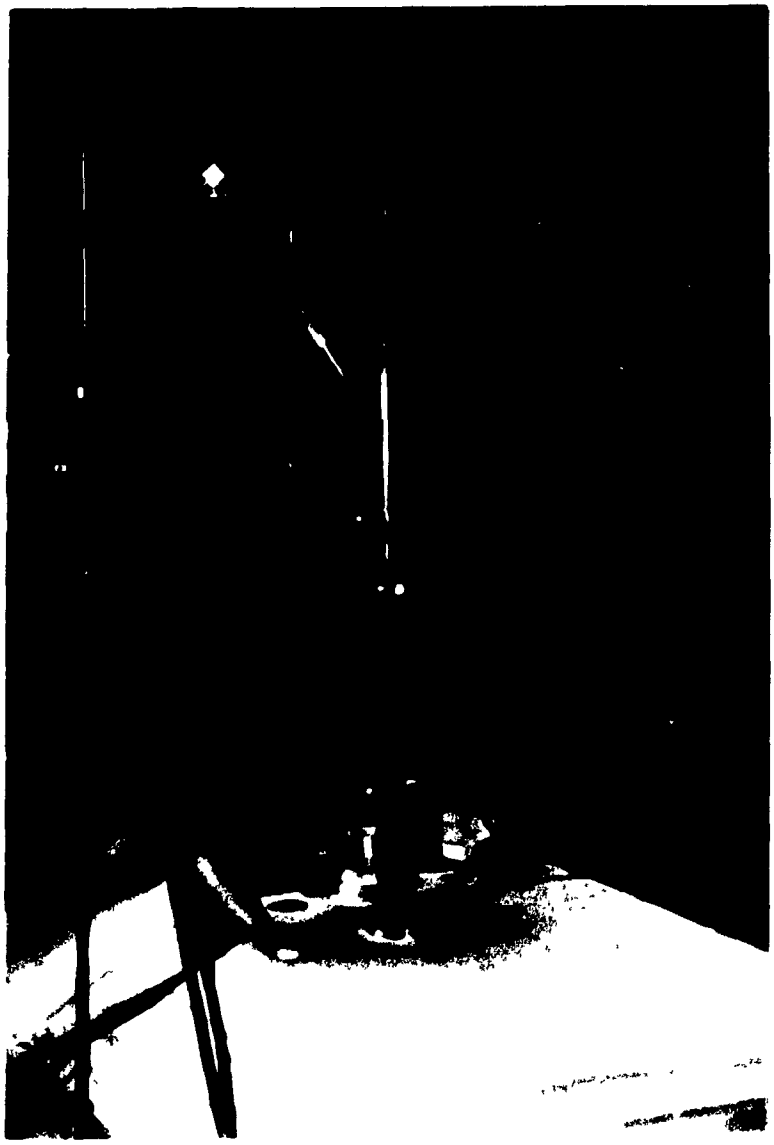

Figure 6.7 : LSHPIL Tests at NTC: Furnace Temperature = 1200 °C, Gas Flowrate = 90 l/min, Fan, Pressure = 0.62 atm, Condenser length = 23 cm

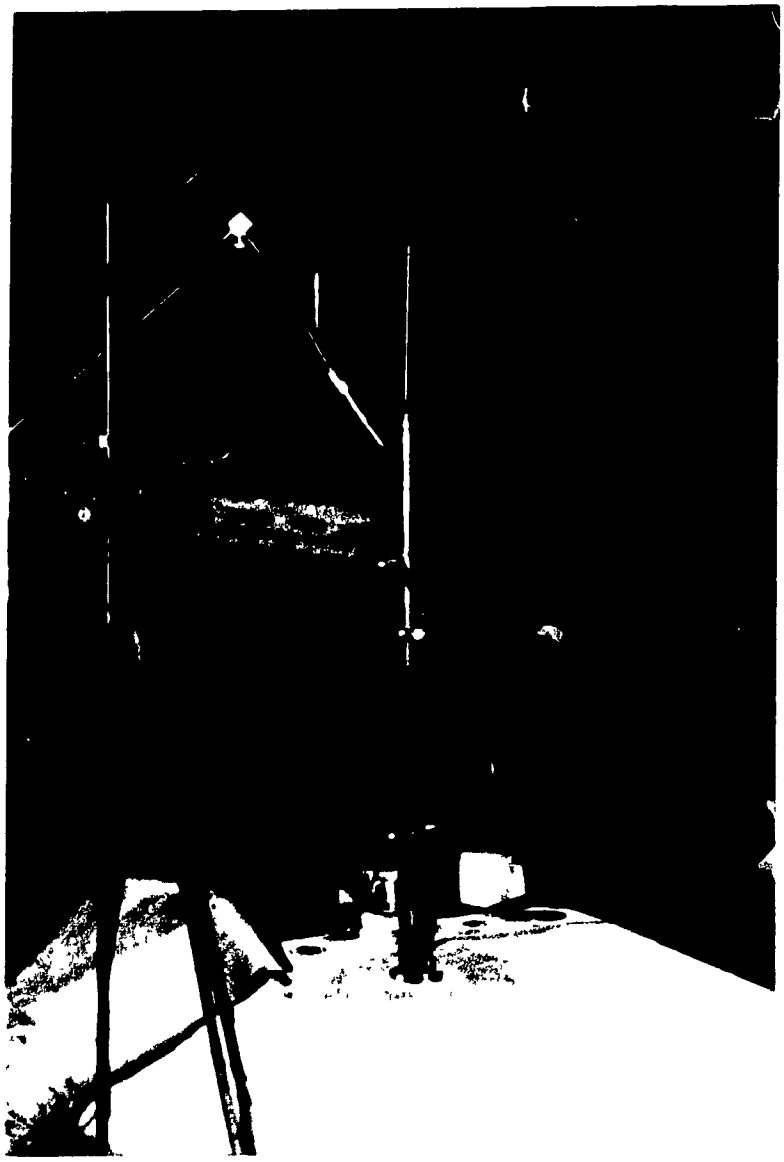

Figure 6.8 : LSHPIL Tests at NTC: Furnace Temperature = 1200 °C, Gas Flowrate = 50 l/min, Fan, Pressure = 0.65 atm, Condenser length = 24 cm

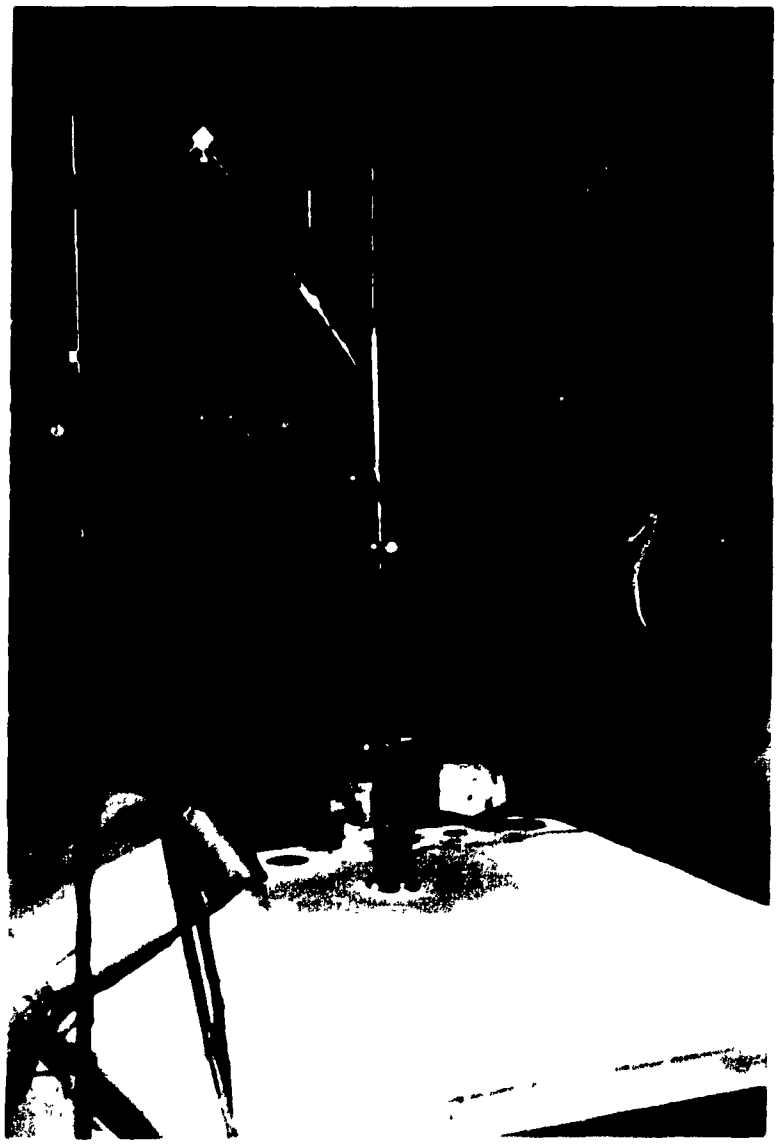

Figure 6.9 : LSHPIL Tests at NTC: Furnace Temperature = 1200 °C, Gas Flowrate = 0 l/min, Fan, Pressure = 0.68 atm, Condenser length = 30 cm

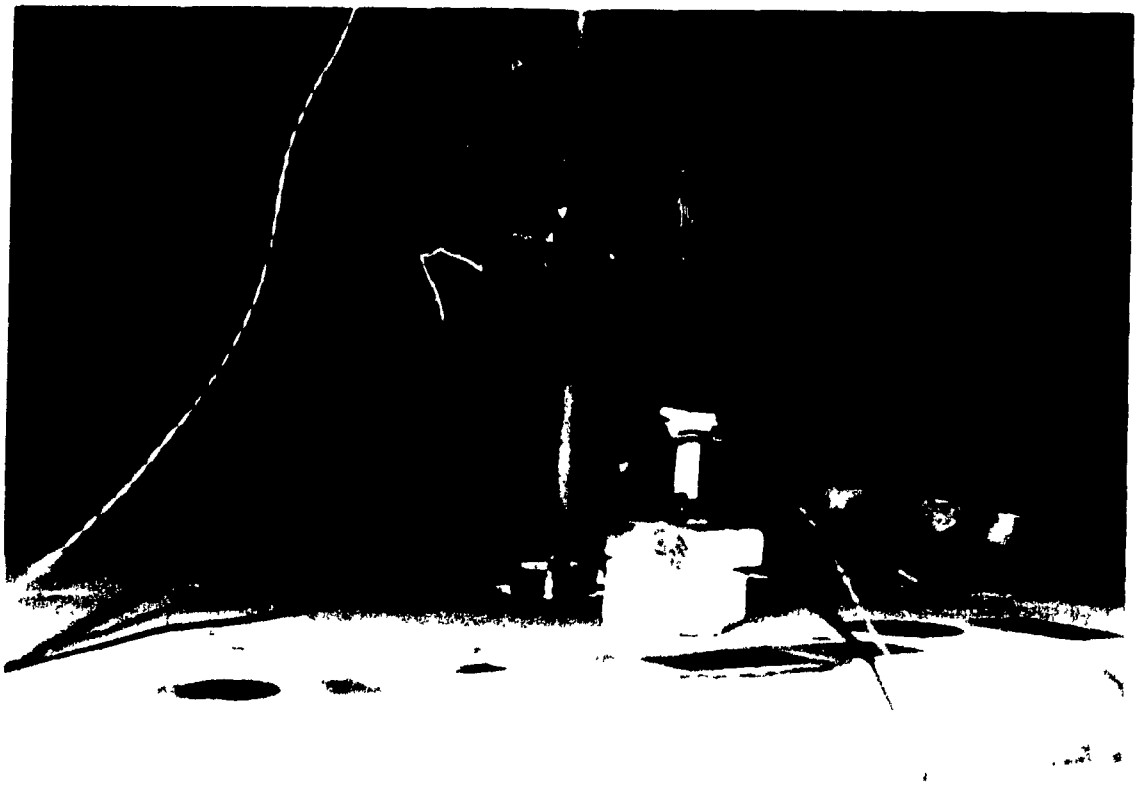

Figure 6.10 : LSHPIL Tests at NTC: Close-up of Condenser depicting the Red Hot Glow of the Lance

By comparing Figures 6.3 and 6.4, we can see the effect of changing the furnace temperature on the outer condenser. When the temperature was raised by 50 °C and everything else was left constant, the outer condenser rose by approximately 20 %. When the gas through the middle was then turned on to 50 l/min, Figure 6.5, the condenser dropped from 48 cm to 43 cm, a 10% change. The pressure also changed by 10%. When the gas was further increased to 90 l/min, Figure 6.6, the condenser fell by only 5%, whereas the pressure in the lance fell significantly; by 17%. This illustrates conclusion 4: the internal condenser of the annular pipe was modified to account for the pressure drop while the outer condenser remained more or less the same, resulting in a slanted inert gas/sodium vapour interface. When the fan is then turned on, Figure 6.7, the outer condenser falls drastically, 44%, but the pressure only changes by 15%. Again illustrating the slanted interface concept. In Figures 6.8 and 6.9 the gas through the middle is turned down to 50 l/min and then to 0 l/min, respectively, causing the condenser to rise and the pressure to rise in each case.

It is clear that the simulation provided valuable information regarding potential lance behaviour in the industrial furnace. The evaporator/condenser ratio of 1 for the standard test (experiment 1) provided the basis for choosing the length of the pilot scale heat pipe lance. The calculations in Appendix C using the wall temperatures and pressure from a typical simulation experiment enabled the approximation of the vapour and condensate velocities that could be expected in a pilot scale lance. These calculations are shown at the end of Appendix C.

For an LSHPIL experiment with an operating pressure of 1.43 atmospheres, the following results were calculated:

$q_{dissipated} = 2.6$ kW

$v_{vapour} = 3.68$ m/s

$v_{condensate} = .091$ m/s

Chapter 7

The Mark I Heat Pipe Injection Lance

7.1 Introduction

With the success of the preliminary heat pipe lance work, the construction of a pilot scale heat pipe lance could begin. The tests were to be carried out in the C-furnace (converting furnace), at the Kidd Creek smelter in Timmins, Ontario, Canada. Discussions with the plant metallurgical engineer in charge of the lancing operation, Dr. Mike Kozlowski, and Ernest Mast of the Noranda Technology Centre (NTC), were on-going during the construction of the first pilot scale heat pipe lance, Mark I, in an effort to understand the set-up of their furnace and the conditions the lance would be subject to. The data obtained from the simulations would serve as the basis for the engineering of the lance. The materials would be provided by the NTC, based on the design parameters established by McGill, taking into account the aforementioned discussions.

The assembly, welding, cleaning, charging and some conditioning of the Mark I lance took place at McGill. The lance was then shipped to Kidd Creek where Dr. Kozlowski had prepared the experimental set-up. The first set of tests began on August 13, 1991 and finished on August 16, three days later. In the following section the development of the Mark I lance and the results of those tests will be discussed.

7.2 The Making of the Mark I Lance

The selection of materials for the Mark I lance was based on the work done with the laboratory scale heat pipe injection lance and the procedures outlined in that section of this work. The steel used for the lance, however, was not exactly the same. The laboratory simulations which used a 316 stainless steel showed that such a material was a good candidate. The comprehensive list of criteria outlined in the LSHPIL section of this work also strongly

supported the use of stainless steel for the lance material. The stainless steel chosen for the Mark I lance was type 310, containing approximately 20% Ni and 24% Cr. Such a steel was decided upon primarily for its high temperature corrosion resistance. It was felt that it would behave similarly to the 316 stainless steel used in the LSHPIL tests, but its better corrosion properties could increase its life as a heat pipe lance beyond that of 316 stainless steel. In the end, both the inner and outer pipes of the lance were made of 310 SS, as well as the end plates.

The following illustration shows a schematic of the Mark I injection lance with the inner and outer pipe materials and dimensions labelled. The proposed insertion depth into the furnace is also illustrated:

Mark I - 5.08 cm SCH 80, 310 SS
2.54 cm SCH 80, 310 SS

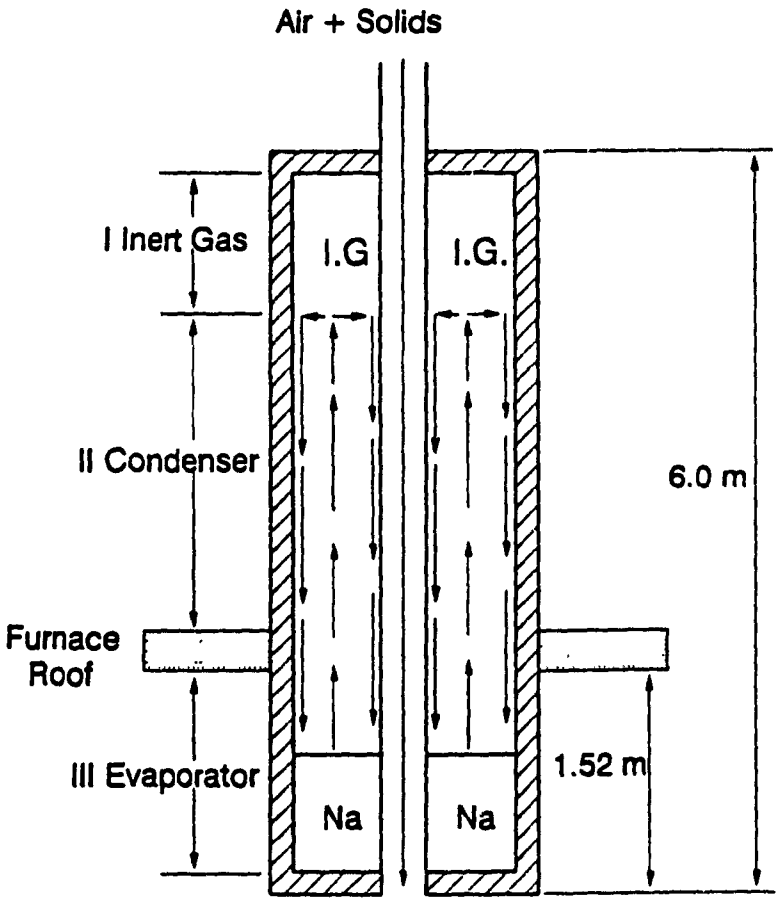

Figure 7.0 : Mark I, Pilot Scale Heat Pipe Injection Lance

The construction of the lance took place at McGill University, once both the inner and outer pipes and the end plates were received from the manufacturers. The NTC dealt with the shipment and payment of the 310 stainless steel pipes. The pipes were all seamless, containing no welds. The end plates were then machined from 0.635 cm thick plates so that they could be securely fit and welded between the two pipes. The machining of the pipes was done by the staff of the McGill metallurgical machine shop. The welding was done by the Chemical engineering machine shop staff, at McGill. Upon completion of the welding, the lance assembly was checked for leaks. The same cleaning procedure was used as was for the LSHPIL. The fittings and valves were the appropriately sized *Swagelok* type. Two feed tubes were attached to the Mark I lance. The feed tubes were stainless steel, 0.635 cm in diameter, located near the very top of the lance. Note that there exists a difference between "tube" designations and "pipe" designations. *Swagelok* works on a tube system.

7.3 Charging of the Sodium

After the pipe was cleaned it was ready for charging. From the results of the LSHPIL tests, based on the amount of material that was charged into the pipe and the amount that was lost to oxidation, it was estimated that 50% of the evaporator volume was filled. Calculations were made to determine the amount of sodium required for a 50% evaporator volume charge, based on a submersion depth of approximately 6 ft or 1.82 m into the furnace. The annular volume that the liquid sodium would fill would amount to approximately 1.25 kg of sodium, according to the following calculations:

$$\text{Volume of evaporator} = \pi(2.464^2 - 1.067^2)(.5 \times 6(12)(2.54))$$
$$= 1417 \text{ cm}^3$$

$$\text{At } 300^\circ\text{C } \rho_{\text{sodium}} = 880 \text{ g/l}$$
$$\therefore \text{ Mass Na required} = 1.417 \text{ l} \times 880 \text{ g/l}$$
$$= 1.25 \text{ kg of sodium}$$

To compensate for oxidation and other losses, 1.4 kg was weighed out and charged into the Mark I lance. The sodium was cut into pieces, as illustrated in the LSHPIL section, using

the same apparatus. Once cut, the sodium was held temporarily in nitrogen filled *Ziploc* bags until the sodium could be charged. The following picture illustrates the sodium filled *Ziploc* bags:

Figure 7.1 : Hand Cut Sodium in Nitrogen Filled *Ziploc* Bags

The charging operation was undertaken by E. Mast of NTC and myself. It took place outdoors, in the parking lot next to the metallurgical furnace laboratory. It was felt that this was the best way to ensure everyones' safety. If sodium did catch fire, it would be in the open where it could burn freely and not damage any equipment or harm anyone. The lance was maintained at an angle of approximately 30° during the charging process so that gravity would cause the solid sodium pieces to fall to the bottom of the lance. The charging of sodium into

the lance took place at the two feed tubes located at the top of the lance, illustrated in Figure 7.2. These ports are later connected to the valves and pressure transducer by *Swagelok* fittings. The charging process was long as periodic jamming of the sodium took place. In future great care must be taken to ensure the sodium is cut to the proper size and that it is not fed too quickly, i.e. it is given the time to fall to the bottom of the lance and not plug up near the top. Sodium is slightly sticky in solid form and did not easily slide to the bottom of the lance. More time and energy must be invested into the development of an efficient means of charging sodium if large scale production of sodium filled heat pipe lances becomes a reality.

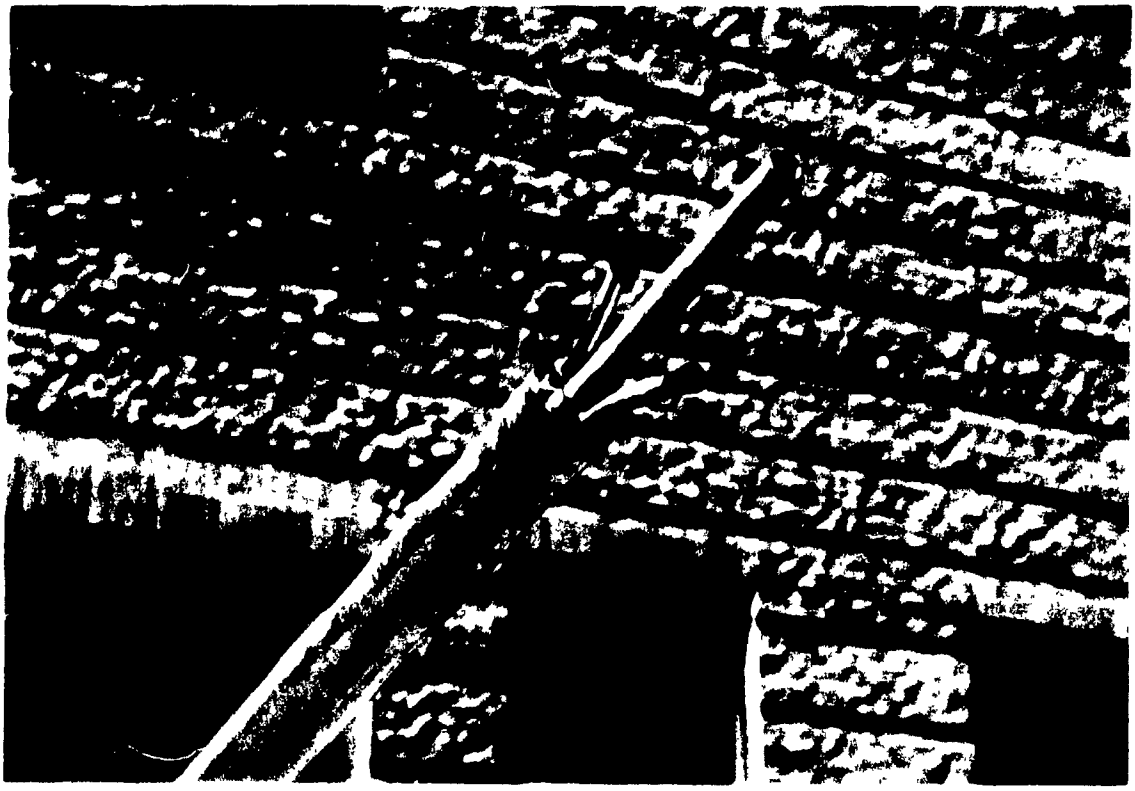

Figure 7.2 : Mark I Sodium Feed Tubes

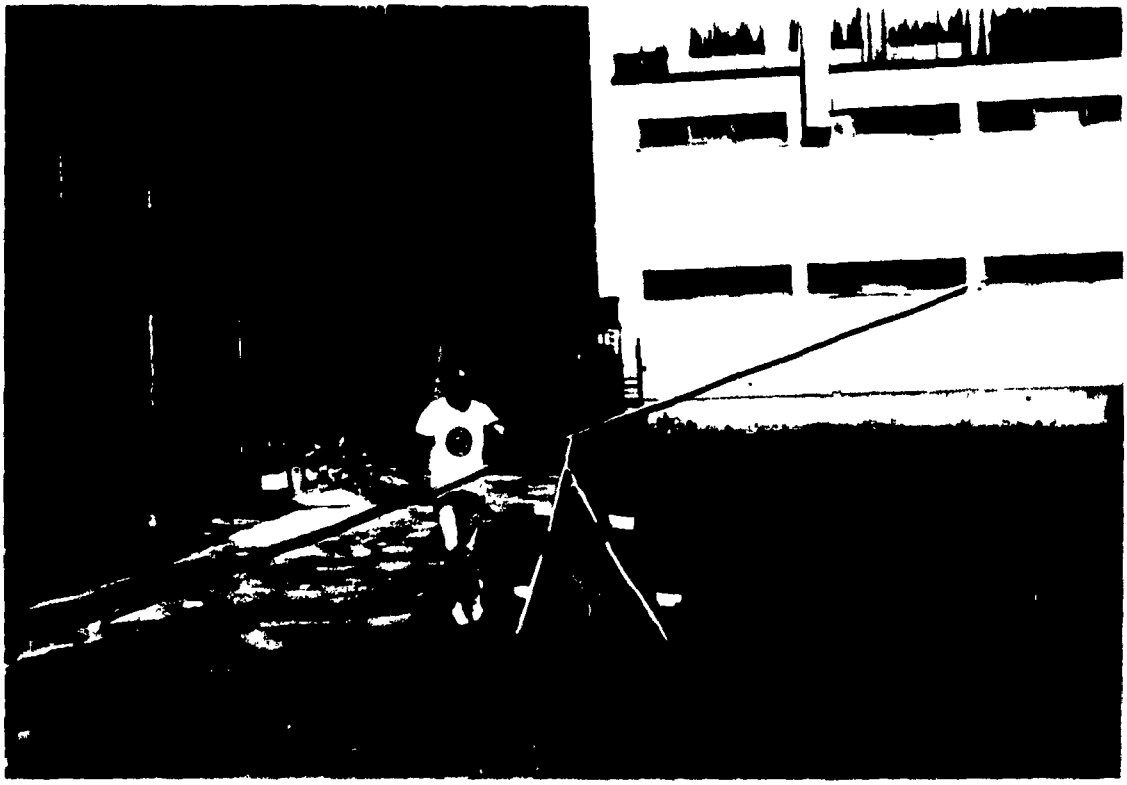

Figure 7.3 : Mark I Lance, Ready for Outdoor Sodium Charging

7.4 Conditioning of the Lance

Once the charging was completed, it was necessary to condition the lance to remove impurities from the sodium and ensure that the majority of the sodium was at the bottom of the lance. The lance was again maintained at an angle to ensure that gravity would cause the sodium to fall to the bottom of the pipe. To condition the lance, a number of portable propane torches were used to melt the sodium between the two pipes and force it to run down to the end of the lance. By melting the sodium it was hoped that some impurities would be forced out of the sodium and that the beginning of the conditioning of the Mark I lance would take place. The remaining conditioning would take place at the plant. Our greatest concern was that the minimum amount of sodium be trapped at the top of the lance so that the evaporator reservoir would not be depleted and the pipe would not get damaged. The following picture shows the torching of the lance to melt the sodium inside of it:

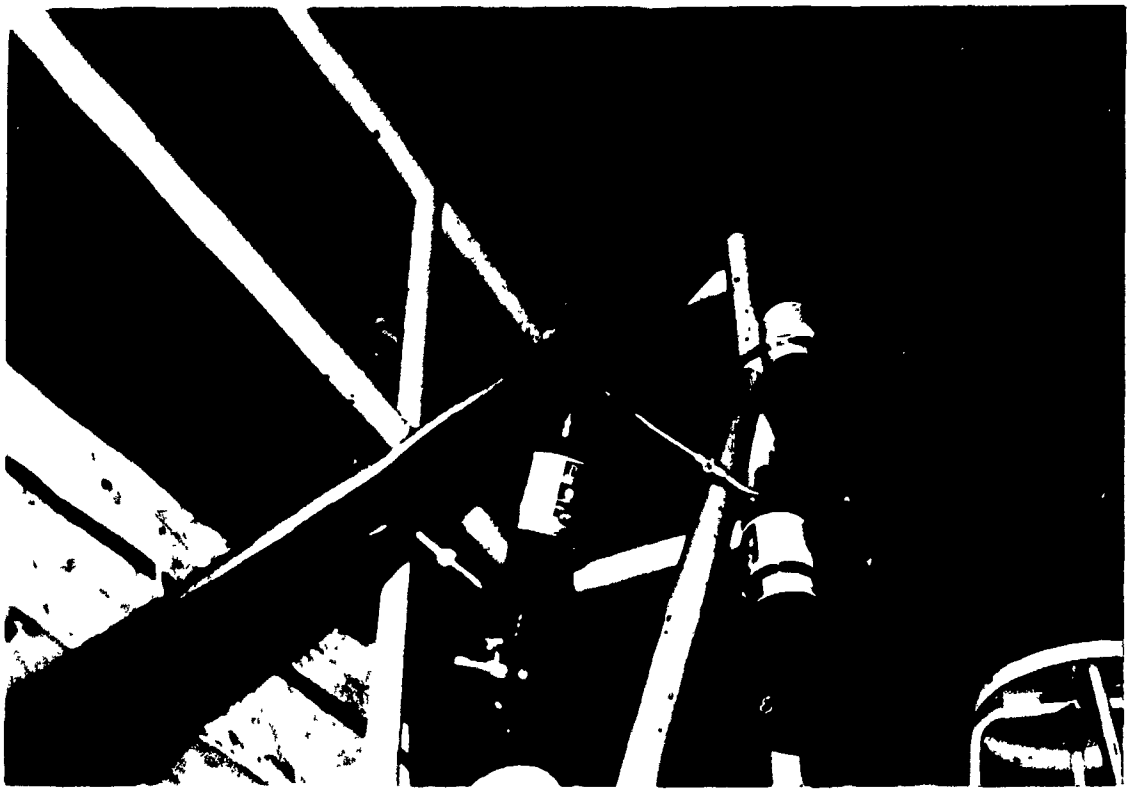

Figure 7.4 : Melting the Sodium Inside of the Mark I Lance, Top Section

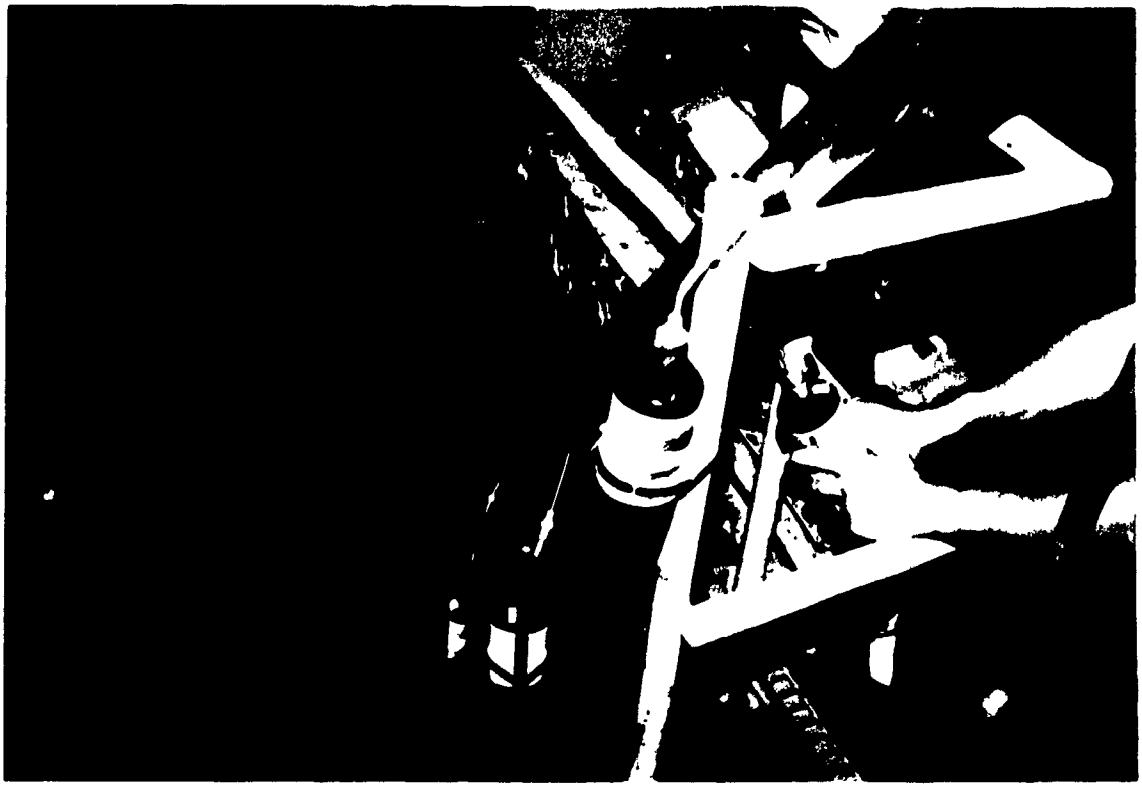

Figure 7.5 : Melting the Sodium Inside of the Mark I Lance, Middle Section

Once the conditioning stage was completed the lance was evacuated and sealed with *Swagelok* fittings. The pressure transducer was connected to the valve Tee-connection. A protective aluminum cover was attached to the head of the lance to protect the fittings and the pressure transducer during shipping.

7.5 Experimental

In its journey to the Kidd Creek smelter, the Mark I lance was mishandled. The protective aluminum cover had been damaged and the top of the valve had either fallen off or been removed. These two factors seemed to have no effect on the lance, however, since it was still in good working condition. The lance was re-evacuated and checked for leaks. Once it was found to have no leaks, preparation of lance insertion into the furnace was begun. The following photograph partially illustrates the set-up at Kidd Creek's C-furnace:

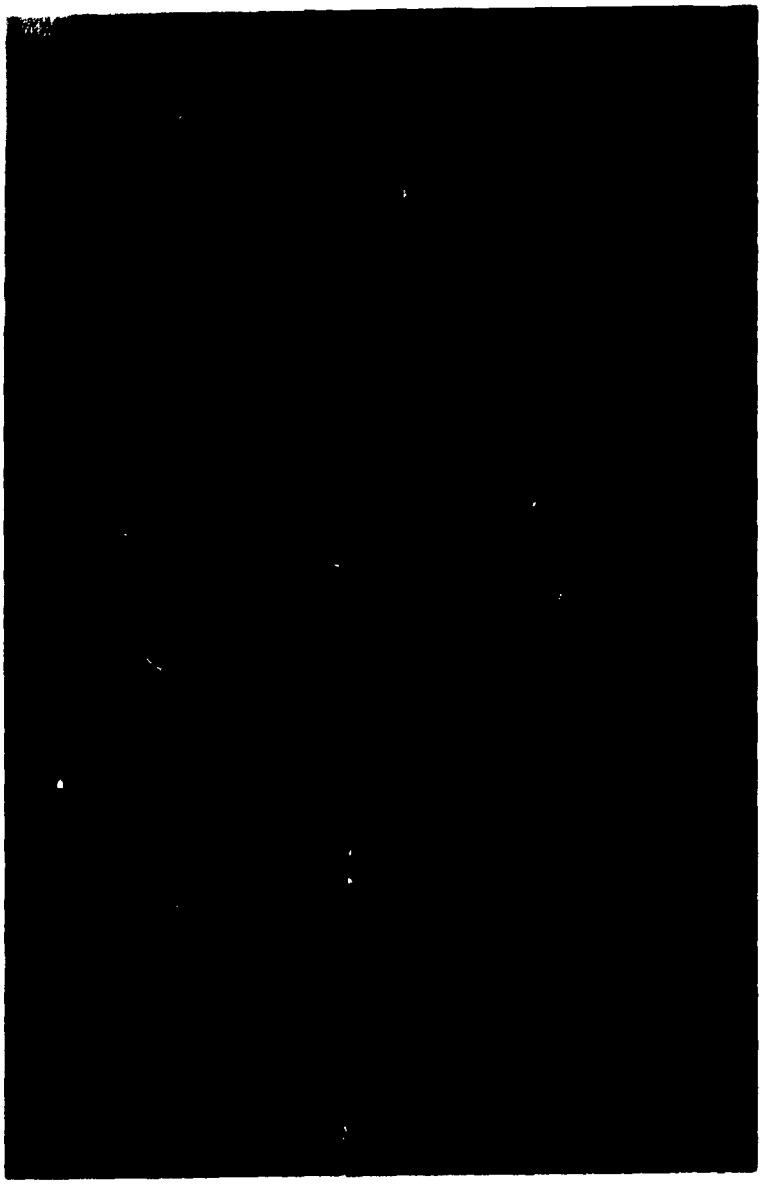

Figure 7.6 : Part of Experimental Set-up for Kidd Creek Pilot Scale Heat Pipe Injection Lance Trials

The set-up consisted of:

- 1 6.1 m Pilot Scale Heat Pipe Lance (Mark I lance)
- Hole in the furnace roof large enough to fit a 6 cm diameter lance
- 1.5 m of space between roof and grated working platform
- 1.5 m protective, rectangular, screened box surrounding Mark I lance
- 1 *Omega* power supply
- 1 *Omega* pressure transducer and wiring
- 1 K-type thermocouple and wiring
- 1 voltmeter
- 1 Macintosh Computer to collect data, situated in the "control room"
- 1 Edwards "Speedvac" vacuum pump
- 1 "air mover" to blow air over surface of lance
- air line and air hose

The lance was manipulated with a manually operated, 5-ton crane and a clamp attached to the head of the Mark I lance. The lance was raised above the roof and slowly inserted into the hole. It was lowered at an approximate rate of 1 centimetre every 10 seconds. The sodium vapour pressure was monitored first by a voltmeter for quick reference and then by a computer outside the plant in the control room, for long-term measurements. The Mark I lance was initially lowered to a height of 0.61 m from the furnace roof; taking into account the roof thickness. Approximately 0.37 m of the lance was subjected to the furnace atmosphere. After a period of 10 minutes, the lance was lowered to a height of 0.91 m, measured from the furnace roof. After a full day of operation at this height, the lance was lowered another 0.3 m. Thus, the lance tip at its lowest point was approximately 1.5 m from the surface of the bath.

7.6 Results and Discussion

The data from the Mark I lance tests was compiled with a Macintosh computer and stored onto a disk. It was then imported into a spreadsheet (Lotus 123), organized, and imported again into the Lotus *Freelance* program. Data was collected every minute by the plant computer. The following are graphs of the sodium vapour pressure and the outer wall temperature located 2.4

m from the tip of the lance, versus time. The measurements taken are graphed on an hourly basis. Note that this temperature is near the upper end of the condenser section. The thermocouple reading thus illustrated when the condenser rose to this section of the Mark I lance. When the condenser did rise to this section, the thermocouple was essentially triggered and read hot temperatures. It served to make the operator aware of whether the condenser was approaching the working platform area, above the furnace roof. It did not, however, necessarily read the condenser temperature; it did so only when the condenser had risen to the level of the thermocouple.

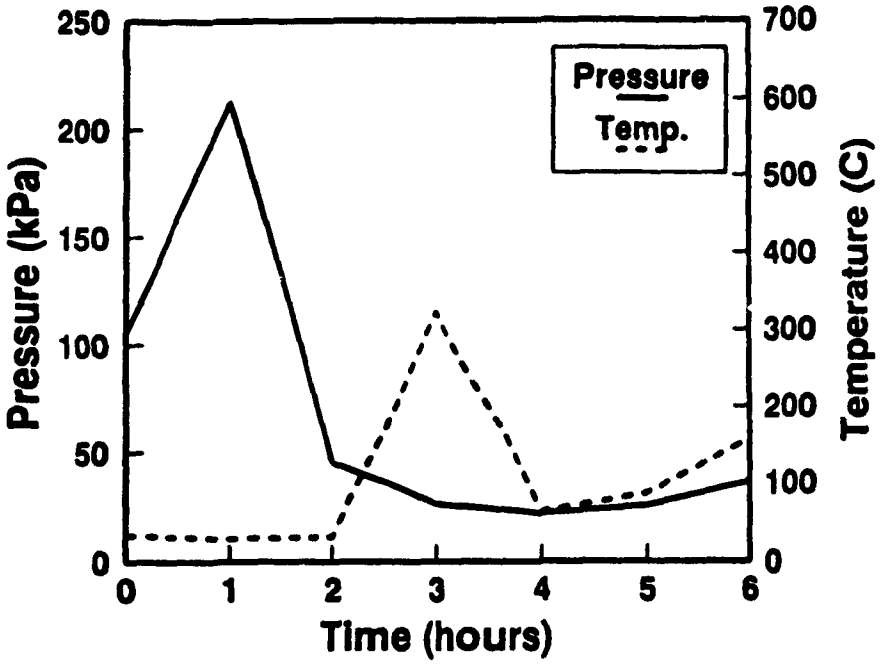

Figure 7.7 : Na Vapour Pressure and Outer Wall Temperature Curves for Mark I Lance Tests, August 13, 1991.

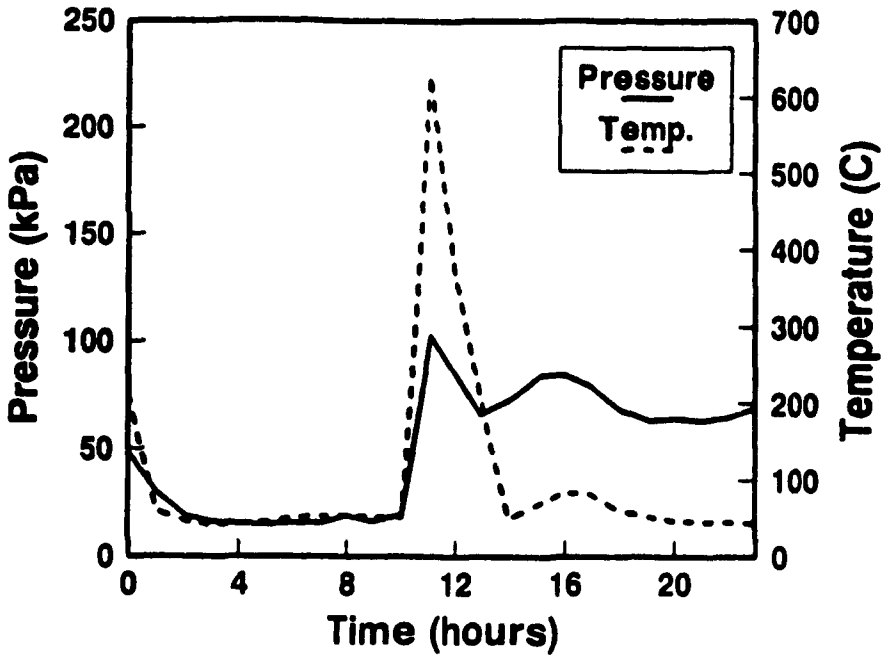

Begins at 0:00

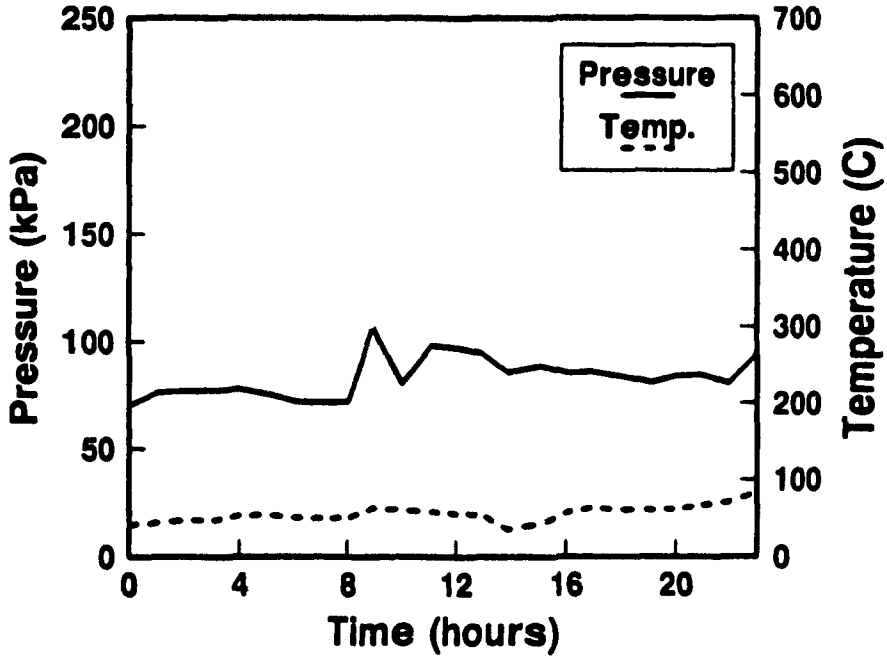

Begins at 0:00

Figure 7.8 : Na Vapour Pressure and Outer Wall Temperature Curves for Mark I Lance Test, August 14 (above), August 15 (below), 1991.

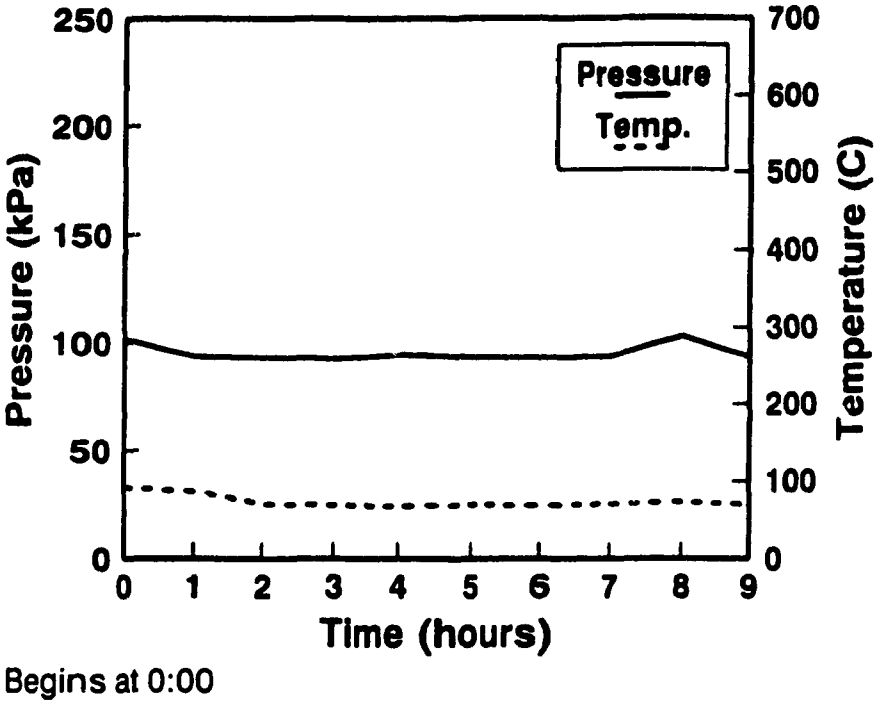

Figure 7.9 : Na Vapour Pressure and Outer Wall Temperature Curves for Mark I Lance Tests, August 16, 1991.

The Mark I lance test began at 18:00 hours on August 13, 1991. Once the lance was inserted to its initial depth of 0.61 m, the pressure in the pipe rose to approximately 2 atmospheres. The initial pressure in the lance, before insertion read 0.04 atmospheres according to the pressure transducer. The pressure reading of 2 atmospheres, Figure 7.7, reflected the vapour pressure of the sodium, and the pressure of the initial non-condensable gases in addition to the non-condensable gases generated from the vaporization of sodium (i.e. oils and grease).

The lance was then re-evacuated to remove some of these inert gases. This is part of the conditioning process that was discussed earlier in this work.

The pressure in the pipe dropped as illustrated in Figure 7.7, while the temperature reading of the thermocouple increased. By evacuating the inert gases in the chamber, the condenser was allowed to rise. As it approached the thermocouple located 2.4 m from the lance tip, it caused an increase in temperature in the region, reflected by the peak in the temperature curve illustrated in the graph. The pressure continued to drop even after the evacuation was stopped.

The rise in the condenser accompanying the evacuation of inert gases and the subsequent drop in pressure was caused by the reduction of inert gas molecules in the system. The pressure in the Mark I lance is the pressure of the inert gas/sodium vapour system. The pressure of the two gases is the same, however, their volumes are not. This is due to the fact that a different number of molecules of each gas exists within a fixed volume. The pressure is dictated by the amount of heat (Watts) which must be removed from the evaporator, by the heat of vapourization of the sodium molecules. By removing inert gas molecules from the system, space was made available for the sodium molecules to occupy, hence the condenser rose. It rose to a height fixed by the new pressure of the system. This pressure was lower, however, since a larger portion of the total gas volume was occupied by sodium molecules, while the heat dissipated by the system remained unchanged. Thus, the pressure of the system dropped since the same number of sodium molecules were needed to dissipate the heat over a larger volume. Once the smaller number of inert gas molecules were compressed to the new equilibrium pressure of the system, the condenser ceased to rise, and a new equilibrium was established.

This equilibrium was maintained until the following day, with only subtle changes reflecting variations in the heat flux within the furnace. At 0:00 hours, on August 14, the lance pressure began to drop from 50 kPa to 20 kPa over the next two hours. It is difficult to pinpoint exactly what caused this change since visual inspection of the lances could be done only when a view hole into the furnace was made by plant personnel. Such view holes require oxygen lancing which involves burning a hole into a section of the furnace, allowing one to see inside. No such person was available to us at that time. The best explanation for the drop in pressure was the building of accretions onto the lance. It is known from previous visual inspections that

accretions form on the standard lances. They form and then fall off, often damaging the lances as they may take sections of pipe with them. If an accretion was formed on the Mark I lance, then as it grew larger, the heat flux entering the lance would be diminished. In Figure 7.8, (August 14) the pressure in the lance drops over a period of two hours and then stabilizes, which may reflect the formation of an accretion. Visual inspections of the Mark I lance at a later time showed evidence of fairly large accretion build-up, supporting this hypothesis.

At around 10:00 o'clock, on August 14, the pressure in the lance jumped from 20 kPa to 100 kPa, resulting from the lance being inserted another 30.5 cm into the furnace. No evacuation of gases took place. It can be seen that the condenser immediately responded to the increased heat which the Mark I lance must dissipate, indicated by the surge in the temperature reading which is synchronized with the pressure spike. The response of the lance to the increased heat load is the vaporization of more sodium, hence an increased sodium vapour pressure. The increased pressure compresses the inert gas to a point where the pressures are equal and this is where the condenser remains. In this case, it was in close proximity to the thermocouple.

It should be noted that the lance requires fairly long periods of time to reach equilibrium as the walls are relatively thick and stainless steel has poor conductivity. The lance responds quickly to changes in external conditions but requires fairly long periods of time for the heat to fully soak into the pipe walls and equilibrate the system. Temperature and pressure peaks are often followed by oscillations as the lance attempts to regain equilibrium. However, equilibrium in an industrial furnace is almost impossible to achieve as the process is continually changing and never steady. The drop in pressure after the pressure surge and the following oscillations are indicative of the Mark I lance attempting to equilibrate itself.

On August 15, a small pressure peak appears followed by a more gradual peak. These peaks reflect changes in furnace temperature. It illustrates an added benefit of using a heat pipe lance versus a normal lance. Besides longevity of life and improved control over the Mitsubishi process, the heat pipe lance appears to be a good sensor of what is happening inside the furnace. Perhaps good enough that correlations can be drawn between the pressure inside the pipe and the operating conditions of the furnace. This is not investigated in this work but is something that should be kept in mind for future study.

The Mark I lance failed at approximately 1:00 o'clock in the morning, on August 16, 1991. The pressure reading in Figure 7.9 illustrates this. The pressure read 97 kPa for a seven hour period following a peak in the graph. Visual inspection of the condenser revealed that it had fallen into the furnace. The reading of 97 rather than 101,3 kPa resulted from the calibration of the pressure transducer being slightly off. The Mark I lance was thus reading atmospheric pressure without any condenser. This could only mean that the lance had failed. The tiny peak at the end of the graph resulted from the removal of the pipe.

The Mark I lance tests proved to be very successful as the lance had remained in the furnace for 2 days and 15 hours. Type 304 stainless steel lances are consumed upon insertion into the furnace at a rate in the order of centimeters per hour. The Mark I lance survived for 2 days and 7 hours before a leak developed. Only then did any significant consumption begin.

7.6 Failure of the Mark I Lance

After failure, the lance remained in the furnace for 8 hours. During this time, it behaved as a normal lance, since sodium cooling ceased and the heat pipe principles no longer applied. Fortunately, the lance was retrieved, which was not planned at the beginning of the experiment. This allowed some investigations into its operation and failure.

Visual inspection of the lance revealed that failure had occured at the tip of the lance, since approximately .3 m of the lance edge was destroyed. Figure 7.10, which follows, shows the severely attacked tip section next to a segment of the condenser which was approximately 1.5 m above the furnace roof. During the welding of the lance, a small pin hole had developed. When the hole was filled, it is unlikely that the steel weld material penetrated deeply into the tiny crevice, resulting in a superficial weld. Thus, the pipe wall at the pinhole location could be very thin rendering that point on the lance susceptible to a leak. It is obvious from the figure that the greatest amount of damage took place at the tip. It appears that deterioration of the lance began at the tip and worked its way backward.

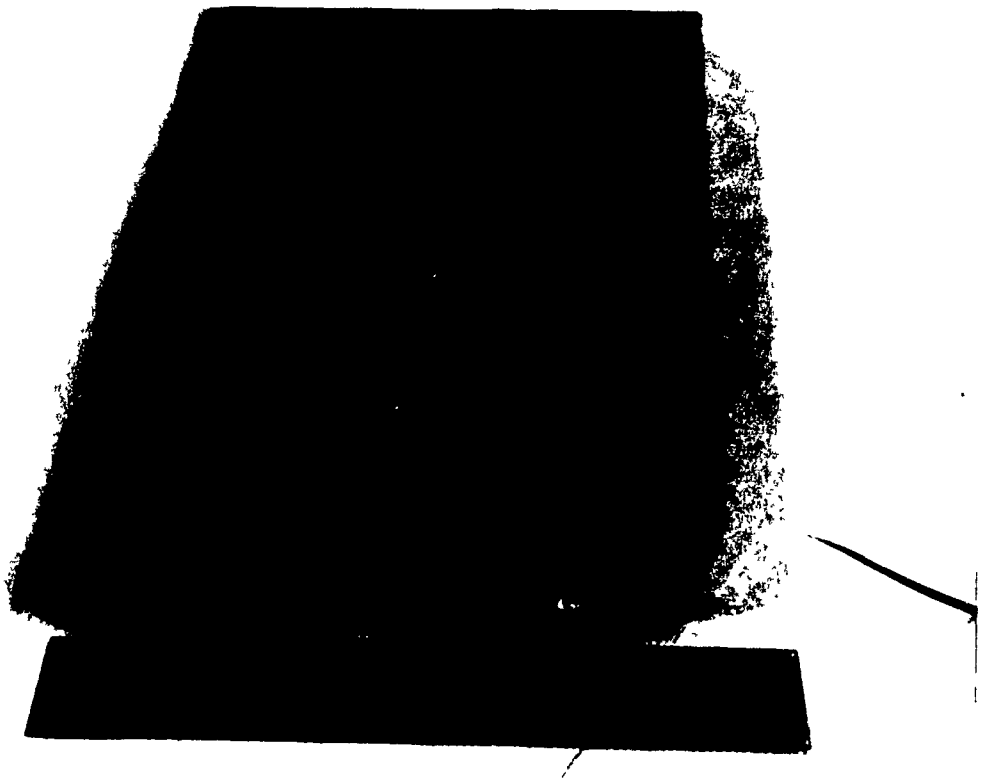

Figure 7.10 : Chemical Attack of Mark I Lance Tip Versus Undamaged Condenser Section

The remainder of the lance section inside the furnace was for the most part intact, suffering only a mild attack, most likely occuring after the failure of the lance when it no longer behaved as a heat pipe. The moderate attack can be seen in the following photograph which compares the lance section inside the furnace with the condenser section outside the furnace. The mild attack on the remainder of the section inside the furnace versus the severe attack of the tip section also suggests that the tip of the lance was the origin of failure.

Figure 7.11 : Top View of a Lance Section Inside the Furnace next to a Condenser Section

Chapter 8

Scanning Electron Microscope Analysis of Mark I Lance

8.1 Introduction

SEM analysis was conducted on the Mark I injection lance with two objectives in mind:

i) to determine the high temperature effects of sodium on stainless steel

ii) to evaluate the damage done by the environment of the C-furnace on the Mark I lance

The samples taken from the Mark I lance had the following dimensions:

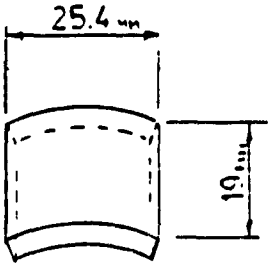

OUTER PIPE SAMPLE DIMENSIONS

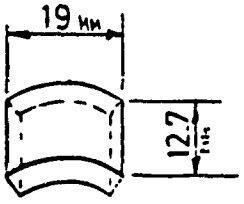

INNER PIPE SAMPLE DIMENSIONS

Figure 8.0 : Sample Dimensions of Mark I Lance

The samples were taken from three sections of the pipe. The first set, section 1, was taken at a distance of 2.6 m from the bottom of the lance. This section is outside the furnace but within the operating regime of the sodium in the heat pipe. The second set of samples, section 2, was taken from a region just inside the furnace, 1.5 m from the bottom of the lance. The last section, section 3, was taken at a location on the pipe that was 0.76 m from the lance bottom.

8.2 Sample Preparation and Analysis

The inner and outer pipe cross-sections were mounted in bakelite and fine-ground to reveal the interfaces between the pipe and the working substance and the pipe and the environment. The samples were ground using standard procedures.

The samples were all examined using the secondary electron mode of the SEM. The accelerating voltages used were 15 and 20 kV with a working distance of 39 mm. These settings were thought to provide the best resolution. X-ray analysis was done on all three samples to qualitatively determine what was present.

8.3 Results and Discussion

When comparing Micrographs 1 and 2, on the following page, the air interface with the sodium interface, it can be seen that the wall is coarser on the sodium side. This is illustrated by the slightly granular nature of the interface in Micrograph #2. Note that the dark background is bakelite. This attack of the interface appears to be very even. This was the case when the entire sample was examined. The morphology of the interface could be a result of chemical attack or a physical erosion of the interface due to the sodium. The latter would be preferred from a heat pipe materials point of view and will be shown to be the case in the discussion which follows.

The granulation of the sodium side becomes much more distinct when the images are magnified (Micrographs 3 and 4). The depth of penetration of this attack is approximately 12.5 micrometers. This is over a period of nearly 65 hours.

Micrographs 5 and 6 illustrate the outer pipe section taken at the same location, 2.6 m from the lance bottom. Similar results to those of the inner pipe can be seen.

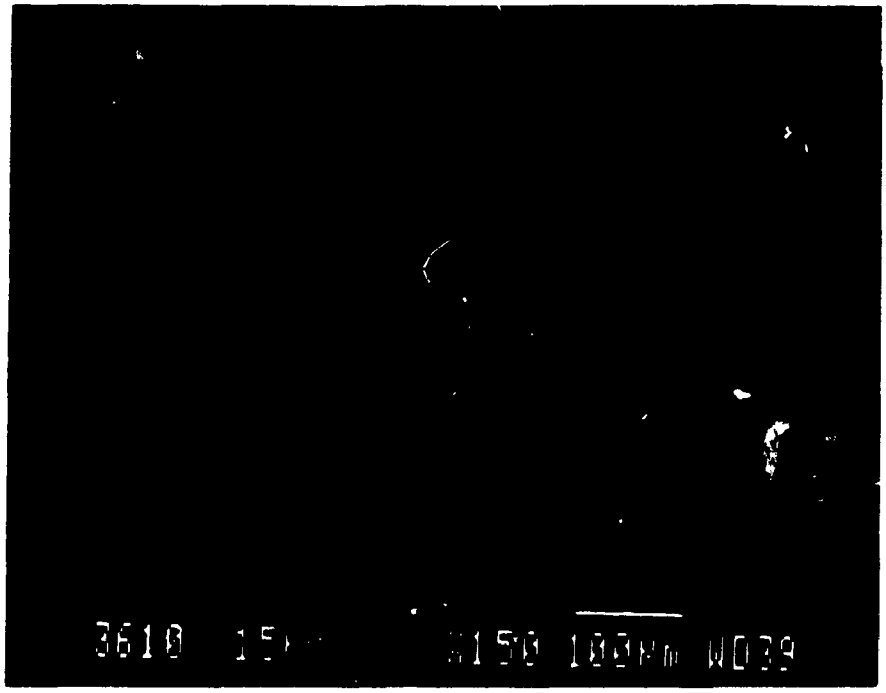

Micrograph #1- Inner Pipe and Air Interface, Section 1, 150X

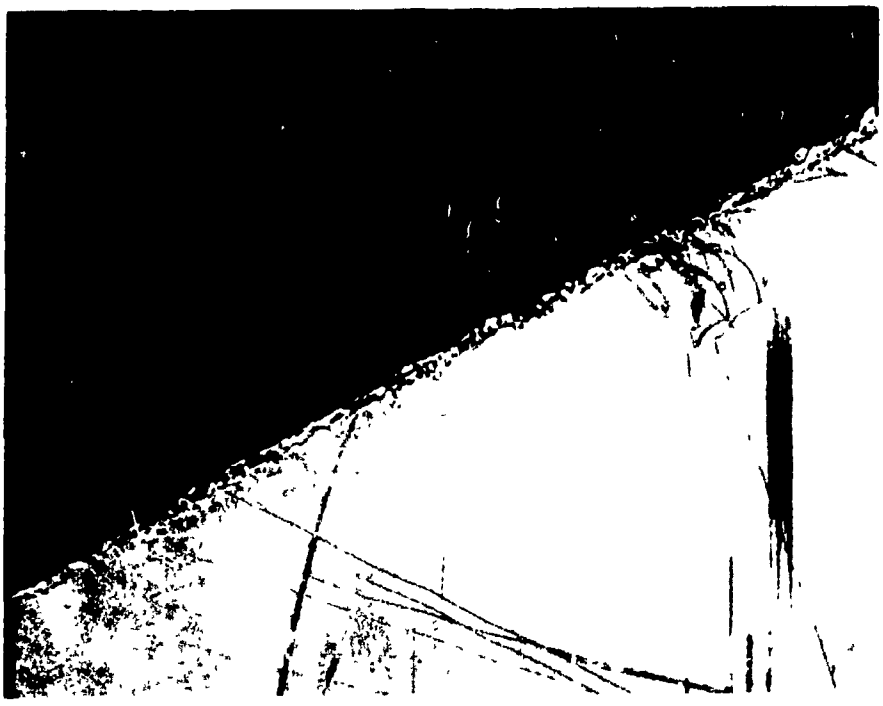

Micrograph #2- Inner Pipe and Sodium Interface, Section 1, 150X

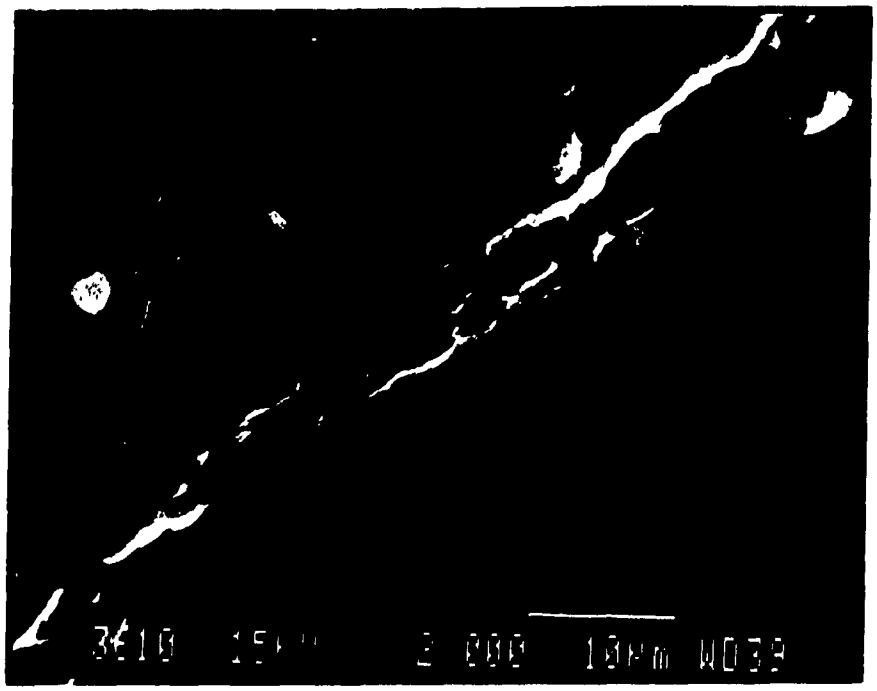

Micrograph #3- Inner Pipe and Air Interface, Section 1, 2000X

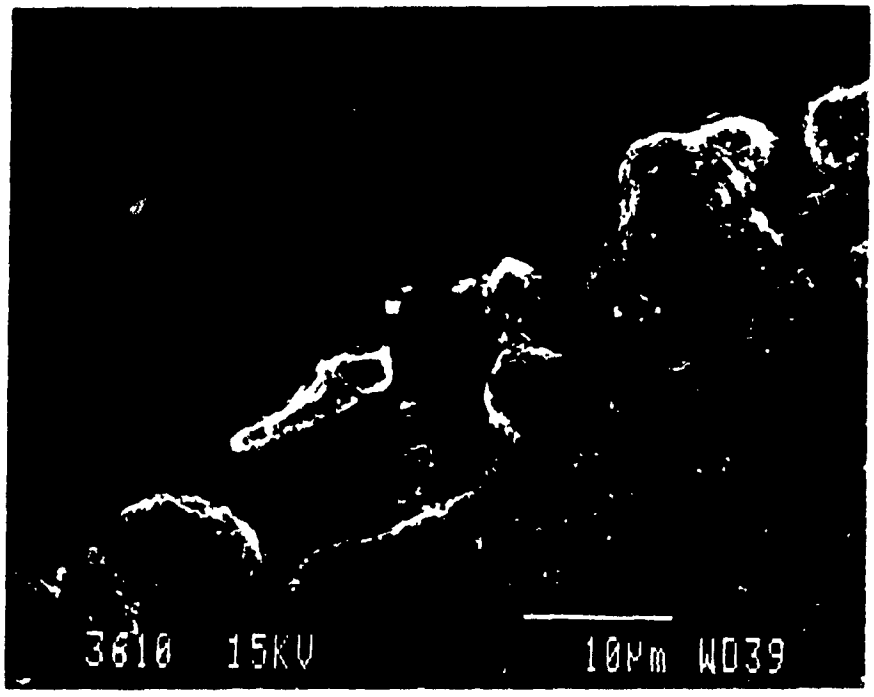

Micrograph #4- Inner Pipe and Sodium Interface, Section 1, 2000X

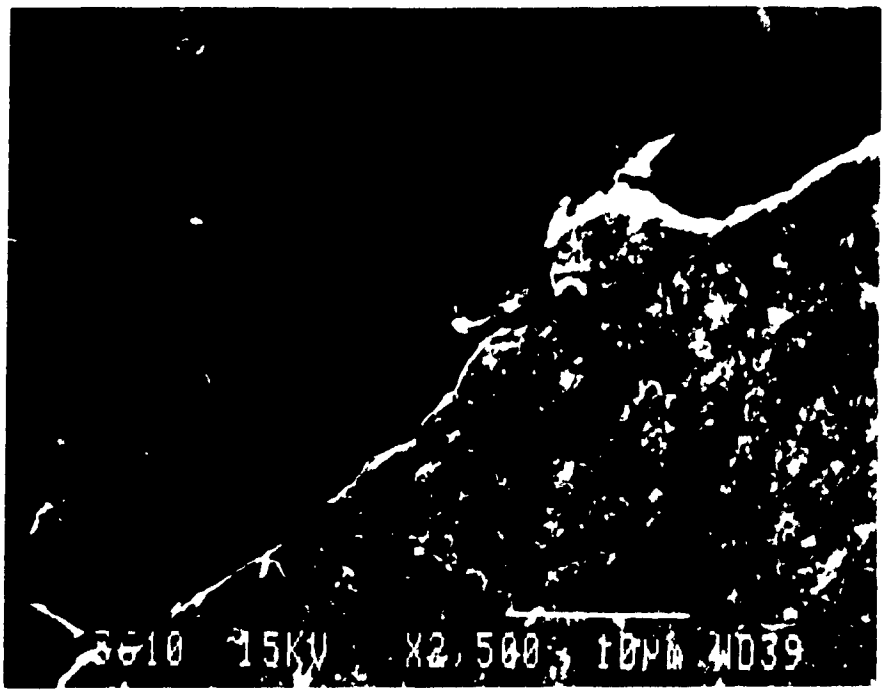

Micrograph #5- Outer Pipe and Air Interface, Section 1, 2500X

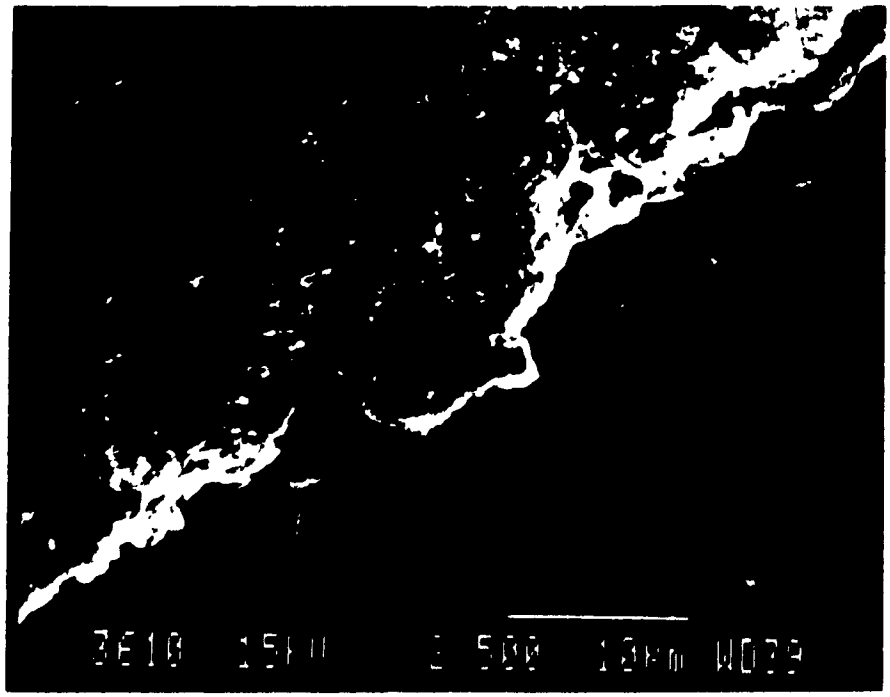

Micrograph #6- Outer Pipe and Sodium Interface, Section 1, 2500X

The attack on the inner surface of the outer pipe, Micrograph #6, is granulated as this is where the sodium is flowing. The penetration depth of the outer pipe attack is approximately 12 micrometers when measuring straight from the micrograph and taking magnification into account. This number agrees very well with the 12.5 micrometer attack on the inner pipe. Taking the average of the two measurements, a consumption rate of the pipe can be estimated assuming uniform consumption at a constant rate:

$$\text{Consumption rate} = 12.25\ \mu\text{m}/65\ \text{hrs.}$$
$$= 0.19\ \mu\text{m-hr}^{-1}$$

Assuming a linear consumption rate, a 0.635 cm thick heat pipe would last:

$$\#\text{Days} = 0.00635\ \text{m}/(.19\text{x}10^{-6}\text{m-hr}^{-1} \times 24\ \text{hrs/day})$$
$$= 1370\ \text{days}$$
$$= 3.8\ \text{years}$$

X-ray analysis was done on all sides of samples 1 and 2 and on all samples which follow. Little difference existed between the sodium interface side and the air interface side. Sodium was detected in some areas of the sodium interfaces but not in all. An explanation for this could be the fact that the sodium oxide present in the samples was sometimes lost by grinding and handling.

No information was found regarding a binary allov of Fe and Na. The sodium used was commercial purity implying small amounts of additional elements are present. However, from the previous calculations, due to the very small granulated layer and the elevated temperature of the system ($\sim$900 °C), the phenomena taking place is most likely an erosion of the steel surface by the vapour and liquid flow that it is subjected to and not a chemical attack of the surface. Evidence of this can be found in the following micrographs.

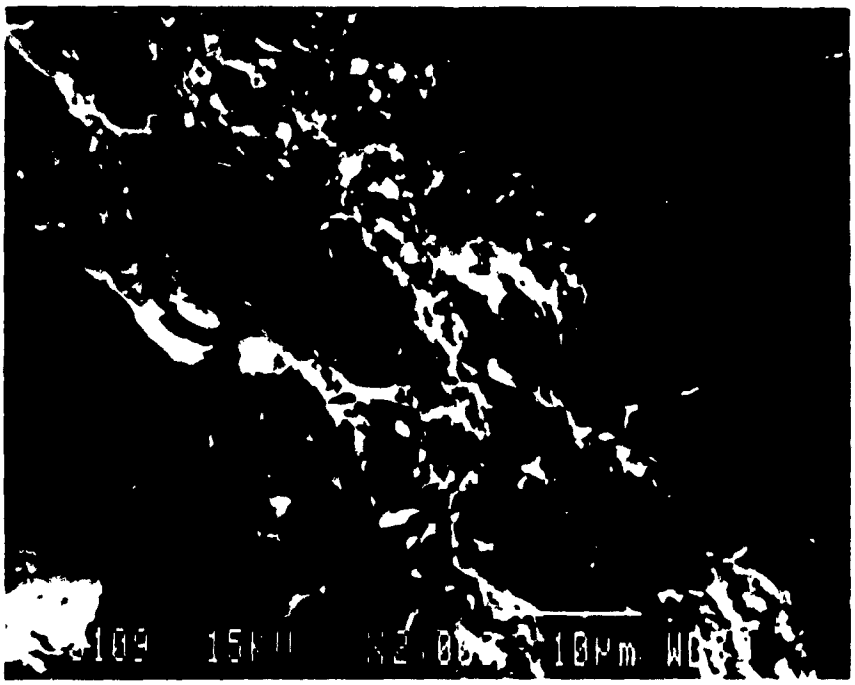

Micrograph #7- Inner Pipe and Furnace Atmosphere Interface, Section 2,2000X

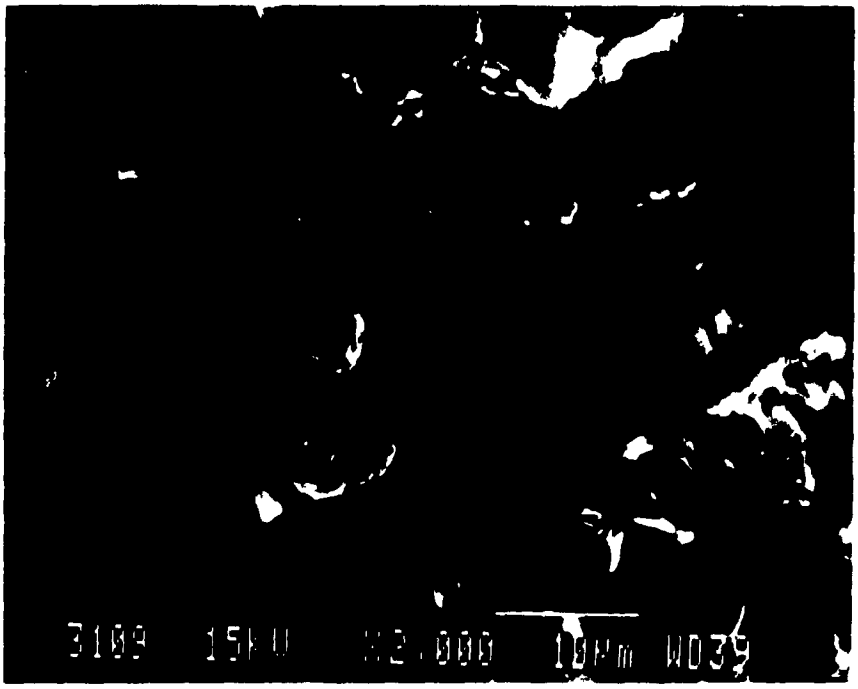

Micrograph #8- Inner Pipe and Sodium Interface, Section 2, 2000X

Unfortunately for the results of this work, after the Mark I lance had failed, it took approximately 10 hours before it was removed from the furnace. Micrographs 7 and 8 are not good representations of the effects of sodium on stainless steel. They do, however, illustrate the effects of chemical attack. The ten hours the lance was exposed to the furnace atmosphere caused the lower end of the lance to experience chemical attack by the furnace gases (predominantly SO_2 and enriched air).

At the higher section previously discussed, damage from the atmosphere was minimal since the hot SO_2 gases could not easily reach the upper part of the pipe. This is due to the fact that the pipe failed when it was operating near one atmosphere, so there was only a small pressure gradient at best to drive the SO_2 furnace gases into the top end of the pipe. As the sodium was slowly consumed and the sodium vapour began to condense due to the temperature drop in the upper portions of the pipe, more furnace gases could find their way into the pipe. The sodium, however, preferentially oxidized so that the steel pipe could only be attacked once all the sodium was consumed. Due to the relatively small annulus, this was a slow process. Perhaps most importantly, the low temperatures at the upper portion of the pipe reduced the corrosion rate of the pipe exponentially. As such, the micrographs presented from section one are not as influenced by the failure of the pipe and do illustrate the effect of sodium on the pipe. The micrographs from the lower end of the pipe illustrate the furnace attack on the steel; the lower the section, the greater the attack.

Comparisons of the micrographs from the different sections support the previous statements. The surface of Micrograph 8 is rough and uneven unlike its counterpart in section one, Micrograph 4. The latter is granular and uniform, appearing to have undergone an erosion process on the surface. The former is rougher and uneven, resembling a surface which has experienced chemical reaction. The hot SO_2 and air from the furnace atmosphere and the temperature of the surroundings increased the reaction rates noticeably in the lower sections of the pipe.

Micrograph 9 which follows, taken from section 3, 0.76 m from the lance tip, further supports chemical attack of the lower sections by the furnace gases versus erosion of the upper portion by sodium. An even more severe attack can be seen on this surface.

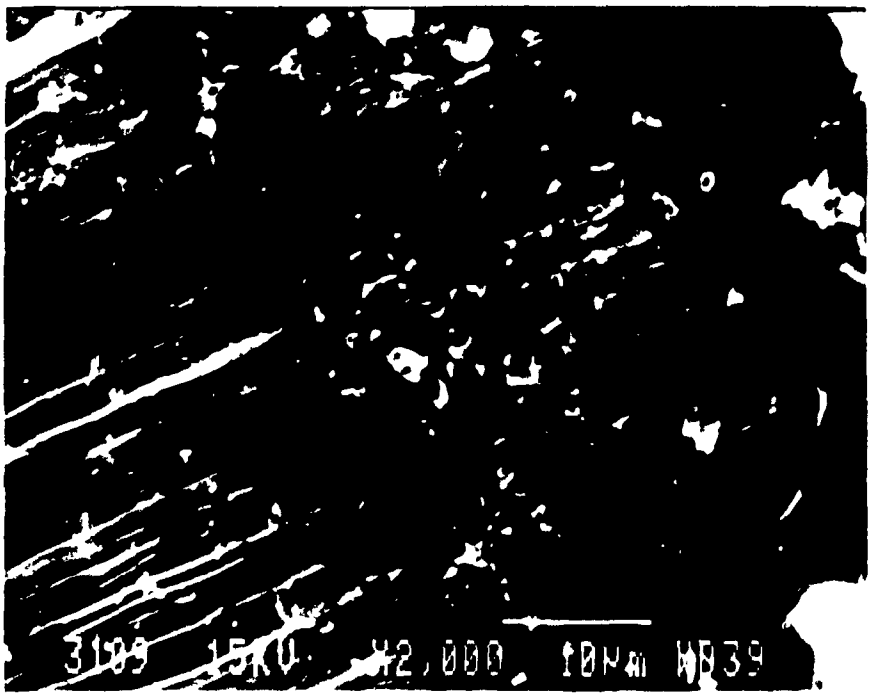

Micrograph #9- Inner Pipe and Sodium Interface, Section 3, 2000X

When Micrograph 9 is compared with Micrograph 4 the different mechanism of attack becomes obvious. The lower sections show how the furnace atmosphere of the C-furnace at Kidd Creek reacted with the stainless steel pipe and began to consume it. The morphology of the two micrographs are very different. Comparing Micrographs 8 and 9 we can see that the lower down the lance, the greater the attack. Note that this section was located well above the bath surface where the attack on the stainless steel is not nearly as severe as it is down by the tip of the lance.

If we compare the x-ray graphs of the upper section to the lower section, evidence of chemical attack at the bottom of the pipe is revealed.

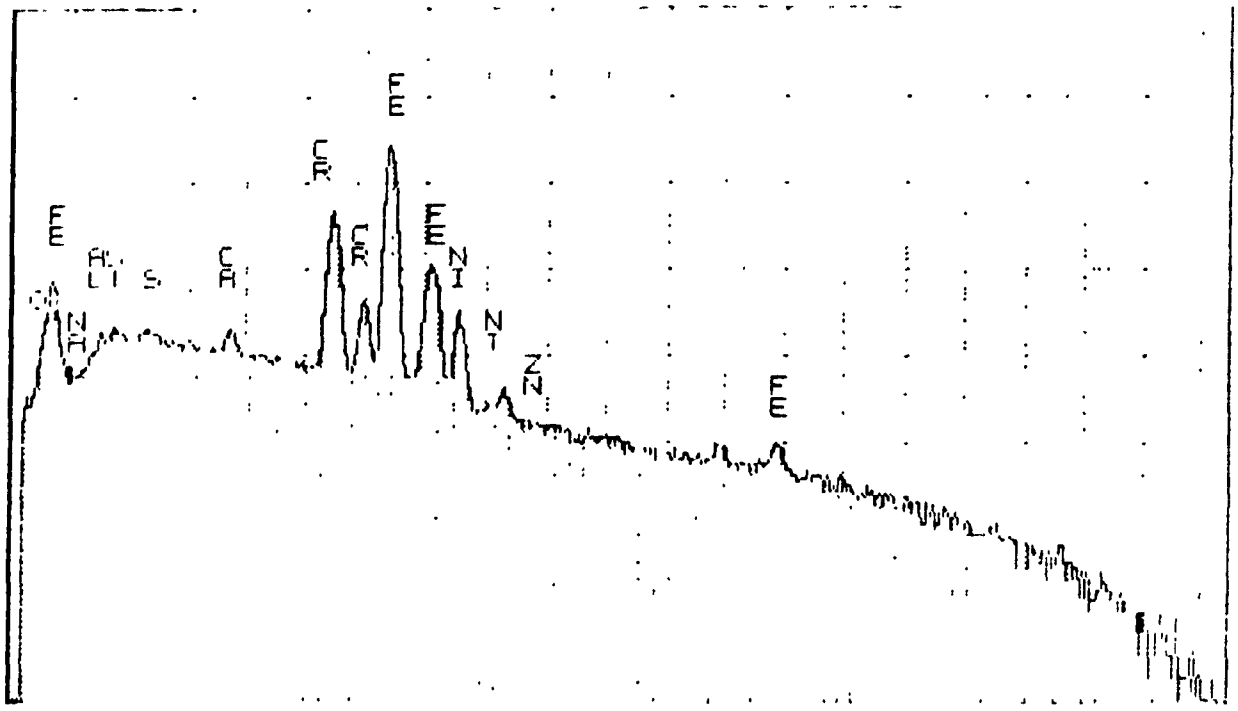

Figure 8.1 : X-Ray Analysis of Outside Pipe and Sodium Interface, Section 1, 17000X

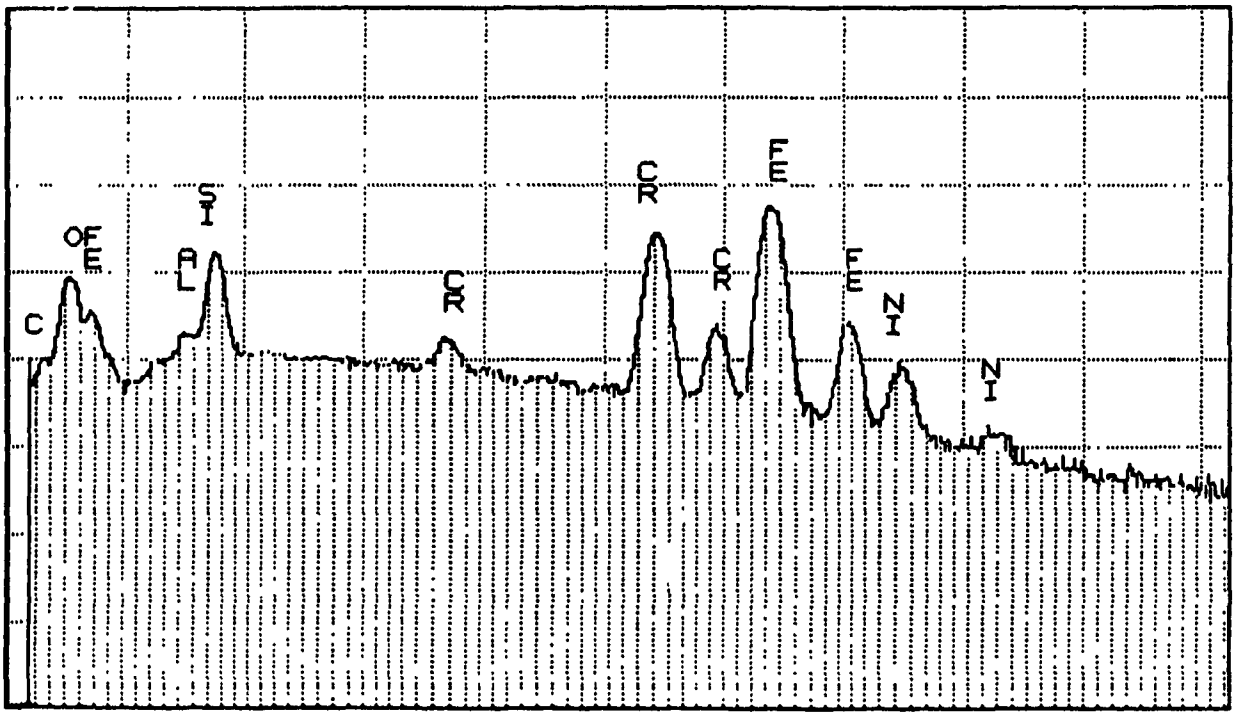

Figure 8.2 : X-Ray Analysis of Inside Pipe and Sodium Interface, Section 2, 8000X

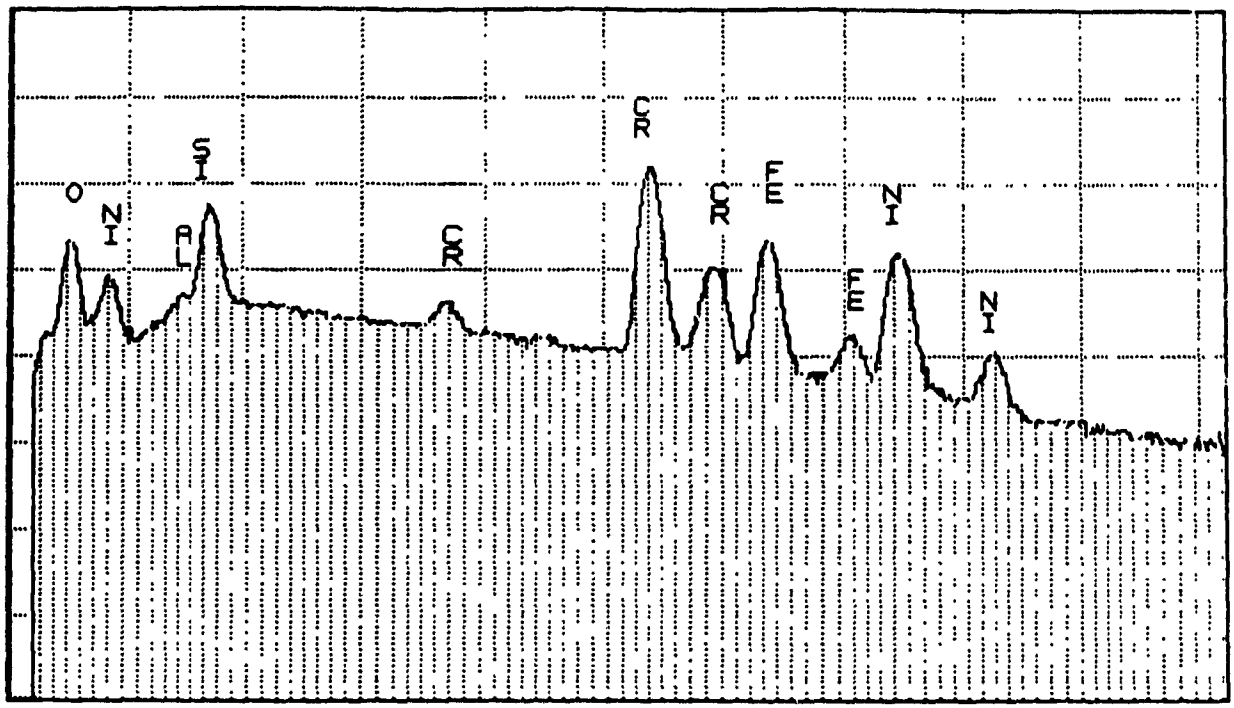

Figure 8.3 : X-Ray Analysis of Inside Pipe and Sodium Interface, Section 3, 9000X

Figures 8.2 and 8.3 show the presence of oxygen in the interface. Figure 8.3 of section 1 reveals no oxygen in the interface. The oxygen must exist as metal oxide and in a large enough amount to show up in x-ray analysis. Oxygen is often difficult to analyze for on the SEM. This implies the presence of corrosion products such as iron-oxides on the surfaces of sections 2 and 3. This can only result from a chemical reaction taking place at the interface between the furnace gases and the steel. As no oxides were detected on the surface of section one we must assume that no corrosion has taken place. If we consider this and the other evidence presented, the mechanism causing the granulation that was illustrated in Micrograph 4, is erosion.

Chapter 9

The Mark II Heat Pipe Injection Lance

9.1 Introduction

Motivated by the success of the Mark I lance tests, construction and testing of a second lance was planned shortly after. Discussions were held on how to improve the heat pipe lance based on the knowledge acquired from the previous experiments. The major points of those discussions were as follows:

i) From the results of the S.E.M. analysis and the Mark I lance tests, it was clear that sodium should remain as the working fluid since it proved to be compatible with stainless steel and it served its purpose well as a coolant.

ii) From the visual inspection of the remains of the Mark I lance based on our knowledge of the pinhole which developed during welding, it was clear that failure had taken place at the tip of the lance and that this problem must be dealt with.

iii) Past experience with lances operating at Kidd Creek showed that HD alloy lances last longer than 310 stainless steel lances. Thus a small change in materials selection was decided upon.

These points were implemented into the engineering of the Mark II lance. The lances were otherwise similar in all regards.

9.2 Construction of the Mark II Lance

Kidd Creek had a contract with Kuboto, a Japanese based company that manufactures the HD alloy lances tested in Kidd Creek's C-furnace. They were contracted to do the bulk of the

Mark II lance construction. Their HD alloy lances are spun cast so that they are not available in a large variety of sizes. The size required for the inner pipe of the Mark II lance assembly was not available in HD alloy material, so a 309 stainless steel was chosen instead. The HD alloy lances were larger in diameter than the 310 stainless steel lances resulting in a greater overall weight of the lance. This also implied that the heat entering the lance would be greater due to the larger surface area. Calculations were made using the methodology in Appendix C, revealing that the vapour velocity would be well within all of the limits mentioned in the theory section.

To solve the problem of the lance tip failure, a much thicker plate was welded to the bottom of the pipes, resulting in welds that were removed from the edge of the lance where it is felt the greatest amount of attack takes place. These welds were also tested non-destructively (x-ray testing) to ensure their integrity. The thicker plate would ensure a longer life for the tip assuming that is where the greatest problems occur.

The sodium working substance was not changed and came from the same supply that was used for the Mark I lance.

9.3 Experimental

The cleaning and feeding procedures are the same as those outlined in the Mark I lance section. The pressure transducer and valving system was identical to the one used for the Mark I lance. The only difference in experimental set-up between the two tests was that the Mark II lance had an average air flowrate through the middle of the lance of 90 Nl/s, which was maintained for the entire duration of the test. In the previous lance experiments, air was not available at the beginning of the test so that the Mark I lance ended up plugging.

9.4 Results and Discussion

The Mark II lance test began on December 11, 1991 and finished on December 19, 1991. The data was compiled in the same manner as mentioned in the previous section. The following figures show the pressure and temperature curves for the Mark II lance.

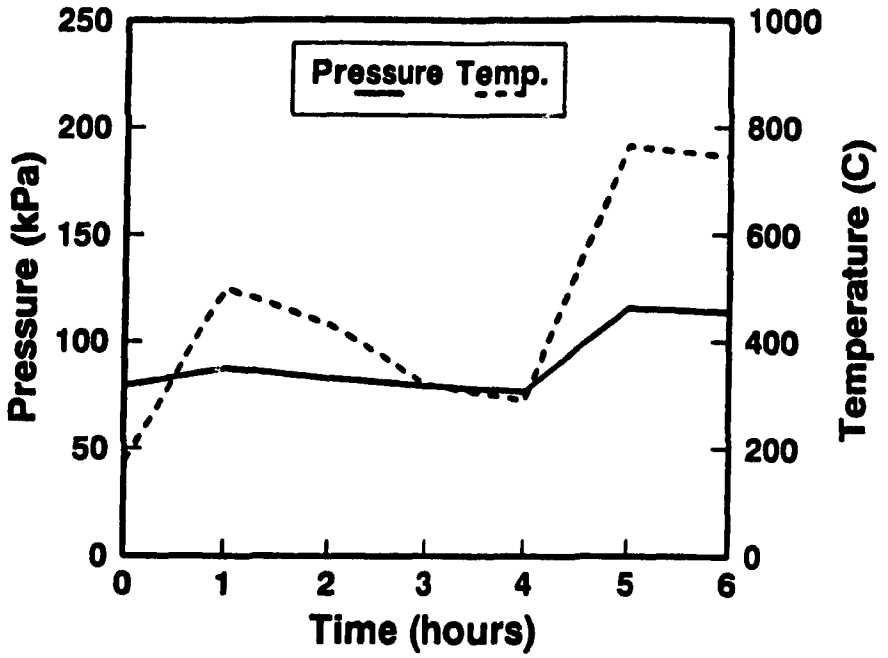

Begins at 17:12

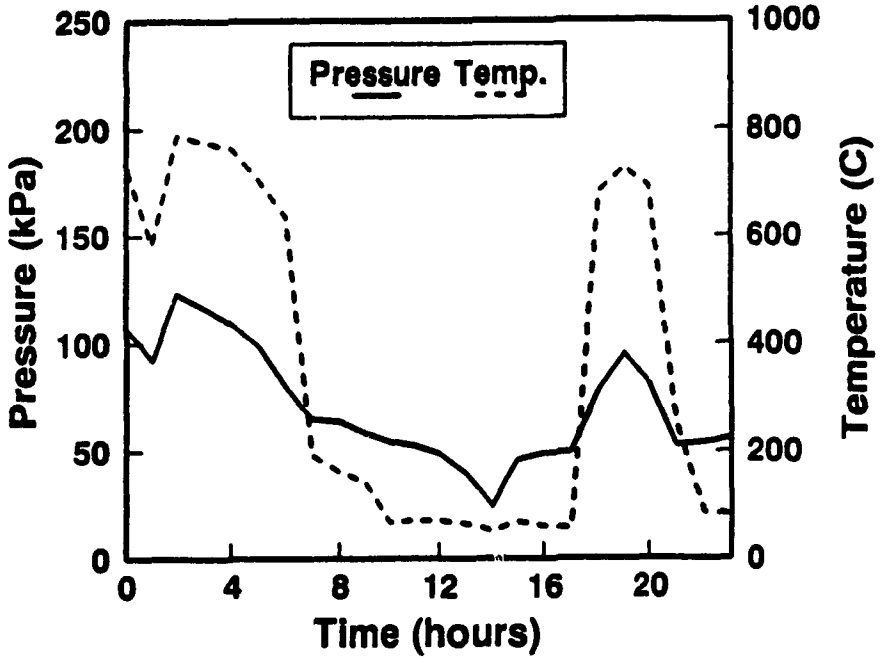

Begins at 12:12

Figure 9.0 : Na Vapour Pressure and Outer Wall Temperature Curves for Mark II Lance Test, December 11 (above), December 12 (below), 1991.

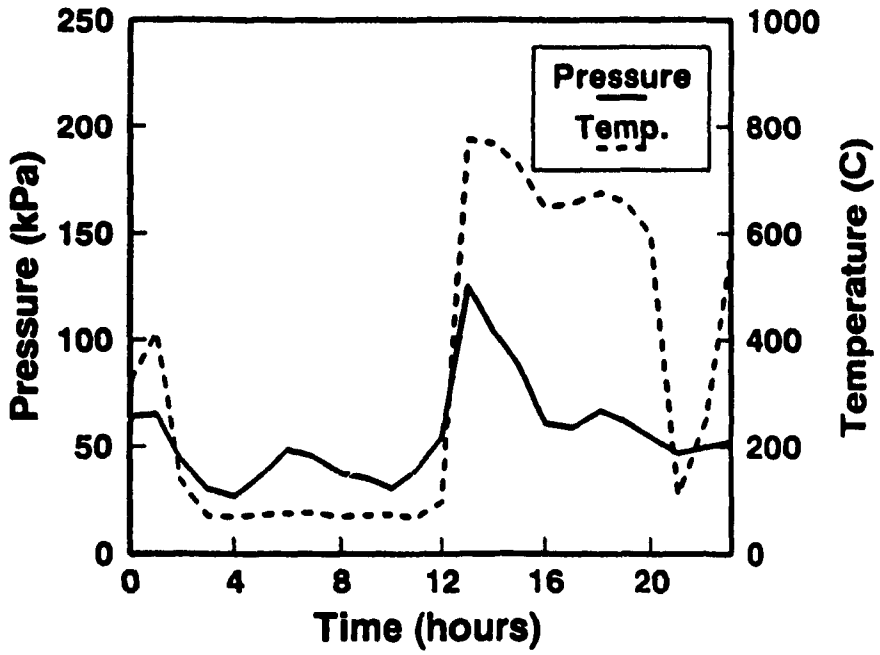

Begins at 12:12

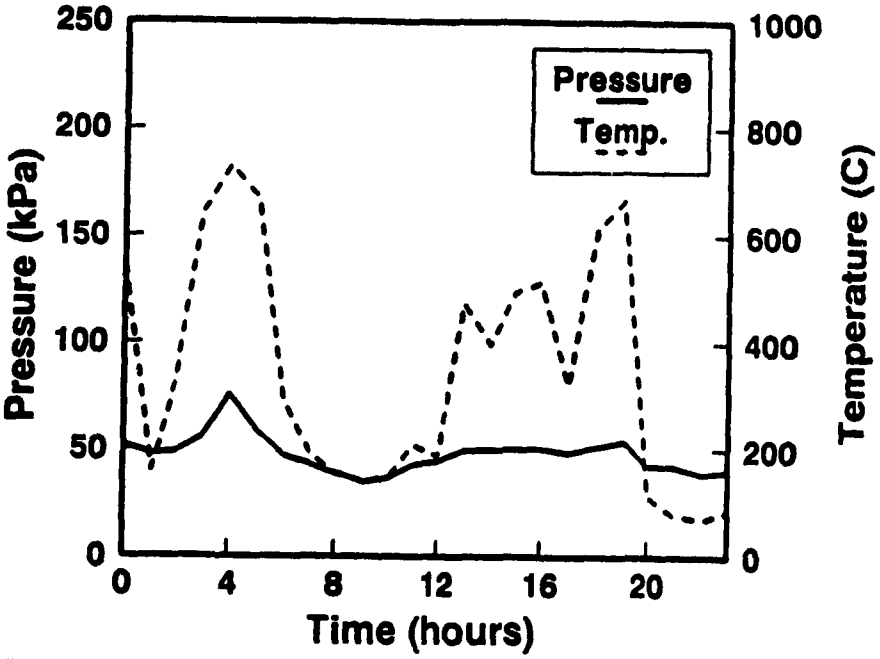

Begins at 12:12

Figure 9.1 : Na Vapour Pressure and Outer Wall Temperature Curves for Mark II Lance Test, December 13 (above), December 14 (below), 1991.

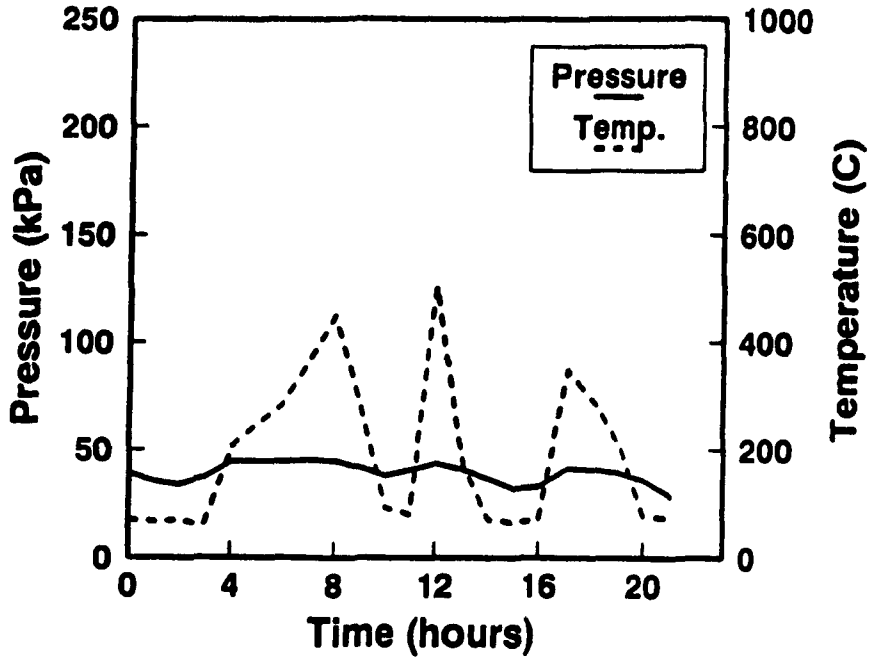

Begins at 12:12

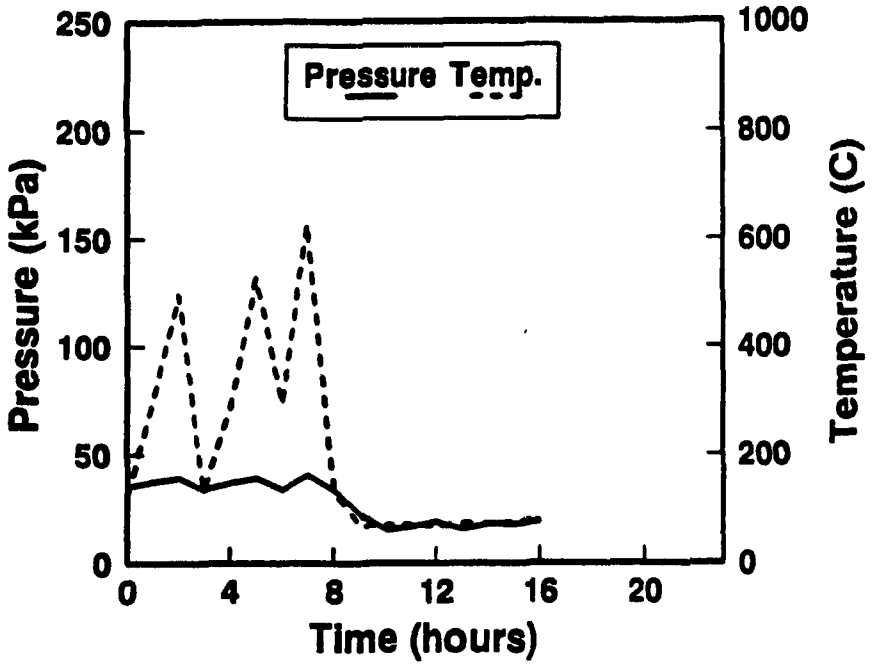

Begins at 6:47

Figure 9.2 : Na Vapour Pressure and Outer Wall Temperature Curves for Mark II Lance Test, December 15 (above), December 16 (below), 1991.

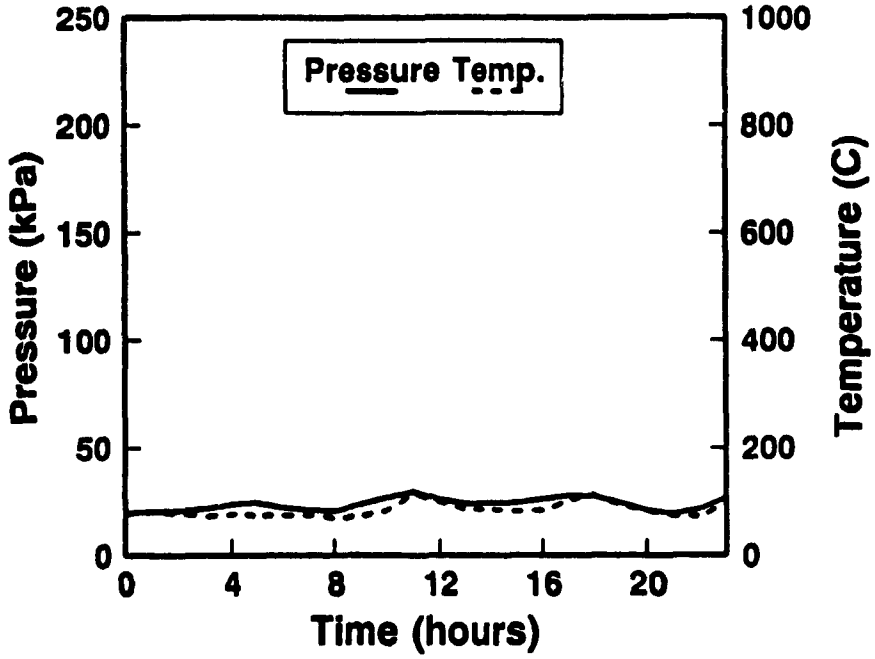

Begins at 12:00

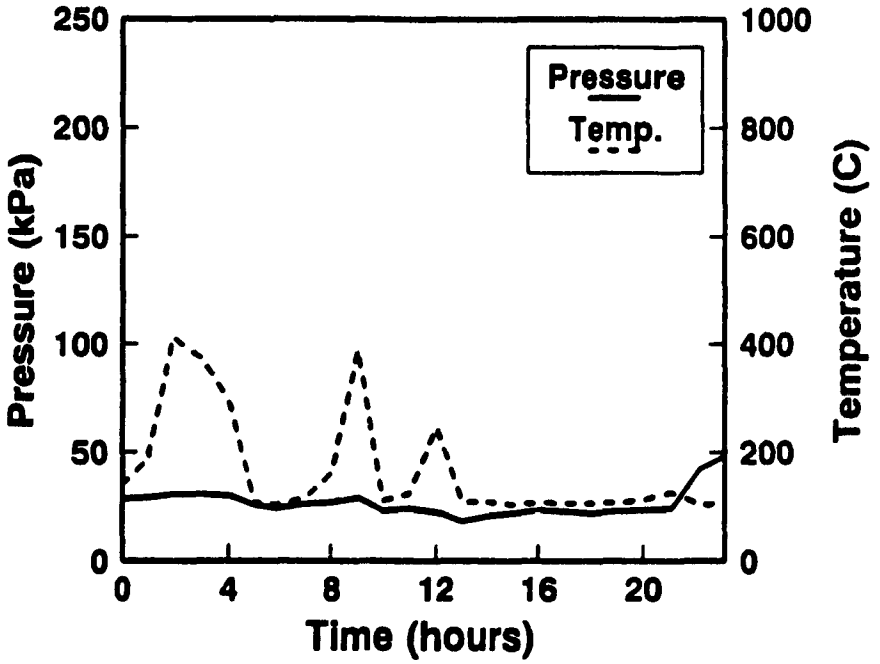

Begins at 12:00

Figure 9.3 : Na Vapour Pressure and Outer Wall Temperature Curves for Mark II Lance Test, December 17 (above), December 18 (below), 1991.

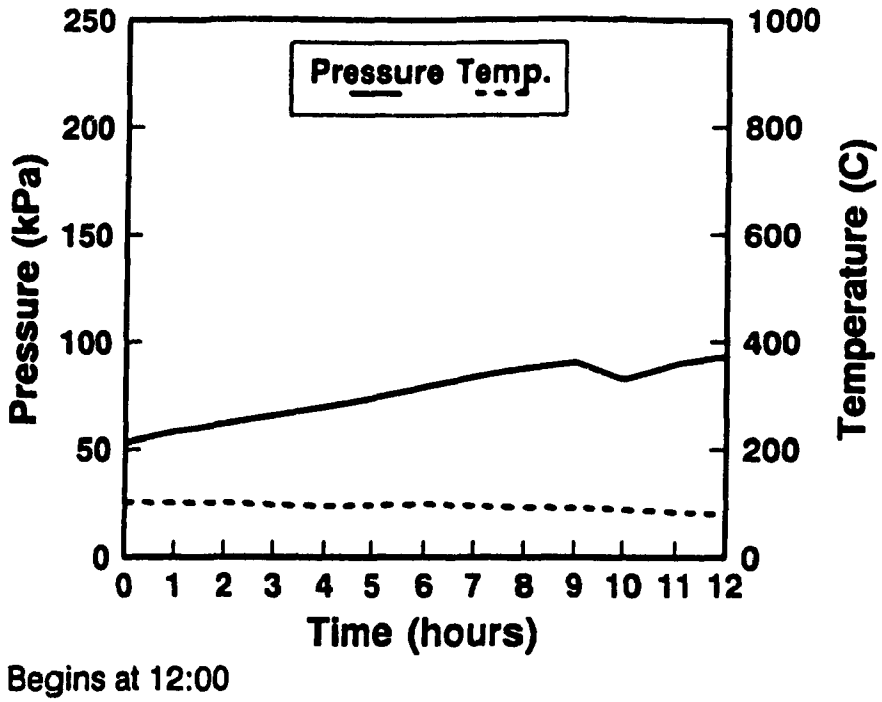

Figure 9.4 : Na Vapour Pressure and Outer Wall Temperature Curves for Mark II Lance Test, December 19, 1991.

On December 11, the Mark II lance was inserted into the furnace to a depth of 1.8 m, leaving 1.57 m of the lance subject to the furnace atmosphere, when the roof is taken into account. The Mark II lance was left in this position for the entire test. The experiment was observed by Dr. M. Kozlowski, E. Mast, Dr. F. Muccіardi, and myself over a period of two days before it was left to the plant engineers and workers to look after.

From the temperature and pressure curves and from our visual observations of the Mark II lance during its operation at Kidd Creek, the behaviour of the lance was essentially the same as the Mark I lance. In the following section, only the important inferences from the graphs are discussed.

Upon insertion into the furnace, the response of the lance was smooth, without any large fluctuations in the pressure readings. This is because the data that is graphed in Figure 9.0 was taken after the conditioning process, wherein the lance was evacuated over 5 second intervals, a number of times, to remove the impurites generated from the vaporization of sodium. Thus, the Mark II lance was well conditioned before the data was recorded. The jump in the pressure after four hours resulted from a change in the furnace conditions and not from a deeper insertion. On the days which followed the pressure and temperature curves seemed to fluctuate more than in the previous lance experiment. Two factors contribute to this behaviour: firstly, daily lance inspections are carried out to re-adjust the lance heights if required, which involve turning off the furnace, and secondly, a seemingly greater instability in furnace operations during the Mark II lance test as compared with the Mark I lance test.

On December 15 and 16, Figure 9.2, there is a discontinuity in the data. This was a result of improper storage of data in the computer and had nothing to do with the operation of the Mark II lance. Up until December 18, Figure 9.3, the lance was left in place with little supervision; only the occasional inspection to make sure everything was in order. The lance operated smoothly, responding to the changes in furnace conditions as expected. On December 18, at approximately 9:00 pm, a leak developed in the Mark II lance causing the pressure to gradually rise to 1 atm over a period of 15 hours. At 9:00 am, there was a decrease in the pressure for a 1 hour period before the curve returned to the gradually increasing slope it had before. The dip in the pressure resulted from a lance inspection. When the furnace was down, the temperature dropped inside the lance causing the gases to contract and the pressure reading to fall. After an hour, the furnace was turned back on and the pressure reading in the lance began to climb again.

Upon completion of the test, we were satisfied that the improvements in the engineering of the Mark II lance served their purpose. The life of the lance was extended to 7 and 1/2 days from the previous 2 and 1/3 days.

9.4 Failure of the Mark II Lance

Once the Mark II lance failed, attempts were made to remove the lance from the furnace.

In the end, the evaporator section of the lance could not be retrieved. The lance tip was therefore, not inspected. However, the condenser section was examined revealing valuable information regarding the failure of the lance.

During the operation of the Mark II lance, a spiral shadow of darker material appeared on the condenser section. The following figure illustrates this point.

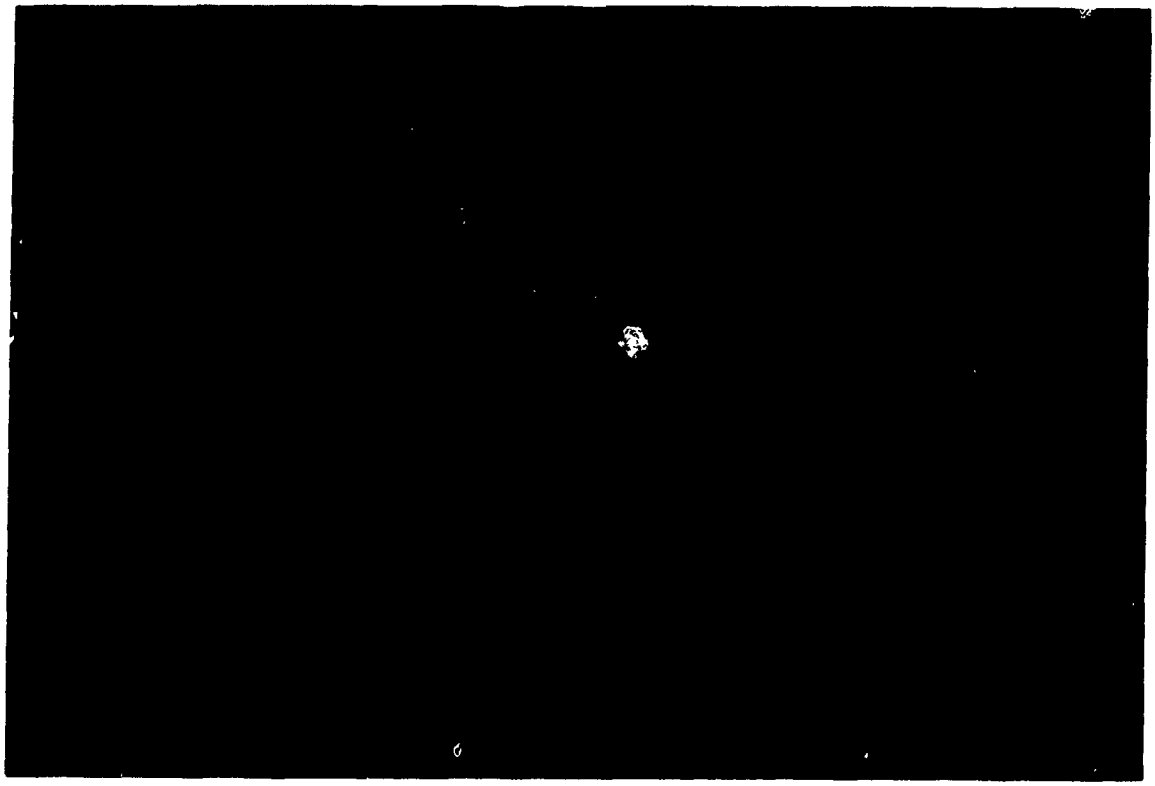

Figure 9.5 : Spiral Shadow of Darker Material on the Condenser Section of the Mark II Lance

After the lance was retrieved and disassembled, it was discovered that the bottom portion of the inner pipe had warped, illustrated in the following figure.

Figure 9.6 : Inner Pipe of the Mark II Lance After Kidd Creek Tests

The warping of the inner pipe must have come about from a differential expansion of the two pipes. This was a sensible explanation since not only were the materials different steels, but their dimensions, i.e. wall thicknesses, were different. This caused a disparate degree of expansion in each pipe. Since the pipes were welded at the ends, the inner pipe was not permitted to expand in length, causing it to warp.

Two cracks were also discovered on the inner pipe. Leak testing conducted at NTC demonstrated that one of the leaks penetrated the full thickness of the pipe. The cracks were longitudinal, as can be seen in Figure 9.7.

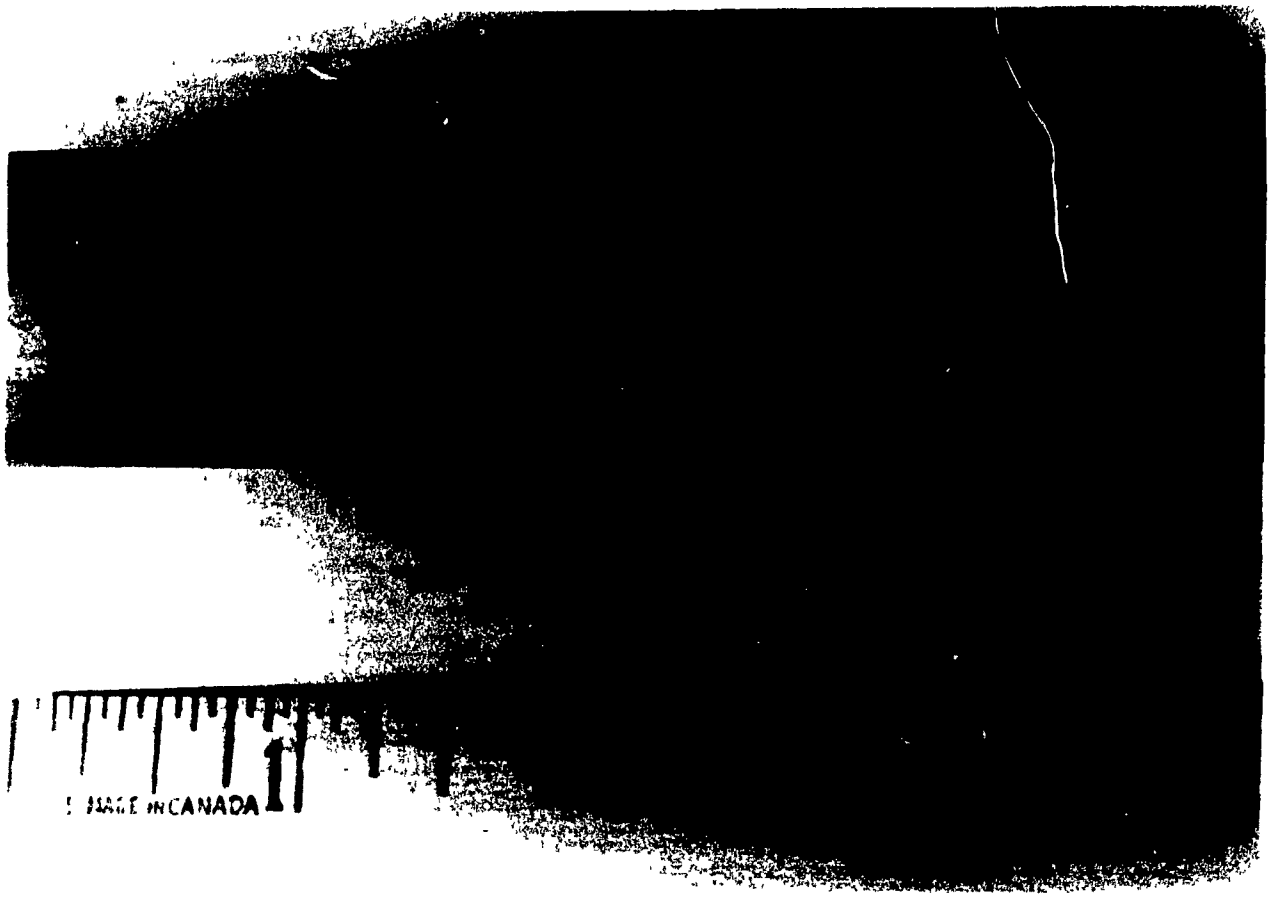

Figure 9.7 : Longitudinal Crack on Inner Pipe of Mark II Lance

A metallographic study undertaken by NTC personnel was conducted on sections of the pipe. The study revealed that a brittle intermetallic, known as sigma phase, was found in the heated parts of the inner pipe. Details of the study are found in an internal report and are not available for referencing. The failure resulted from the combination of differential expansion and sigma phase embrittlement of the inner pipe. The differential expansion caused stresses in the inner pipe while the sigma phase provided a location of decreased ductility were the stresses could concentrate and lead to a crack.

Chapter 10

Conclusions

A transparent heat pipe was constructed and studied. The two-phase, liquid and vapour, flow was visualized and values for the heat flux, vapour velocity and fluid velocity were determined mathematically. The mathematical value obtained for the condensate velocity (Appendix B) agreed with visual measurements. The methodology used in the calculations became the basis for the heat pipe injection lance calculations (Appendix C).

Simulations for the Kidd Creek process with a Laboratory Scale Heat Pipe Injection Lance were carried out. It was discovered that a 1/1 ratio of condenser to evaporator length could be expected in the industrial size C-furnace at Kidd Creek. It was also learned that the sodium vapour pressure and the visible condenser length could be reduced by as much as 40 % of their original values when external air cooling was used on the condenser section of the laboratory scale heat pipe injection lance.

Two pilot scale heat pipe injection lances were developed and tested based on the preliminary work done and the results of the simulation experiments. The second heat pipe injection lance, Mark II, lasted 7 and 1/2 days in Kidd Creek's C-furnace; orders of magnitude longer than the regular 304 stainless steel lances which were being used at that time. The results of the simulation experiments proved to be accurate. The behaviour of the Mark I and Mark II lances corresponded well with the values obtained in the simulation trials. From our visual inspection inside the furnace and from the fact that the lance was operating properly, it was clear that the lance location with respect to the bath surface was unchanged from its original insertion depth. Thus, its exact location was known unlike the standard lances.

A novel, self-cooling, heat pipe injection lance (patent pending) was developed and successfully tested.

Appendix A

Heat Pipe Theory Calculations

Capillary limit

Determination of capillary limit in example 1 of theory section. Assume the distribution of heat flux is uniform along the length of the evaporator and the condenser and that the pipe operates at 373.15 K.

Properties of water at 373.15 K:

liquid density, $\rho_l = 961$ kg/m^3
liquid viscosity, $\mu_l = 2.82 \times 10^{-4}$ kg/m-sec
liquid thermal conductivity, $k_l = 0.68$ W/m-K
surface tension coefficient, $\sigma = 5.84 \times 10^{-2}$ N/m
heat of vaporization, $\lambda = 2.254 \times 10^6$ J/kg
vapour density, $\rho_v = 0.58$ kg/m^3
vapour viscosity, $\mu_v = 1.28 \times 10^{-5}$ kg/m^3

Maximum effective pumping pressure P_{pm}:

capillary radius, $r_c = 1/2N = 6.4 \times 10^{-5}$ m
maximum capillary pressure, $P_{cm} = 2\sigma/r_c = 1.82 \times 10^3$ N/m^2
normal hydrostatic pressure, $\Delta P_\perp = \rho_l g d_v \cos\psi = 189$ N/m$_2$
axial hydrostatic pressure, $\rho_l g L_t \sin\psi = 0$
maximum effective pumping pressure, $P_{pm} = P_{cm} - \Delta P_\perp - \rho_l g L_t \sin\psi$
$= 1631$ N/m^2

Liquid frictional coefficient, F_l:

wick cross-sectional area, $A_w=\pi(d_l^2-d_v^2)/A=6.63 \times 10^{-5}m^2$

wick crimping factor, $S=1.05$

wick porosity, $\epsilon=1-\pi SNd/4=0.594$

wick permeability, $K=d^2\epsilon^3/122(1-\epsilon)^2=4.07 \times 10^{-11}m_2$

liquid frictional coefficient, $F_l=\mu/KA_w\rho_l\lambda=48.2\ (N/m^2)/(W-m)$

Vapour frictional coefficient, F_v:

vapour core cross-sectional area, $A_v=\pi d_v^2/4=3.17 \times 10^{-4}\ m^2$

vapour core hydraulic radius, $r_{h,v}=1.005 \times 10^{-2}m$

Drag coefficient, $(f_vRe_v)=16$

vapour frictional coefficient,

$F_v=(f_vRe_v)\mu_v/(2A_vr_{h,v}^2\rho_v\lambda)=2.45 \times 10^{-2}\ (N/m^2)/(W-m)$

Capillary heat transport factor, $(QL)_{c,max}$:

$(QL)_{c,max}=P_{pm}/(F_l+F_v)=33.8$ W-m

Capillary heat transport limit, $Q_{c,max}$:

$$Q_{c,max}=\frac{(QL)_{c,max}}{0.5L_c+L_a+0.5L_e}=84.5W$$

Sonic Limit

Determination of sonic limit for example 1. Same assumptions as those of capillary limit calculations.

vapour core cross-sectional area, $a_v = 3.17 \times 10^{-4} m^2$

vapour density, $\rho_v = 0.58$ kg/m^3

latent heat of vaporization, $\lambda = 2.254 \times 10^6$ J/kg

vapour molecular weight, M = 18

vapour specific heat ratio, $\gamma_v = 1.33$

universal gas constant, $R = 8.314 \times 10^3$ J/kg-mol-k

vapour constant, $R_v = 8.314 \times 10^3 / 18 = 462$ J/kg-k

vapour temperature, $T_v = 373.15$K

sonic limit,

$$Q_{s,max} = A_v \rho_o \lambda \left[\frac{\gamma_v R_v T_o}{2(\gamma_v + 1)}\right]^{1/2}$$

$= (3.17 \times 10^{-4})(0.58)(2.254 \times 10^6)[1.33(462)(373.15)/[2(1+1.33)]]^{1/2}$

$= 9.19 \times 10^4$ W

Entrainment Limit

Determination of entrainment limit for example 1. Same assumptions hold as in capillary limit section.

vapour core cross-sectional area, $a_v = 3.17 \times 10^{-4} m^2$

heat of vaporization, $\lambda = 2.254 \times 10^6$ J/kg

surface tension coefficient, $\sigma = 5.84 \times 10^{-2}$ N/m

vapour density, $\rho_v = 0.58$ kg/m^3

$r_{h,s} = 2A_s/C_s = 1/2N\text{-}d/2 = 3.225 \times 10^{-5}$m,

note that for screen wicks the hydraulic radius is equal to half of the wire spacing

$$Q_{e,max}=A_v\lambda(\frac{\sigma\rho_v}{2r_{h,s}})$$

$=(3.17x10^{-4})(2.254x10^{-6})[(5.84x10^{-2})(0.58)/[2(3.225x10^{-5})]]^{1/2}$

$=1.64 \times 10^4$ W

Boiling Limit

Determination of boiling limit for example 1. Same assumptions hold as in capillary limit section.

critical nucleation radius, $r_n=10^{-5}$ in. $= 2.54 \times 10^{-7}$ m

effective thermal conductivity of wick (see Chi p.76), $k_e=1.61$ W/m-K

surface tension coefficient, $\sigma=5.84 \times 10^{-2}$ N/m

vapour temperature, $T_v=373.15$K

heat of vaporization, $\lambda=2.254 \times 10^6$ J/kg

vapour density, $\rho_v=0.58$ kg/m^3

Radius ratio, $r_l/r_v=2.21/2.01=1.1$

critical pressure for nucleation, $2\sigma/r_n=2x5.84x10^{-2}/2.54x10^{-7}$

$=4.6 \times 10^5$ N/m^2.

This is much larger that the maximum possible capillary pressure in the capillary limit calculations ($P_c = 1.82 \times 10^3$ N/m^2), therefore P_c can be neglected and the equation becomes:

$$Q_{b,max}=\frac{2\pi L_e k_e T_v}{\lambda\rho_v \ln(r_l/r_v)}(\frac{2\sigma}{r_n})$$

substituting into the above equation,

$$Q_{b,max} = 2\pi(.1)(1.61)(373.15)(4.6 \times 10^5)/[(2.254 \times 10^{-5})(0.58)\ln 1.1]$$

$$= 1394 \text{ W}$$

Appendix B

Transparent Heat Pipe Calculations

All the following equations and data can be found in "Heat Transfer" by J.P Holman and "Fundamentals of Heat and Mass Transfer" by Incropera and De Witt :

Calculations derived from a typical transparent heat pipe experiment where:

$L_{condenser}$ = 0.775 m

$r_{outside}$ = 0.0145 m

r_{inside} = 0.013 m

k_{pyrex} = 1.13 W/m-K

$T_{ambient}$ = 295 K

Heat Losses Due to Natural Convection from the Pipe to the Environment

Convective Heat Transfer Equation:

$q_{conv} = hA(T_w - T_\infty)$

To find h for natural convection we must first determine the Grashof number:

$$Gr_x = \frac{g\beta(T_{w,o} - T_\infty)x^3}{\nu^2}$$

here T_∞ = 295 K

g = 9.81 m/s^2

ν_{air} = 15.252x10^{-6} m/s$_2$

evaluating the film temperature we get:

$$T_f = 1/\beta = (T_{w,o} + T_\infty)/2 = (T_{w,o} + 295)/2$$

now $\beta = 2/(T_{w,o} + 295)$

If we plug everything back into the Grashof relationship we get:

$$Gr_{x,T_{w,o}} = 8.434x10^{10}[\frac{T_{w,o}-295}{T_{w,o}+295}]x^3$$

Now we can determine the Nusselt number from the relation:

$Nu = C(Gr_f Pr_f)^m$, where $Pr_f = 0.709$

from table 7-1 of "Heat Transfer", C=0.59 and m=1/4, so that:

$$Nu = 291.76[\frac{T_{w,o}-295}{T_{w,o}+295}]^{1/4}x^{3/4}$$

we know that:

$Nu = h_x * x/k$

$h_x = Nu * k/x$ where $k_{air} = 0.026$ W/m °C

and

$$h = \frac{\int_0^L h_x dx}{\int_0^L dx}$$

where L = 0.775 m, the length of the condenser.

Here h is $h_{air,avg}$, for the condenser section. Making the appropriate substitutions and integrating we get:

$$h_{air,avg}=10.71[\frac{T_{w,o}-295}{T_{w,o}+295}]^{1/4}$$

Heat Lossess Due to Radiation

The equation describing radiation from a body onto a large open surrounding is:

$$q_{rad}=\sigma\epsilon A(T_1^4-T_2^4)=\sigma\epsilon A(T_{w,o}^4-T_\infty^4)$$

Assuming an emissivity of one and calculating the area as:

$A=2\pi rl=2\pi(0.0145m)(0.775m)=0.0706m^2$

substituting into the previous equation gives us:

$$q_{rad}=4.00x10^{-4}[T_{w,o}^4-295^4]$$

Total Heat Losses from the Transparent Thermosyphon

$$q_T=0.756\frac{[T_{w,o}-295]^{5/4}}{[T_{w,o}+295]^{1/4}}+4.00x10^{-4}[T_{w,o}^4-295^4]$$

Conduction Through the Walls of the Pipe

$$q_{cond} = \frac{-2\pi kL(T_{w,i} - Tw,o)}{\ln(r_o/r_i)}$$

where k(pyrex)= 1.13 W/m-K

L = 0.775m

r_o/r_i= 0.0145/0.013 = 1.1154

$q_{cond} = -50.38(T_{w,i}-T_{w,o})$

Laminar Film Condensation on the Inside Surface of the Pipe

After having observed the flow in the transparent thermosyphon, the convection inside the pipe may be best approximated by laminar film condensation on a vertical plate.
The average heat transfer coefficient for the entire plate is:

$$h_{avg,L} = 0.943\left[\frac{g\rho_l(\rho_l - \rho_v)k_l^3 h_{fg}'}{\mu_l k_l (T_{sat} - T_s)L}\right]^{1/4}$$

where the physical properties of Refrigerant 11 are:

ρ_l @25°C = 1467 kg/m^3

ρ_v @ B.P. = 5.86 kg/m^3

h_{fg} @ B.P. = 180 689 J/kg

k_l @25°C = 8.65 x 10^{-2} W/m-K

μ_l @25°C = 0.42 x 10^{-2} kg/m-s

$c_{p,l}$ @25°C = 871.52 J/kg

now $h_{fg}' = h_{fg} + 0.68\, c_{p,l}(T_{sat}-T_s)$ = 180 689 + 0.68(871.52)(2)

= 181 874 J/kg

note that we assumed a $(T_{sat}-T_s)=2$, after first assuming $h_{fg}'=h_{fg}$ and calculating for $(T_{sat}-T_s)$.

Substituting:

$$h_{avg,L}=0.943\left[\frac{9.81(1467)(1467-5.86)(8.65x10^{-2})^3 181874}{.42x10^{-2}(T_{sat}-T_s).775}\right]^{1/4}$$

$h_{avg,L} = 880/(T_{sat}-T_s)^{1/4}$

The equation then becomes:

$$q_{lam.cond.}=\frac{880A_{cond}[T_{sat}-T_{w,i}]}{[T_{sat}-T_{w,i}]^{1/4}}$$

Calculation of Heat Dissipated by Transparent Heat Pipe

we have now determined three equations describing the system:

$$q_{cond} = -50.38(T_{w,i}-T_{w,o})$$

$$q_T=0.756\frac{[T_{w,o}-295]^{5/4}}{[T_{w,o}+295]^{1/4}}+4.00x10^{-4}[T_{w,o}^4-295^4]$$

$$q_{lam\ cond.}=\frac{880A_{cond}[T_{sat}-T_{w,i}]}{[T_{sat}-T_{w,i}]^{1/4}}$$

We have here four equations and four unknowns. If the first two equations are solved simultaneously, q_T can be isolated on one side (take note that $q_T = q_{cond} = q_{lam\ cond}$). $T_{w,o}$ is isolated in the conduction equation and substituted into the natural convection equation to give:

Solving by trial and error and educated guessing based on the experimentation done, we

$$q_T = .756\frac{[(T_{w,i}-q_T/50.38)-295]^{5/4}}{[(T_{w,i}-q_T/50.38)+295]^{1/4}} + 4x10^{-4}[(T_{w,i}-q_T/50.38)^4-295^4]$$

substitute values of q_T and $T_{w,i}$ that make the left side equal the right side. We know that $T_{w,i}$ should be in the vicinity of the normal boiling point of freon 11 which is 296.82 K.

The only solution found was 297 K and 100.7 W for $T_{w,i}$ and q_T, respectively. If $T_{w,i}$ was varied only slightly in either direction the system of equations diverges very quickly. Therefore the only possible solution within reasonable limits of q_T was $T_{w,i}$ = 297 K and q_T = 100.7 W. When these values are substituted into the $q_{lam\ cond}$ equation we see that they make good sense.

First solve for $T_{w,i}$,

$$q_{cond} = 50.38(T_{w,i}-297)$$
$$100.7/50.38 = T_{w,i}-297$$
$$T_{w,i} = 298\ K.$$

then, $q_{lam.cond.} = 879\ A\ (T_{sat}-T_{w,i})/(T_{sat}-T_{w,i})^{1/4}$

$$100.7 = 879\ (.775)\pi(26x10^{-3})(T_{sat}-298)/(T_{sat}-298)^{1/4}$$
$$T_{sat} = 298 + 2.2\ K = 300.2\ K$$

Mass Flowrates and Velocities

The heat which is transported by the heat pipe is done so by the vaporization and condensation of the working fluid. Neglecting any losses, the following equations hold:

$$q_T = dm/dt\ h_{fg} \quad \text{and} \quad dm/dt = \rho Av$$

therefore, the amount of sodium needed to dissipate the previous heat calculated is:

$$100.7\ W = dm/dt\ (171.6\ J/g)$$
$$dm/dt = .59\ g/sec\ of\ sodium$$

The maximum vapour velocity of this sodium is:

$$v_{vapour} = dm/dt(1/\rho A)$$

$$v_{vapour} = .59 /(6320\pi(13x10^{-3})^2)$$

$$= 0.176 \text{ m/s}$$

To estimate the condensate velocity we must first calculate a film thickness. Rosler et al.[1], provide an equation which follows Nusselt's theory. Assuming constant fluid properties and neglecting interfacial shear stress, the film thickness in a thermosyphon device of uniform cross section can be determined from the following equation:

$$\delta_o = \left(\frac{3 q_e \mu_l L_e}{\rho_l(\rho_l - \rho_v) g h_{fg}} \right)^{1/3}$$

$$\delta_o = \left(\frac{3(100.7/L_e)(.42x10^{-2})(L_e)}{1467(1467-5.86)9.8(180689)} \right)^{1/3}$$

$$\delta_o = .07 \text{ mm}$$

Now we must calculate the cross sectional area of the film,

$$A_{xs} = \pi[.013^2 - (.013 - .07x10^{-3})^2]$$

$$= 5.7 \times 10^{-6} \text{ m}^2$$

Now, the condensate velocity can be calculated

$$v_{condensate} = .59 \times 10^{-3} / (1467 \times 5.7 \times 10^{-6})$$

$$= 0.07 \text{ m/s}$$

Appendix C

Laboratory Scale Heat Pipe Injection Lance Calculations

This section refers to the schematic of the Laboratory Scale Heat Pipe Injection Lance, Figure 6.0. The results of a test not indicated in the Table 6.1 and 6.2, are used in the following calculations. The parameters of the test were as follows:

$P = 1.43$ atm — From F*A*C*T (a thermodynamic computation program),

$T_1 = 866$ °C — at this pressure, $T_{Na,vapour} = 1188$ K or 915 °C

$T_2 = 847$ °C — Condenser length = 0.275 m

$T_3 = 140$ °C — $T_{ambient} = 25$ °C

$T_4 = 50$ °C — Evaporator length = 0.305 m

$r_{outside}$, $r_o = 0.0165$ m

r_{inside}, $r_i = 0.0125$ m

Condenser, Section II

Take the average temperature of the condenser as $T_{cond,avg} = (866 + 847)/2 = 857$ °C

Area of condenser: $A_{cond} = 2\pi r_o l_{cond}$

$= 2\pi(0.0165)(0.275)$

$= 0.0285\ m^2$

Heat dissipated through radiation (mostly) and convection:

Radiation: surface radiation to a large enclosure, from Holman[42]:

$$q = \sigma A_{cond} \epsilon_{ss} (T_{wall}^4 - T_{amb}^4)$$

from C.R.C. handbook $\epsilon_{ss} = .9$ for oxidized stainless steel

$$q = 5.669 \times 10^{-8}(.0285)(.9)(1130^4 - 298^4)$$

$q_{II,rad} = 2.36$ kW

Convection (Free): From vertical cylinders, from Holman:

$$Nu_{f,avg} = C\ (Gr_f Pr_f)^m$$

where $T_f = (T_{amb} + T_w)/2 = (298 + 1130)/2 = 714$ K

$$Gr_{f_x} = \frac{9.8\beta(T_w - T_{amb})x^3}{\nu^2}$$

$\nu_{700K,air}$ = 66 x 10^{-6} m^2/s $\beta = 1/T_f = 1/714$

$$Gr_{f_x} = \frac{9.8(\frac{1}{714})(1130-298)x^3}{(66x10^{-6})^2}$$

take x_{avg} = 0.1375 (middle of section)

therefore, $Gr_{f,avg}$ = (2.6215 x 10^9) x_{avg}^3

$Gr_{f,avg}$ = 6.815 x 10^6

From Table 7-1 of Holman: Pr_f = 0.684

using $Gr_{f,avg}Pr_f$ = 4.66 x 10^6

we get C = 0.59 and m = 1/4

therefore, $Nu_{f,x}$ = 0.59 (1.793 x 10^9 x^3)$^{1/4}$

$Nu_{f,x}$ = 121.4 $x^{3/4}$

we know that, $h_x = Nu_x k/x$

and $k_{air,700k}$ = 0.05 W/m°C

to find h_{avg} we must integrate as follows:

$$h_{avg} = \frac{1}{L}\int_{.35}^{625} \frac{Nu_{f_x}(.05)dx}{x}$$

integrating gives h_{avg} = 7.3 W/m^2°C

using Newton's law of cooling we get,

$q_{II,conv}$ = 7.3 A_{cond} (T_w - T_{amb})

$$= 7.3\ (.0285)\ (1130 - 298)$$

$$q_{II,conv} = 173\ W$$

It is clear that convection is very small compared to radiation.

Inert Gas, Section I

The heat losses in this section have been calculated only for radiation, since convection losses for this section are negligible compared to the rest of the losses. Using the same procedure for radiation as in the previous section:

$$q_{II,rad} = 65\ W$$

Total Heat Dissipated by the LSHPIL

$$q_T = q_{I,rad} + q_{I,conv}(\text{negligible}) + q_{II,rad} + q_{III,conv}$$

$$= 0.065 + 0 + 0.173 + 2.36\ kW$$

$$= 2.60\ kW$$

Evaporator, Section III

To calculate Radiation and Convection in the evaporator, first we must calculate the other temperature of the outside pipe.

Conduction: As a first estimate, let us assume the inside wall temperature to be that of the sodium vapour. The heat conducted through the walls of the cylinder and the bottom, in the evaporator section equals the heat dissipated by sections I and II.

$$q_T = 2600 = \frac{2\pi kL(T_w - T_i)}{\ln(r_o/r_i)} + \frac{KA}{\Delta x}(T_w - T_i)$$

$$k_{ss(20\%Cr,15\%Ni)} = 15\ W/m^{\circ}C$$

$$25.1 = T_w - 915$$

$$2600 = \frac{2\pi(15)(.3)(T_w - 915)}{\ln(.0165/.0125)} + \frac{15(7.86x10^{-4})(T_w - 915)}{.00625}$$

$$T_w = 940\ ^\circ C$$

This value is lower than what it should be as a gradient must exist between the inner wall and the sodium for the heat to be transported away by the sodium. A 10 °C gradient assumption will be made. Therefore, $T_w = 25.1 + (915 + 10) = 950\ ^\circ C$

Radiation:

We must calculate the radiation leaving the furnace walls, then calculate the fraction of this absorbed by the lance.

The walls are fireclay brick with $\epsilon_F = 0.75$ (Holman)

$$\therefore\ q_{Furn \to pipe} = \sigma \epsilon_F A_F F_{F \to pipe}(T_{F4} - T_{pipe4})$$

we know that, $A_F F_{F \to pipe} = A_{pipe} F_{pipe \to F}$

$$A_{pipe}(1) = A_F F_{F \to pipe}$$

$$q_{F \to pipe} = \sigma \epsilon_F A_{pipe}(1473^4 - 1223^4)$$

$$= 5.667 \times 10^{-8}(.75)(2\pi(.0165)(.3))(1473^4 - 1223^4)$$

$$= 1.322 \times 10^{-9}\ (2.47 \times 10^{12})$$

$$= 3265.8 \text{ Watts}$$

According to Kirchoff's law, the absorptivity of a surface equals its emissivity which equals 0.8 for the stainless steel pipe.

$$\text{then } q_{into\ pipe} = 3265.8\ (.9)$$

$$= 2939.2\ W$$

This value is subject to the accuracy of the emmisivity of the fireclay brick. Emissivities for brick material vary immensely from one type to another. Changing the emissivity value from .75 to .7 results in a incident heat flux of 3048 W. This changes the $q_{into\ pipe}$ to 2743, which agrees better with the 2600 W of heat dissipated by the lance, calculated in the previous section. If the gradient of 10 °C is raised to 20 °C, this further improves the agreement as the $q_{into\ pipe}$ becomes 2661 W. A 20 °C gradient from the inner wall of the pipe to the sodium vapor gives us a $T_{wall,out}$ of 960°C in a 1200°C environment. This implies that the heat pipe injection lance

is able to maintain a temperature 240 °C below the radiative temperature it is subject to.

Calculation of the Working Substance Flowrates

Once at steady state, the heat is removed from the evaporator, through the heat of vaporization of the sodium, where:

$$q = dm/dt\ h_{fg} \quad \text{where } dm/dt = \rho A_{xs} v_{fluid}$$

$$h_{fg} = 4636437.26 - 180.817\ T \quad J/kg \quad (C.R.C)$$

$$@\ 915\ °C \qquad h_{fg} = 4422 \quad J/g$$

$$dm/dt = 2.6\ kJ/s\ (1/4.422\ g/kJ)$$

$$dm/dt = 0.59\ g/s$$

$$\text{Now,} \quad dm/dt = \rho A_{xs} v_{fluid}$$

$$\text{and} \quad v_{fluid} = dm/dt(1/(\rho_{Na} A_{xs}))$$

$$\text{where,} \quad A_{xs} = \text{annulus cross section of the lance}$$

$$= \pi r_{i,op}^{\ 2} - r_{o,i\,p.}^{\ 2}$$

$$= \pi(.0127)^2 - \pi(.003175)^2$$

$$= 4.75 \times 10^{-4}\ m^2$$

$$\rho_{vapour} = PV/RT \quad mol/m^3$$

$$\rho_{vapour} = 1.43 \times 101.3 \times 10^3/(8.314 \times 1188)$$

$$= 14.66\ mol/m^3$$

$$V_{vapour} = .59/(23 \times 14.66 \times 4.75 \times 1/10^6)$$

$$= 368\ cm/s$$

$$V_{vapour} = 3.68\ m/s$$

To estimate the condensate velocity we must first calculate a film thickness. Using the same equation as in Appendix B:

$$\delta_o = \left(\frac{3 q_e \mu_l L_e}{\rho_l(\rho_l - \rho_v) g h_{fg}} \right)^{1/3}$$

$$\delta_o = \left(\frac{3(8.22)(.387x10^{-2})(30.5)}{.8(.8-337.2x10^{-6})980x4422} \right)^{1/3}$$

$$\delta_o = 0.102 \text{ mm}$$

The cross section of the film becomes:

$$A_{xs,film} = \pi(1.27^2 - 1.2598^2)$$

$$A_{xs,film} = .081 \text{ cm}^2$$

$$dm/dt = \rho A V_{fluid}$$

$$V_{condensate} = dm/dt \; / \; (\rho A_{xs})$$

$$= .59 \; / \; (.8 \times .081)$$

$$V_{condensate} = .091 \text{ m/s}$$

The Mark I Pilot Scale Heat Pipe Injection Lance

We assume that the heat flux in the industrial furnace is the same as that in the simulation experiments:

$$q'' = 2.6 \text{ kW}/(2\pi(1.65)(30.5))$$

$$= 8.22 \text{ W/cm}^2$$

Area of heat pipe injection lance:

Dimensions Outer Pipe O.D. = 6.01 cm

I.D. = 4.85 cm

Inner Pipe O.D. = 3.3 cm

I.D. = 2.54 cm

Area of evaporator, $A_{cylinder} = 2\pi(3)(6)(2.54)(12)$

$$= 3447.2 \text{ cm}^2$$

$$A_{bottom} = \pi r_1^2 - \pi r_2^2$$

$$= \pi(3)^2 - \pi(1.27)^2$$

$$= 23.21 \text{ cm}^2$$

$$A_{tot} = 3470 \text{ cm}^2$$

$$\text{Heat into Lance, } q = 8.22 \text{ W/cm}^2 \times 3470 \text{ cm}^2$$
$$= 28\,527 \text{ W}$$

Vapor velocity in the Pilot Scale Heat Pipe Lance

$$\rho_{vap} = 14.66 \text{ mol/m}^3 \times 23 \text{ g/mol} \quad @ \ 915 \text{ °C}$$
$$= 337.2 \text{ g/m}^3$$

$$A_{xs} = \pi(2.425)^2 - \pi(1.65)^2$$
$$= 9.92 \text{ cm}^2$$

$$q = dm/dt \ (h_{fg})$$
$$dm/dt = 28\,527 / 4422$$
$$= 6.45 \text{ g/s}$$

$$dm/dt = \rho A v$$
$$v_{vap} = 6.45 / (14.66(23)(9.92)(10^{-6}))$$
$$= 1927 \text{ cm/s}$$
$$v_{vap} = 19.27 \text{ m/s}$$

Condensate Velocity:

Using film thickness equation:

$$\delta_o = [3(8.22)(.00387)(182.88)/(.8(.8\text{-}337.2\text{x}10^{-6})(980)(4422)]^{1/3}$$
$$= 1.84 \times 10^{-2} \text{ cm}$$

$$A_{xs,film} = \pi(2.42^2 - (2.42\text{-}.0184)^2)$$
$$= 0.27 \text{ cm}^2$$

$$dm/dt = \rho A v$$

$$v_{condensate} = dm/dt/(\rho A_{xs,film})$$

$$= 6.45 / [(.8)(.27)]$$

$$v_{condensate} = 29.86 \text{ cm/s}$$

References

1. Gaugler, R.S. **Heat Transfer Device.** US Patent 2350348, Published 6 June, 1944.

2. Grover,G.M. **Evaporation-Condensation heat transfer device.** US Patent 3229759. Published 18 January, 1966.

3. Feldman, K.T., and Whiting, G.H. **The Heat Pipe and its Application.** Engrs. Dig., London, vol.28, No.3, pp 86-96, 1967.

4. Eastman, G.Y. **The Heat Pipe.** Scientific American, vol. 218, No.5, pp38-46, 1968.

5. Feldman, K.T., and Whiting, G.H. **Application of the Heat Pipe.** Mech. Engng., Nov., Vol.90, pp 48-53, 1963

6. Chi, S.W., **Heat Pipe Theory and Practice: A Sourcebook.** Hemisphere Publishing Corporation, U.S.A., 1976.

7. Feros Patenter Aktiebolaget **FR-PS 2,507,290.**

8. Ying Manufacturing Corp. **US-PS 4,184,477.**

9. Levenspiel, O, and Chan, R.T. **US-PS 4,408,656.**

10. Daimler-Benz AG **DE-PS 2,839,365.**

11. Institut de Recherches de la Siderurgie Francaise (IRSID)
FR-PS 2,520,101.

12. Elderfield, R. **US PS 4,398,703**
UK PS 8,013,470

13. Nagano,T. **Progress of Copper Sulfide Continuous Smelting,** Phys. Chem. Of Ext. Met., Met.Soc. AIME. Warrendale, P.A., 1985 pp 311-326.

14. Shibasaki, T., and Hayashi, H. **Top-Blown Injection Smelting and Converting: The Mitsubishi Process.** JOM, September 1991, pp 20-26.

15. Sweetin, R.M., Newman, C.J., and Storey, A.G. **Start-Up of the Kidd Smelter: Early Operating Results.** JOM, October 1983, pp36-41.

16. Kimura, E. **Fundamental Research of Lancing Mechanism in Mitsubishi Continuous Smelting Furnace,**Trans.

17. Moto Goto, **The Mitsubishi Continuous Process: Operation and Design, Mitsubishi Metal Corporation**, Tokyo, Japan, February 1988.

18. Incropera, F.P., and De Witt, D. P. **Fundamentals of Heat and Mass Transfer, Third Edition**, John Wiley and Sons, U.S.A., 1990.

19. Griffith, P., and Wallis, J.D. **The Role of Surface Conditions in Nucleate Boiling.** ASME-AIChE Heat Transfer Conference, August 1959.

20. Negishi, K., and Sawada, T. **Heat Transfer Performance of an Inclined Two-Phase Closed Thermosyphon.** Int. J. Heat Mass Transfer. Vol 26 No 8, 1983, pp 1207-1213.

21. Neda, T., Miyashita, P. **Heat Transport Characteristics of a Closed Two-Phase Thermosyphon.** JSME, Series II, Vol 32, No.2, 1989.

22. Basiulus, A., Prager, R.C., Lamp, T.R. **Compatibility and Reliability of Heat Pipe Materials.** Hughes Aircraft Company. Electron Dynamics Division, Torrance California, USA.

23. Fukano, T., Kadoguchi, K., Tien, C. **Oscillation Phenomena and Operating Limits of the closed Two-Phase Thermosyphon.** Proceedings of the Eigth International Heat Transfer Conference. California, USA., 1986, pp 2325-2330.

24. Faghri, A., Parvani, S. **Numerical Analysis of Laminar Flow in a Double-Walled Annular Heat Pipe.** J. Thermophysics. Vol 2, No 2, April 1988. pp 165-171.

25. Faghri, A., Chen, M. **A numerical Analysis of the Effects of Conjugate Heat Transfer, Vapour Compressibility and Viscous Dissipation in Heat Pipes.** Numerical Heat Transfer, Part A, Vol. 16, 1989, pp 389-405.

26. Faghri, A., Thomas, S. **Performance Characteristics Of a Concentric Annular Heat Pipe: Part I-Experimental Prediction and Analysis of the Capillary Limit.** Transactions of the ASME, Vol 111, November 1989, pp 844-850.

27. Faghri, A. **Performance Characteristics of a Concentric Annular Heat Pipe: Part II-Vapour Flow Analysis.** Journal of Heat Transfer, November 1989, Vol 111, pp 851-857.

28. Faghri, A., Chen, M.M., Morgan, M. **Heat Transfer Characteristics in Two-Phase Closed Conventional and Concentric Annular Thermosyphons.** Journal of Heat Transfer, Vol. 111, August 1989, pp 611-618.

29. Faghri, A., et al. **Mathematical Modeling and Analysis of Heat Pipe Start-Up from the Frozen State.** Transactions of the ASME, Vol 112, August 1990, pp 586-594.

30. Ivanovsky, M.N., Subbotin, V.I., et al. **Investigation of Heat Transfer Capillary Limit in Sodium Heat Pipes.** International Heat Pipe Conference. Bologna, 1976, pp 733-739.

31. Fukano, T., Chen, S.J., and Tien, C.L. **Oscillation Phenomena and Operating Limits of the Closed Two-Phase Thermosyphon**. Proc. ASME/JSME Thermal Engineering Conference, Vol. 1, 1983, pp. 95-101.

32. Dobran, F. **Steady-State Characteristics and Stability Thresholds of a Closed Two-Phase Thermosyphon**. Int. J. Heat Mass Transfer., Vol 28, No.5., 1985, pp 949-957.

33. Dobran, F. **Suppression of the Sonic Heat Transfer Limit in High-Temperature Heat Pipes**. Journal of Heat Transfer, Vol 111, August 1989, pp 605-610.

34. Negishi, K., and Sawada, T. **Heat Transfer Performance of an Inclined Two-Phase Closed Thermosyphon**. Int. J. Heat and Mass Transfer, Vol. 26, No. 8, 1983, pp. 1207-1213.

35. Bahadori, M.N. **Control of Solidification Rate by Application of Heat Pipe Principle**. Cast Metals Research Journal, Vol.6, No.1, March 1970, p. 38.

36. Zuzanak, A. **Control of Solidification Rate by Application of Heat Pipe**. AFS Transactions 89-69, pp 1035-1037.

37. Zuzak et al. **Heat Pipe: An Active Chill in the Thermal Steel Casting Sand Mold System**. AFS Transactions 90-20, pp 559-563.

38. Wells, K.J., Berry, J.T. **Two Dimensional Numerical Simulation of Casting Solidification With Heat Pipe Controlled Boundary Conditions**. AFS Transactions, 84-95, pp 429-434.

39. Choi, H.C. **Techniques for the Continuous Measurement of Melt Temperature** Ph.D. thesis, McGill University, Montreal, Canada, 1991.

40. Buontempo, S., et al. **The Heat Pipe**. Undergraduate Report for Mech Laboratory II, McGill University, 1991.

41. Dunn, P.D., Reay, D.A. **Heat Pipes**. Pergamon Press, 1982.

42. Holman, J.P. **Heat Transfer (Fifth Edition)**. McGraw-Hill, New York, 1981.